

H3K9 demethylation is required for reproduction in *Arabidopsis*

Dissertation

zur Erlangung des

Doktorgrades der Naturwissenschaften (Dr. rer. nat.)

der

Naturwissenschaftlichen Fakultät I

-Biowissenschaften-

der Martin-Luther-Universität

Halle-Wittenberg

vorgelegt

von Frau M.Sc. Jinping Cheng

Geboren am 07.10.1991 in Changzhi City, China

verteidigt am 16.05.2022

Gutachter:

1. Juni.-Prof. Dr. Hua Jiang

2. Prof. Dr. Wenhui Shen

Table of Contents

1 Introduction	4
1.1 Histone modifications in Eukaryotes.....	4
1.1.1 Histone methyltransferases in Eukaryotes.....	5
1.1.2 Histone demethylases in Eukaryotes	8
1.1.3 The role of histone demethylase in <i>Arabidopsis</i>	9
1.1.4 Recruitment of histone methyltransferases and demethylases	12
1.1.5 Histone modifications and gene expression	13
1.2 Anther development and pollen wall formation	14
1.2.1 Anther development	14
1.2.2 Pollen wall formation	15
1.2.3 Mechanisms of tapetum development and pollen wall formation	16
1.3 Meiosis	18
1.3.1 Overview of meiosis in plants.....	19
1.3.2 Homologous chromosome pairing and synapsis.....	20
1.3.3 Homologous recombination.....	21
1.3.4 Histone modifications in meiosis.....	22
1.3.5 The cohesin complex in meiosis	23
1.4 Aims of the study	26
2 Materials and methods.....	27
2.1 Plant Materials and Growth Conditions.....	27
2.2 In vivo histone demethylation assay.....	27
2.3 Chromatin Immunoprecipitation (ChIP) followed by qRT-PCR or sequencing (ChIP-seq)	28
2.4 RNA extraction followed by qRT-PCR or sequencing (RNA-seq).....	29
2.5 Cytological analysis.....	29
2.6 Yeast two-hybrid assays	30
2.7 Pollen viability assay.....	30
2.8 Bimolecular Fluorescence Complementation assay (BiFC).....	31
2.9 Construction and transformation	31

2.10 Co-immunoprecipitation (Co-IP)	31
2.11 Affinity Purification Mass Spectrometry (AP-MS).....	32
3 Results	33
3.1 H3K9 demethylation is required for meiosis in Arabidopsis.....	33
3.1.1 The mutation of <i>IBM1</i> leads to enlarged or collapsed pollen.....	33
3.1.2 The <i>ibm1</i> mutants produced abnormal microspores.....	34
3.1.3 <i>IBM1</i> and <i>JMJ27</i> were functionally redundant	36
3.1.4 The <i>ibm1</i> and <i>ibm1 jmj27</i> mutants showed multiple defects in meiosis....	42
3.1.5 Many genes obtained ectopic H3K9me2 in <i>ibm1 jmj27</i>	48
3.1.6 <i>IBM1</i> directly bind at targets to remove H3K9me2	51
3.1.7 Genes with ectopic H3K9me2 were downregulated in <i>ibm1 jmj27</i>	52
3.1.8 Meiosis essential genes were downregulated with increased H3K9me2 levels in <i>ibm1 jmj27</i>	54
3.1.9 <i>IBM1</i> interacts with PDS5 family proteins.....	58
3.1.10 PDS5s act downstream of H3K9 demethylation to activate gene expression.....	62
3.2 H3K9 demethylation is required for pollen wall formation.....	68
3.2.1 H3K9 demethylation is required for exine formation	68
3.2.2 <i>AMS</i> interacts with <i>IBM1</i>	70
3.2.3 <i>IBM1</i> and <i>JMJ27</i> activate <i>TEK</i> expression to regulate nexine formation....	72
4 Discussion.....	76
4.1 Cooperation of H3K9 demethylases in plant development.....	76
4.2 H3K9me2 removal is required for Arabidopsis meiosis.....	78
4.3 PDS5s act downstream of H3K9me2 to regulate meiotic gene expression	81
4.4 H3K9me2 removal is required for pollen wall development mediated by <i>AMS</i> recruitment	82
5 Summary	84
6 Reference	86
7 Appendix	101
8 Acknowledgement	105
9 Curriculum Vitae	107
10 Eidesstattliche Erklärung/Declaration under Oath.....	109

11 Erklärung über bestehende Vorstrafen und anhängige
Ermittlungsverfahren/Declaration concerning Criminal Record and Pending
Investigations.....110

1 Introduction

1.1 Histone modifications in Eukaryotes

Chromatin is composed of DNA and histones in eukaryotes. The basic unit of chromatin, nucleosome, is typically composed of two repeats of histones H2A, H2B, H3, and H4, and 146 base pairs of DNA (Luger et al. 1997). Each histone contains an unstructured N-terminal tail, usually consisting of 25-40 amino acid residues subjected to various posttranslational modifications, such as acetylation, phosphorylation, methylation, and ubiquitylation (Arnaudo and Garcia 2013) (Figure 1.1). Methylation is an extensively studied modification that primarily occurs on the side chains of lysines (K) and arginines (R). Both K and R can be mono- and di-methylated, and K can be further tri-methylated (Ng et al. 2009). In addition to the number of methyl groups, the sites of methylation can also be different. The methylation at lysine 4 (K4), lysine 9 (K9), lysine 27 (K27), and lysine 36 (K36) are common sites. Generally, H3K4me₃, H3K36me₃, and H3K79me₃ are involved in gene activation, whereas H3K27me₃ and H3K9me₂ are involved in transcriptional repression (Black, Van Rechem, and Whetstine 2012). Thus, histone lysine modifications have different functions depending on the position and number of methyl groups.

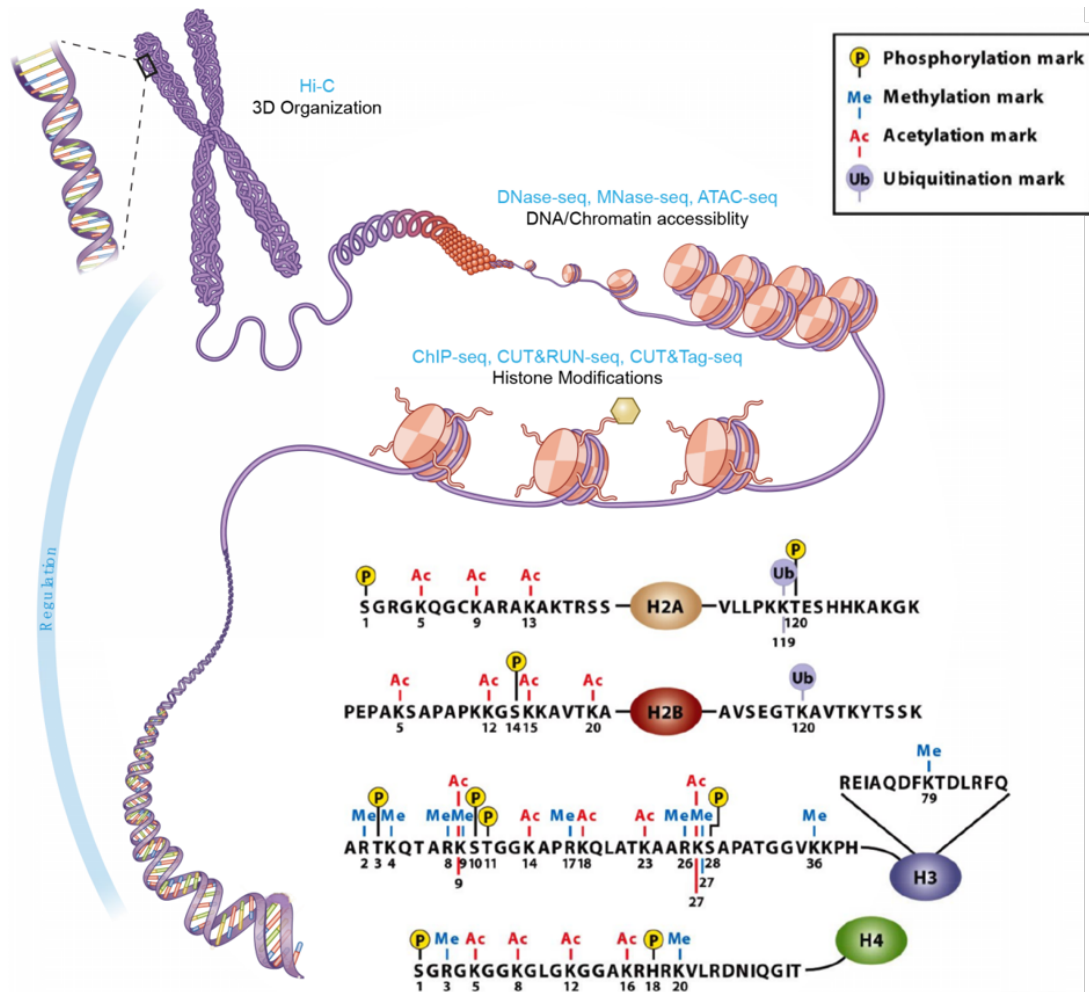


Figure 1.1. Histone modifications. Post-translational modifications of histones, including phosphorylation, methylation, acetylation, and ubiquitination, regulating chromosome structure and gene expression, modified from Zou J. *et al.*, 2019.

1.1.1 Histone methyltransferases in Eukaryotes

Histone methylation is precisely regulated by methyltransferases and demethylases. The methyl group can be added by the histone methyltransferases called “writer”. The first identified histone lysine methyltransferase (HKMT), SUV39H1, mainly methylates H3K9 (Rea et al. 2000). More HKMTs are identified afterward, and most of HKMTs are conserved between animals and plants. These HKMTs usually contain the SET domain responsible for enzymatic activity. One exception is Dot1 (Disruption of telomeric silencing 1) that can methylate H3K79 without the SET domain (Dindar et al. 2014; Xiao, Lee, and Wagner 2016). The SET domain was firstly found in *Drosophila melanogaster* and named after three *Drosophila melanogaster* proteins, namely Su(var) 3-9, Enhancer of Zeste, and Trithorax (Jones and Gelbart 1993; Tschiersch et al. 1994; Stassen et al. 1995). Genetic studies showed that the

SET-domain proteins belonging to the Su(var) 3-9 subfamily play vital roles in H3K9 methylation and heterochromatin assembly (Rea et al. 2000; Nakayama et al. 2001). For example, the mice with compromised *SUVH3-9* showed unstable chromosomes, defected heterochromatin assembly, and increased tumorigenesis (Peters et al. 2001). Clr4p, another SET domain-containing protein, is required for centromeres silencing and the mating-type switching in *Schizosaccharomyces pombe* (Ivanova et al. 1998). The *Drosophila* Su(var)3-9 protein plays a vital role in regulating position-effect variegation (PEV) (Tschiersch et al. 1994). In *Arabidopsis*, 46 SET-domain containing proteins have been identified, which are grouped into seven classes, including I) Enhancer of zeste [E(Z)] homologs; II) The ASH1 homologs; III) The trithorax homologs and related proteins; IV) Proteins with a SET and a PHD domain; V) Suppressor of variegation [Su(var)] homologs and relatives; VI) Proteins with an interrupted SET domain; VII) RBCMT and other SET-related proteins (Ng et al. 2007).

The E(Z) class proteins are mainly associated with histone 3 lysine 27 trimethylation (H3K27me₃) (Springer et al. 2003). H3K27me₃ is usually deposited by the Polycomb Repressive Complex 2 (PRC2). The PRC2 complex, including four core subunits named after their *Drosophila melanogaster* homologs, is highly conserved among species. The core subunits include embryonic ectoderm development (EED), enhancer of zeste homologue 1/2 (Ezh1/2), suppressor of zeste 12 (Suz12), and retinoblastoma-binding protein 7/4 (RBBP7/4) (Ciferri et al. 2012). The PRC2 component EZH1 or EZH2 is responsible for catalyzing H3K27 methylation. H3K27 can be mono (H3K27me₁), di (H3K27me₂), or trimethylated (H3K27me₃). In *Arabidopsis*, there are three E(z) methyltransferase: *MEDEA* (*MEA*), *CURLY LEAF* (*CLF*), and *SWINGER* (*SWN*). *MEA*, a polycomb group protein, is required for proper embryo and endosperm development in a parental imprinted way (Kohler et al. 2005; Kinoshita et al. 1999). *CLF* was shown to mediate H3K27me₃ at *AGAMOUS* (*AG*) and *SHOOTMERISTEMLESS* (*STM*) loci to regulate flowering time via repressing their expression (Schubert et al. 2006; Chanvivattana et al. 2004). *CLF* and *SWN*, two main H3K27 methyltransferases, are redundant in H3K27me₃ deposition (Shu et al. 2019).

The trithorax group (trxG) proteins mainly mediate H3K4 methylation (H3K4me) and activate gene expression. For example, *ATX1* regulates floral development via its H3K4 methyltransferase activity to activate flower homeotic gene expression

(Alvarez-Venegas et al. 2003). H3K4me is mainly deposited at the promoter and enhancer regions in mammals (Cheng et al. 2014), and gene bodies in plants (Zhang et al. 2009), indicating their essential roles in gene expression. In *Arabidopsis*, H3K4me plays a vital role in controlling floral transition and root growth (Jiang et al. 2011; Yao et al. 2013). H3K4me_{2/3} is linked to “memory” of environmental stresses, such as drought and heat in plants (Ding, Fromm, and Avramova 2012; Ding et al. 2012; Lamke et al. 2016). The H3K4me_{2/3} levels at the promoters of ‘heat memory genes’ are elevated after the first moderate stress treatment (Lamke et al. 2016). The increased H3K4me_{2/3} level persists for three days and contributes to more dramatic transcriptional activation and increased stress tolerance upon a second stress treatment, perhaps caused by hyper H3K4me₃ for efficient transcription elongation (Ding et al. 2012; Lamke et al. 2016).

KYP/SUVH4, SUVH5, SUVH6, all belong to the SUV subfamily, are proven to function as histone 3 lysine 9 (H3K9) methyltransferases to maintain the H3K9 methylation levels in *Arabidopsis* (Du et al. 2015; Ebbs and Bender 2006). The above-mentioned proteins, mainly KYP, play critical roles in heterochromatin assembly. H3K9me is mainly deposited on heterochromatin (Barski et al. 2007) but excluded from the gene body. Its deposition on heterochromatin is essential for genome stability through silencing transposable elements (TEs) and other repetitive DNA (Du et al. 2015; Bernatavichute et al. 2008; Liu et al. 2010). H3K9me is highly correlated with DNA methylation (Bernatavichute et al. 2008). In plants, DNA can be methylated at three sequence contexts: CG, CHG, and CHH (where H corresponds to A, T, or C) (Zhang, Yazaki, et al. 2006; Lister et al. 2008; Cokus et al. 2008). CHG methylation can form a feedback with H3K9me₂ (Du et al. 2015). *Arabidopsis* SUVH proteins can bind to the methylated DNA by their SRA domain (SET and RING finger Associated), leading to H3K9 methylation. In turn, CMT3, the CHG methyltransferase, can bind to histones with H3K9me₂ via its chromodomain to maintain CHG methylation (Johnson et al. 2007). Thus, H3K9 methylation and CHG methylation can form feedback to reinforce the methylation states. No obvious development defects are observed in the *kyp* mutant, but further study showed that KYP represses the seed dormancy by decreasing the expression of dormancy-related genes (Zheng et al. 2012). In addition, H3K9me₂ also plays an important role in *Arabidopsis* meiosis. In plants, meiotic recombination mainly happens in chromosome arms but is repressed in centromeric

and pericentromeric regions (Lambing, Franklin, and Wang 2017; Choi and Henderson 2015). Loss of H3K9me2 and CHG DNA methylation activates meiotic recombination near centromeres in *kyp suvh5 suvh6* and *drm1 drm2 cmt2 cmt3* mutants (Underwood et al. 2018), revealing that H3K9me2 is essential for suppressing recombination surrounding centromeres.

1.1.2 Histone demethylases in Eukaryotes

Methylation marks can also be removed by the “eraser”, histone demethylases, to keep the dynamic balance. Histone methylation is believed to be irreversible until the discovery of histone demethylase KDM1A/LSD1. LSD1 can remove H3K4 methylation via its amine oxidase domain with the aid of cofactor flavin adenine dinucleotide (FAD) (Shi et al. 2004). Moreover, the JmjC domain-containing protein KDM2A/JHDM1A can remove H3K36 via its JmjC domain, with the iron as a cofactor mediating an α -ketoglutarate reaction (Tsukada et al. 2006). More histone demethylases catalyzing diverse substrates are characterized after the above discoveries. The identified histone demethylases are clustered into two families: lysine-specific demethylase (LSD) and Jumonji-C (JmjC) domain-containing proteins, with different mechanisms to remove methylation modifications. Hence, histone methylation is dynamically regulated by methylases and demethylases to keep the balance during development.

LSD1 plays an essential role during development, including cell proliferation, cellular differentiation, embryonic development, and cancer (Forneris et al. 2009; Rotili and Mai 2011; Suzuki and Miyata 2011; Lynch, Harris, and Somervaille 2012). It contains three domains: SWIRM domain at N-terminal, FAD-binding domain, and the tower domain (Chen et al. 2006). LSD1 is shown to repress or activate transcription by mediating histone H3K4me1/2 and H3K9me1/2 demethylation, respectively (Shi et al. 2004). The molecular mechanisms underlying this dual substrate specificity remain unknown. LSD1 is responsible for H3K4me1/2 and H3K9me1/2 removal by the amine oxidation reaction together with FAD (Stavropoulos, Blobel, and Hoelz 2006). LSD1 can interact with the transcriptional repressor REST and histone deacetylase HDAC to form a complex, repressing the expression of neuronal genes by removing H3 and H4 lysine acetylation, and H3K4 methylation (Ballas et al. 2001; Battaglioli et al. 2002). Knockdown of *LSD1* leads to increased H3K4 methylation levels at the target

promoters (Shi et al. 2005). LSD1 also demethylate H3K9me to activate transcription. Androgen receptor (AR), a transcription factor, interacts with LSD1 to stimulate the transcription of AR targets by relieving H3K9 methylation. Pargyline, the inhibitor of LSD1, can repress the removal of H3K9 methylation, leading to the reactivation of AR target genes (Metzger et al. 2005). Taken together, LSD1 repress or activate gene expression depending on the specific substrates.

There are four homologs of *LSD1* in *Arabidopsis*, including *LSD1-like 1 (LDL1)*, *LDL2*, *LDL3*, and *flowering locus D (FLD)* (Jiang et al. 2007). *FLD* is shown to regulate *FLC* expression by histone acetylation removal, mutation of *FLD* results in hyperacetylation in *FLC* chromatin, and late flowering (He, Michaels, and Amasino 2003). *LDL1* and *LDL2* are partial redundancy with *FLD* in regulating *FLC* expression (Jiang et al. 2007). *LDL3* specifically removes H3K4me₂ to induce shoot regeneration (Ishihara et al. 2019), indicating the critical roles of H3K4 demethylases during plant development.

The second histone demethylase family, JmjC domain-containing proteins, can also erase a wide variety of histone methylation marks through oxidative reactions. These proteins are widespread from bacteria to eukaryotes, all containing highly conserved JmjC domain. Over 10,000 proteins have been annotated with this domain (Hahn et al. 2008). These proteins are clustered into seven subgroups according to the domains and functions, namely KDM2/JHDM1, KDM3/JHDM2, KDM4/JHDM3, KDM5/JARID, KDM6, KDM7, JmjC-domain only subgroups. The JmjC domain was identified in 1995 (Takeuchi et al. 1995), but its function to eliminate histone methylation was unknown until 2006. JHDM1 (JmjC domain-containing histone demethylase 1) is the first reported demethylase belonging to this family, specifically erasing H3K36 methylation with the cofactors Fe(II) and α -ketoglutarate. Overexpression of *JHDM1* reduces the H3K36 methylation level (Tsukada et al. 2006).

1.1.3 The role of histone demethylase in *Arabidopsis*

Arabidopsis has 21 proteins containing the JmjC domain (Figure 1.2). According to their evolutionary relationship and domain architecture, these proteins are clustered into five groups: KDM5/JARID1, KDM4/JHDM3, KDM3/JHDM2, JMJD6, and JmjC domain-only (Lu et al. 2008).

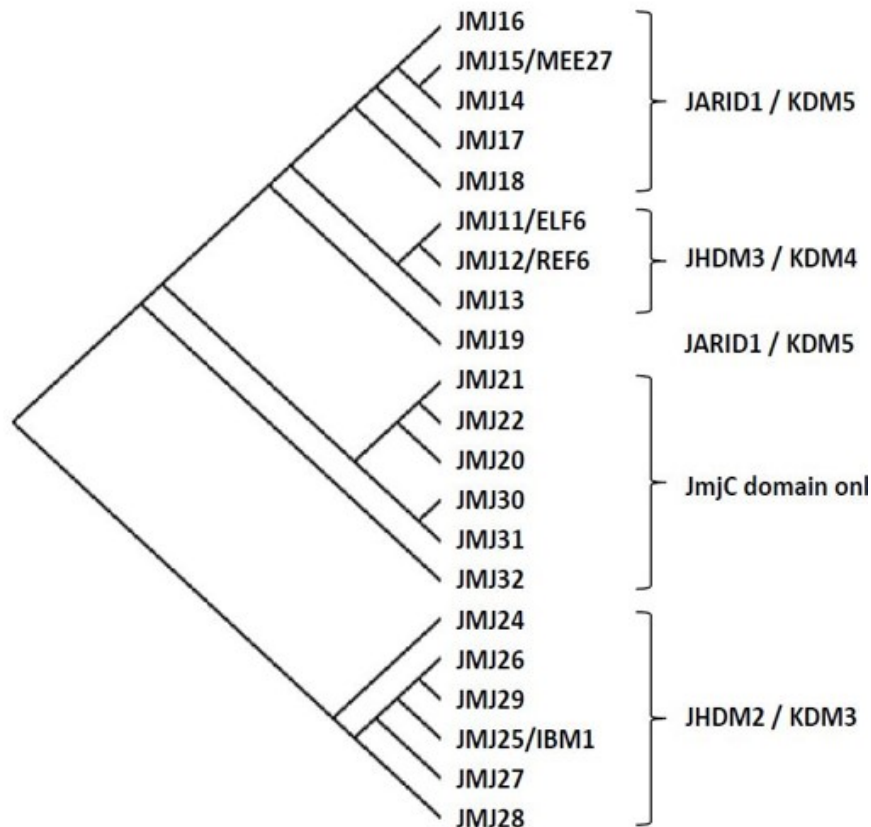


Figure 1.2. Twenty-one JmjC domain-containing proteins in *Arabidopsis*. The JmjC domain-containing proteins are grouped into five groups according to their substrate specificity.

KDM5/JARID1 group contains six members: JMJ14, JMJ15 (MEE27), JMJ16, JMJ17, JMJ18, and JMJ19. JMJ17 contains the JmjC, JmjN, ARID, C5HC2 zinc finger, and the PHD domain, while JMJ19 only contains JmjC, JmjN, and C5HC2 zinc finger domain. The remaining four members have FYRN and FYRC but not C5HC2 zinc finger or PHD domain at the C-terminal. FYRN and FYRC domains are preferentially present in H3K4 demethylases (Lu et al. 2008). Structural study of the JMJ14-H3K4me3 complex explains the substrate specificity of this subgroup. H3R2 and H3Q5 can be recognized by several acidic residues of the Jmj and C5HC2 domains of JMJ14 to further remove H3K4 methylation. The above acidic residues are conserved in plants and animals, indicating the general mechanism to determine the substrate specificity for these proteins (Yang et al. 2018). In addition, FYRN and FYRC domains at the C-terminal of JMJ14 interact with NAC050 and NAC052, two NAC domain-containing transcription factors, to direct the RNA silencing and regulate the flowering time (Zhang et al. 2015). PHD domains of this group are also essential for H3K4 methylation recognition

(Sanchez and Zhou 2011). At last, substrate specificity can be dynamic in different cell-types. JMJ16 only has the H3K4 demethylase activity in somatic cells, and this restriction is probably mediated by the interaction between the C-terminal FYR domain and catalytic domain. MMD1, the meiocyte-specific reader of histone methylation marks, can compete with the catalytic domain of JMJ16 to interact with the C-terminal FYR domain in meiotic cells, thus expanding the substrates from H3K4me to both H3K4me and H3K9me (Wang et al. 2020b).

The KDM4/JHDM3 group contains JMJ11 (ELF6), JMJ12 (REF6), and JMJ13, which are H3K27 demethylases in *Arabidopsis*. These proteins all contain the JmjN and JmjC domains, but have different domains at their C-terminal. JMJ13 contains C4HCHC type zinc finger domain, while REF6 and ELF6 contain four repeat C2H2 zinc fingers. As the zinc finger domain can bind to DNA, this group of proteins is predicted to bind to DNA directly. REF6 can bind to the targets harboring CTCTGYTY motifs through its 4x(C2H2) zinc finger domain and remove the H3K27m3 methyl group (Cui et al. 2016; Lu et al. 2011). JMJ13 represses the flowering in temperature- and photoperiod-dependent pathways. The early flowering phenotype of *jmj13* occurs at high temperatures no matter in LD or SD conditions, but not in SD conditions at low temperature (Zheng et al. 2019). Recently, ELF6 and REF6 are shown to play a critical role in resetting H3K27me3 and H3K27me1 marks during sexual reproduction (Antunez-Sanchez et al. 2020). Moreover, the three proteins can also function together to control the spatial boundaries of H3K27me3, regulating gene expression in a tissue-specific way (Yan et al. 2018).

The KDM3/JHDM2 group contains five members that are predicted to be H3K9me1/2 demethylases, including JMJ25 (IBM1) to JMJ29. Except JMJ28, they all contain conserved Fe (II) and α -KG binding sites required for the demethylase activity (Lu et al. 2008). Mutation of *IBM1* leads to ectopic deposition of H3K9me2 at thousands of gene bodies (Inagaki et al. 2010; Miura et al. 2009). Accordingly, the *ibm1* mutant exhibits pleiotropic developmental phenotypes, indicating its essential roles in plant development (Saze et al. 2008). In addition, JMJ27 is involved in both physiological and developmental regulation in *Arabidopsis*. JMJ27 positively or negatively regulates the expression of specific genes, such as pathogenesis-related (PR) genes *PR1* and *WRKY25*, to against the virulent *Pseudomonas syringae* pathogens. JMJ27

also governs the flowering time in a similar way (Dutta et al. 2017). JMJ29 is required for trichome development (Hung et al. 2020). Although JMJ28 has no conserved Fe (II) and α -KG binding sites, it can remove H3K9me2 at the *CO* locus to activate its expression by interacting with the BHLH transcription factor FBH (Hung et al. 2021). Although JMJ24 is classed into this subgroup, it doesn't harbor the cofactors binding sites and thus the demethylation ability. Alternatively, JMJ24 can destabilize the chromomethylase 3 (CMT3) through its ubiquitin E3 ligase activity, also regulating heterochromatic state (Deng et al. 2016).

1.1.4 Recruitment of histone methyltransferases and demethylases

Recognizing targets is another core question to understand the function of histone methyltransferases and demethylases. Recruiting histone methyltransferases and demethylases to targets is regulated to ensure that the modifications are deposited at the appropriate sites. Two modes are proposed for the targeting, recruited by DNA-binding proteins (Pasini et al. 2010; Eisenberg et al. 1990) or RNAi pathway. Well-identified DNA-binding proteins for the targeting are the Krüppel-associated box (KRAB)-containing zinc-finger proteins (KRAB-ZFPs) in mammals. The KRAB domain interacts with the co-repressor KAP1/Trim28 complex, recruiting SetDB1 methylase to silence the heterochromatic genes (Peng et al. 2000; Schultz et al. 2002; Friedman et al. 1996). Retinoblastoma (Rb) protein is required to recruit SUV39H1–HP1 complex to the euchromatic targets (Nielsen et al., 2001). MAX, the partner of Myc family proteins, is also involved in SUV39H1-mediated specific gene regulation in mouse embryonic stem cells (Maeda et al. 2013). In addition to the aforementioned proteins, transcription factors (TFs) Pax3 and Pax9 also play critical roles in recruiting histone methylases to keep the heterochromatin integrity in mice (Bulut-Karslioglu et al. 2012). The mutation of *pax3* and *pax9* leads to activated satellite transcripts, persistent impairment of heterochromatic marks, and defects in chromosome segregation (Bulut-Karslioglu et al. 2012). Nevertheless, only a limited number of transcription factors are known to recruit the histone demethylases to targets in *Arabidopsis*. JMJ14 interacts with NAC family transcription factors to target specific chromatin regions (Ning et al. 2015). Besides, the transcription factors FLOWERING BHLH (FBH) are shown to recruit JMJ28 to the *CO* locus to activate its expression (Hung et al. 2021). The histone reader MMD1 is shown to interact with JMJ16 to activate gene expression in meiotic cells (Wang et al. 2020a). Hence, histone modifier

interactors are important for recruiting histone methylases and demethylases.

The RNAi pathway is functional in guiding histone methyltransferases to targets in yeast and mammals. In fission yeast, recruiting the H3K9 methyltransferase to the centromeric region requires the RNA intermediates produced by the RNAi machinery, which is essential for heterochromatin formation (Hall et al. 2002). In addition, the RNAi pathway also plays an important role in maintaining the epigenetic inheritance for at least 20 generations in the germline of *C. elegans*, and the germline-specific argonaute HRDE1/WAGO-9 is required for this process. The multigeneration silencing phenomenon does not spread into the somatic cells (Ashe et al., 2012), indicating the tissue-specific functions of the complex. Similar mechanisms are also found in plants. The long siRNAs, produced by the AGO4-mediated silencing system, lead to DNA and histone methylation at the specific region by cooperating with KYP, CMT3, and DRM2 (Zilberman, Cao, and Jacobsen 2003), suggesting similar mechanisms required for the recruitment of histone methyltransferases in plants and animals.

1.1.5 Histone modifications and gene expression

DNA is wrapped around histones forming the nucleosomes. Histones can affect gene expression directly by physically enhancing or blocking the availability of DNA to transcription factors (Luger et al. 1997). Moreover, histones can also affect gene expression indirectly through post-translational modifications. Modified histones further recruit other effectors to regulate chromatin compaction and gene expression (Clements et al. 2003; Wysocka et al. 2006). For instance, H3K4me3 is required to recruit nucleosome remodeling factor (NURF) to activate HOX gene expression in humans (Wysocka et al. 2006).

H3K9me2 is a critical mark of heterochromatin formation and gene silencing in *Arabidopsis*. Deposition and removal of H3K9me2 are regulated by H3K9 methyltransferases and demethylases, both of which are essential for plant development (Fan et al. 2012; Hung et al. 2020; Dutta et al. 2017; Hung et al. 2021; Deng et al. 2016). However, the function of H3K9 demethylases in *Arabidopsis* reproduction is not clear. Moreover, the effectors acting downstream of H3K9 demethylation to activate gene expression are unknown in *Arabidopsis*. So, the first part of my thesis will focus on the function of H3K9me2 demethylation in

Arabidopsis meiosis, and the effectors required for H3K9 demethylation-mediated gene activation.

1.2 Anther development and pollen wall formation

1.2.1 Anther development

The production of pollen grains is essential for plant reproduction and crop yield. Anther is the male reproductive organ of higher plants, where pollen is produced and matured. It is a four-lobed structure, and each lobe is protected by four somatic cell layers, namely epidermis (E), endothecium (En), middle layer (ML), and tapetum (T) from outer to inner (Goldberg, Beals, and Sanders 1993). The innermost tapetum cell layer surrounds the reproductive cells and plays a critical role in pollen maturation (Sanders et al. 1999).

Anther development starts with stamen primordia emergence and ends with anther dehiscence and senescence. The whole process is divided into 14 stages according to the distinctive cellular events observed from the wild-type *Arabidopsis* (Sanders et al. 1999). The 14 stages are further classed into two phases (Figure 1.3). The stamen primordia emerge at stage 1 with L1, L2, and L3 three cell layers. Archisporial cells appear at stage 2, and further divide into the primary parietal layer, secondary parietal layer, and primary sporogenous layer at stage 3. The primary parietal and sporogenous layers differentiate into the four somatic cell layers, and the four-lobed structure is formed at stage 4. At stage 5, the four clearly defined locules are established, and the microspore mother cells arise. Microspore mother cells enter meiosis between stage 5 and stage 7, and the haploid microspores named tetrads are produced at stage 7. During these stages, the middle layer is degenerated, the tapetum cell layer becomes vacuolated, and anther size is increased gradually. The callose wall is degenerated to release microspores at stage 8, indicating the end of phase 1. During phase 2 (stage 9 to stage 14), microspores developed into pollen grains containing both vegetative and generative nuclei for pollination. Several cell layers are degenerated along with stomium cell breakage and pollen release during these stages (Sanders et al. 1999).

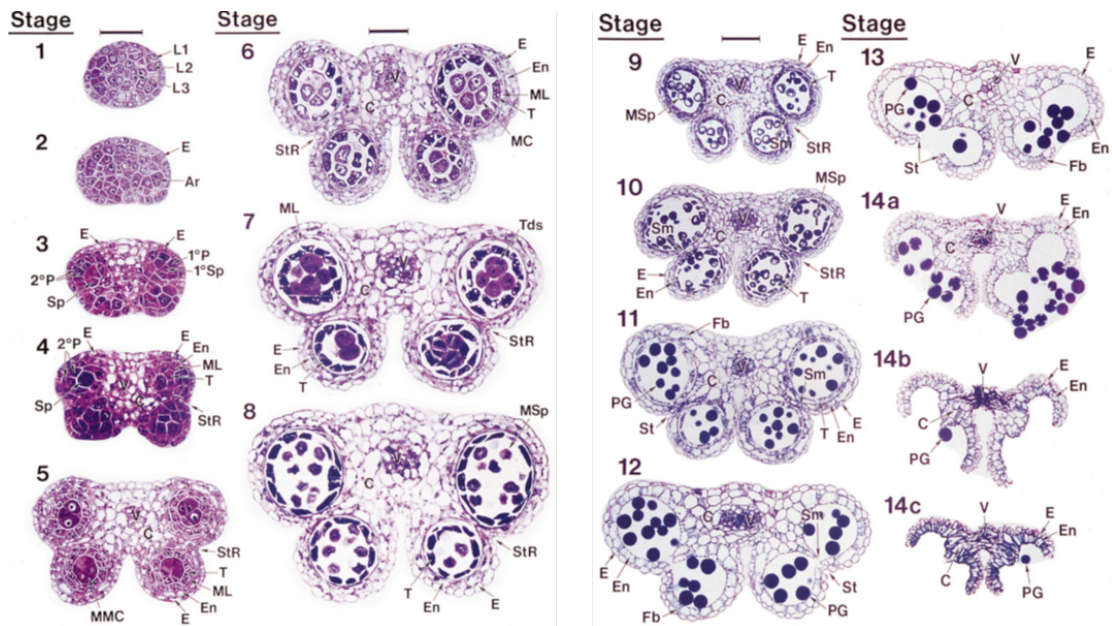


Figure 1.3. Phase one (left) and phase two (right) of wild-type *Arabidopsis thaliana* anther development (Sanders et al. 1999). L1, L2, and L3, the three cell layers of the stamen primordia; E, epidermis; Ar, archesporial; 1°P, primary parietal layer; 2°P, secondary parietal layer; Sp, sporogenous cells; MC, meicyte; ML, middle layer; MMC, microspore mother cell; MSP, microspore; PG, pollen grains; Sm, septum; St, stomium; T, tapetum; Tds, tetrads; V, vascular C, connective; En, endothecium.

1.2.2 Pollen wall formation

Pollen grains are surrounded by a multilayer pollen wall, a structure protecting pollen grains from desiccation, stresses, microbial attacks (Scott, Spielman, and Dickinson 2004). Many genes are involved in pollen wall formation (Figure 1.4). The morphology of the pollen wall varies in different species, but its fundamental structure is conserved (Fraser et al. 2012). The pollen wall is typically composed of an inner intine and an outer exine. The intine is mainly composed of pectin, cellulose, and hemicellulose, while the exine is mainly composed of sporopollenin (Quilichini, Grienenberger, and Douglas 2015; J 1968). The exine is further divided into an inner nexine layer and an outer sexine layer. Sexine is formed in a regular pattern, including the baculum, the rod structure, and the tectum, which is the outside edge covered with the pollen coat (Ariizumi et al. 2003).

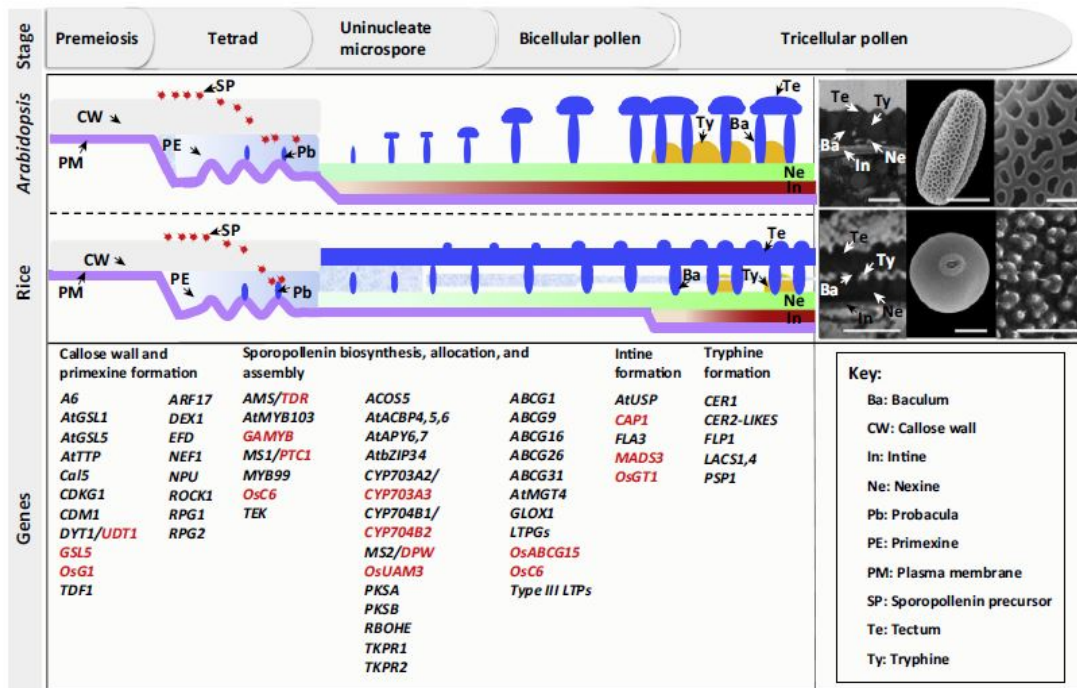


Figure 1.4. Pollen wall development in plants. The pollen wall is a multi-layered structure, and many genes are involved in its formation (Shi et al. 2015).

The pollen wall formation is assumed to start with the degradation of callose by callase secreted by tapetum. Tapetum provides enzymes and chemicals (Goldberg, Beals, and Sanders 1993), responsible for callose secretion, callose wall breakdown, and pollen wall materials synthesis (Xu et al. 2014). For example, sporopollenin, the main component of the exine, is derived from the tapetum. When the tapetal cells are degenerated, microspores will form the primexine that acts as the template for the deposition of sporopollenin precursors (Jiang, Zhang, and Cao 2013; Ariizumi and Toriyama 2011). Deposition of sporopollenin sets up the primexine that will develop into exine. The residue of the primexine is embedded between the precursor of bacula. The intine formation is initiated when the second round of mitosis starts, indicating that the pollen wall is formed.

1.2.3 Mechanisms of tapetum development and pollen wall formation

In *Arabidopsis*, the tapetum, arising from stage 4 during anther development, is highly active during stages 4 to 10. It is degenerated at later stages to promote pollen development (W.Parish and F.Li 2010; Sanders et al. 1999). Many transcription factors regulate tapetum development, including the basic helix-loop-helix (bHLH)

transcription factors *DYSFUNCTIONAL TAPETUM1 (DYT1)*, *ABORTED MICROSPORES (AMS)* (Sorensen et al. 2003; Xu et al. 2010; Zhang, Sun, et al. 2006), and *MALE STERILITY1 (MS1)* that contains a plant homeodomain (Wilson et al. 2001; Yang et al. 2007) (Figure 1.5). All these mutants lead to the failure of pollen formation even they function at different stages. In *dyt1*, tapetal cells are precociously vacuolated before meiosis, leading to abnormal meiotic cytokinesis (Feng et al. 2012; Zhang, Sun, et al. 2006). In addition, DYT1 also regulates callose wall formation and pollen coat biosynthesis, which occurs in tapetal cells and is stored in tapetosomes until the degeneration of tapetal cells (Feng et al. 2012; Hernandez-Pinzon et al. 1999; Hsieh and Huang 2005). AMS regulates the expression of various tapetum-expressed genes, including genes for lipid transportation, fatty acid synthesis and metabolism, methyl-modification, pectin dynamics. The *ams* mutant shows the enlarged tapetal cells that occupy the whole locular space, leading to the failure of tetrads releasing (Xu et al. 2010; Zhu et al. 2011). AMS exhibits a biphasic expression pattern during the anther development, and its expression had two peaks: pollen meiosis to tetrad stage and pollen wall development stage (Ferguson et al. 2017). MS1, another tapetum development regulator, is mainly expressed in the late stages of anther development (Yang et al. 2007). The mutation of MS1 leads to the failure of tapetum development due to lacking programmed cell death (PCD), affecting the deposition of pollen wall materials (Alves-Ferreira et al. 2007; Ito et al. 2007). The above three transcription factors, together with other proteins, form the network to regulate the anther development.

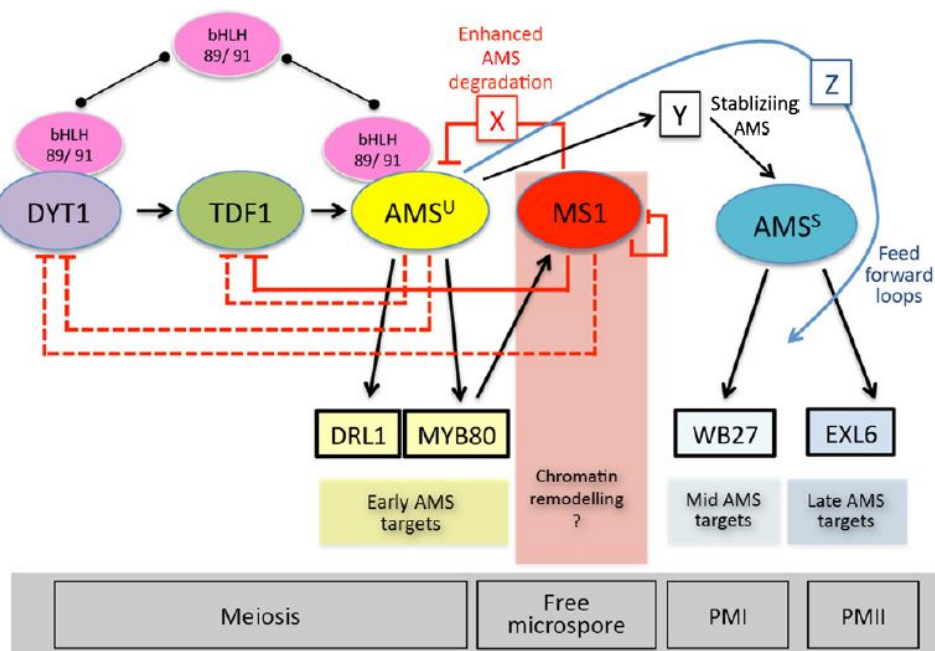


Figure 1.5. The regulatory network for the regulation of tapetum transcription factors during anther development in *Arabidopsis*. AMS has two expression peaks during the anther development with different targets and functions (Ferguson et al. 2017).

The synthesis and degradation of diverse chemicals required for pollen wall are regulated by the complicated regulation networks. The callose wall plays a critical role in the process, and the mutation of callose synthase *CALS5* leads to a defective exine (Dong et al. 2005). *CALS5* expression is decreased in *dex1* with a compromised plasma membrane protein expression. The pollen wall is also abnormal in *dex1*, indicating that *DEX1* is required for exine formation and sporopollenin secretion (Ma, Yang, and Zhang 2013). The exine is composed of inner nexine and outer sexine. Several tapetal-specific genes are involved in the exine formation, including *CYP703A2* and *MS2* for sporopollenin biosynthesis (Chen et al. 2011; Morant et al. 2007), and *ABCG26* for precursor transportation (Choi et al. 2011; Quilichini et al. 2010). *TEK*, an AT-hook containing protein, regulates nexine formation. AMS can bind to the *TEK* promoter and form the regulation pathway (*DYT1-TDF1-AMS-TEK*) to regulate nexine formation. Besides, AMS can also bind to the *MS188* promoter, involved in the regulatory module *DYT1-TDF1-AMS-MS188* to control the sexine formation (Lou et al. 2014).

1.3 Meiosis

1.3.1 Overview of meiosis in plants

Meiosis is a special type of cell division with one round of DNA replication followed by two rounds of chromosome segregation. This process is divided into meiosis I and meiosis II, both of which contain four phases: prophase, metaphase, anaphase, and telophase (Figure 1.6). Homologous chromosomes segregate into two poles in meiosis I, and sister chromatids separate in meiosis II, leading to reduced ploidy. Prophase I is a long process, which is further divided into five substages: leptotene, zygotene, pachytene, diplotene, and diakinesis, based on the cytological features of chromosomes (Armstrong and Jones 2003; Dawe 1998; Zickler and Kleckner 1999b). DNA replication has been completed at leptotene, and chromatin begins to condense, forming thread-like structures called the axial element. Homologous chromosomes pairing starts at zygotene. Synapsis also happens following the synaptonemal complex (SC) structure (Roeder 1990). Homologous chromosomes are fully synapsed and continue to condense at pachytene. At diplotene, the SC is disassembled, and homologous chromosomes start to be partially separated. The cytological features of chiasmata can be detected, where homologous chromosomes are still tethered together at those positions. At diakinesis, the chromosomes further condense and form highly compacted bivalents, indicating the end of prophase I. Homologous chromosomes complete recombination at prophase I, and crossovers form between non-sister chromatids, which are essential for the proper segregation of homologous chromosomes. At metaphase I, paired chromosomes move to the cell center, aligning at the equatorial plane. Homologous chromosomes segregate to opposite poles at anaphase I, and become decondensed at telophase I. Chromosomes are condensed again and separated by the organelle band at prophase II. At metaphase II, two groups of chromosomes are aligned vertically to each other. At anaphase II, sister chromatids are separated and segregated to form four clusters of chromosomes. Chromosomes become decondensed at telophase II. Afterward, four haploid nuclei are packaged through cytokinesis, producing four microspores (Ma 2006).

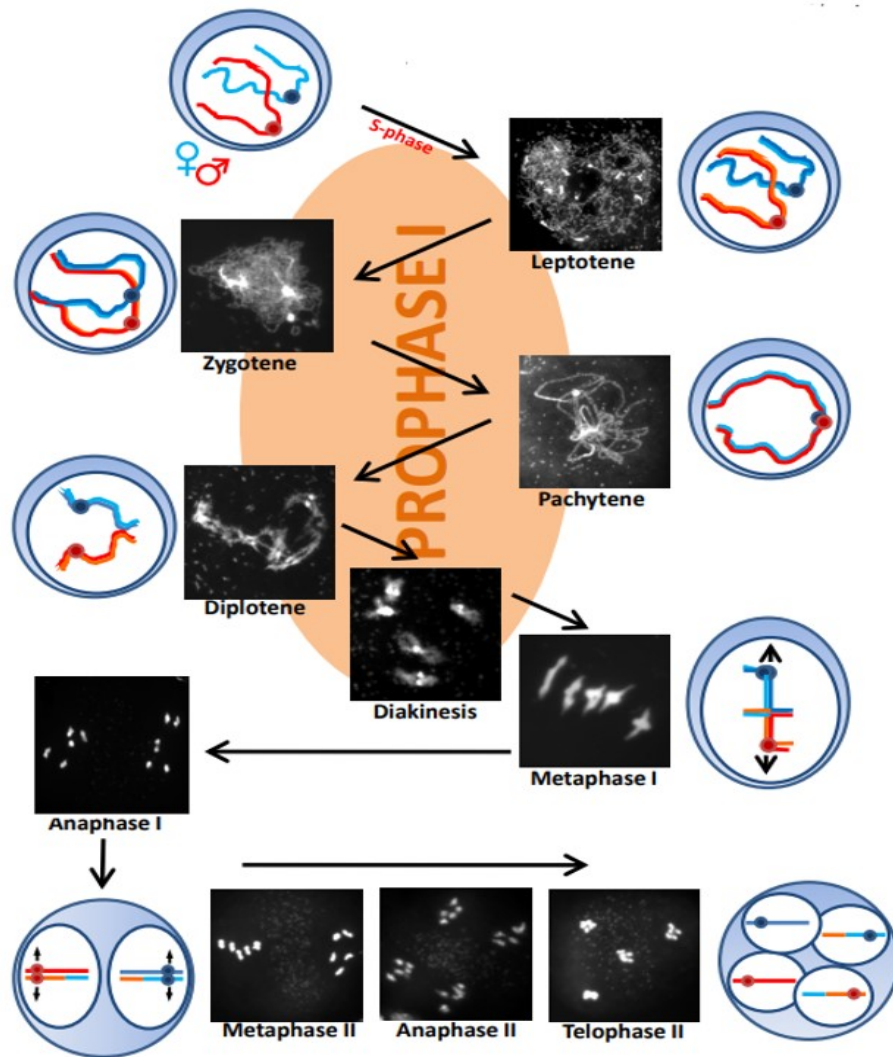


Figure 1.6. Chromosome morphology at different stages in male meocytes. Modified from West A et. al., 2015. Many special events happen in meiosis, such as DNA double-strand breaks (DSBs), homologs recombination, and crossover (CO) formation. These events are essential for the correct segregation of homologous chromosomes.

1.3.2 Homologous chromosome pairing and synapsis

The initiation of alignment and pairing between homologous chromosomes occurs from leptotene through zygotene. The axial elements (AEs) is initially formed between the paired sister chromatids in early prophase I, and the homologous chromosomes are increasingly aligned closely with each other from leptotene through zygotene. During these stages, the AEs will develop into parts of the SC structure that are referred to lateral elements (LEs), and LEs at the two sides of SC are connected by the transverse filaments (TFs), forming the SC structure. At

pachytene, the completely synapsed homologous chromosomes are linked by the SC along their entire length, and the four chromatids are held together tightly by the SC. The SC is disassembled during diplotene, and the homologous chromosomes are separated at chromosome arms, only linked together by chiasmata at reciprocal crossover sites.

The structure of SCs is highly similar in eukaryotic organisms. However, the sequences of the protein components are not conserved. For example, the TF proteins Zip1 in yeast, SYP1 in *C. elegans*, C (3)G in *Drosophila*, and SCP1 in mammals do not show some sequence similarity even sharing the similar structure (Page and Hawley 2001; MacQueen et al. 2002; Zickler and Kleckner 1999a; Heyting 1996). In *Arabidopsis*, two Zip1 homologs, AtZYP1a and AtZYP1b have been identified, both of which are required for plant fertility. The mutation of *ATZYP1a* leads to the reduced crossover, multivalent and univalent formation (Higgins et al. 2005; Capilla-Perez et al. 2021). DSBs are required for homologous synapsis in *Arabidopsis*. Loss of SPO11, a protein catalyzing the formation of meiotic DNA DSBs (Bergerat et al. 1997; Hartung et al. 2007; Grelon et al. 2001), leads to the abolishment of chromosome pairing and synapsis (Grelon et al. 2001). The phenotype is the same in yeast and mammals but different in *C. elegans* that synapsis occurs without the DSBs formation (McKim et al. 1998; Lichten 2001; Burgess 2002).

1.3.3 Homologous recombination

Homologous recombination is initiated by the formation of DSBs at leptotene. SPO11, the highly conserved protein, catalyzes meiotic DNA DSBs (Bergerat et al. 1997; Hartung et al. 2007; Grelon et al. 2001). There are three SPO11 proteins in *Arabidopsis*, namely AtSPO11-1, AtSPO11-2 in A subunit, and MTOPVIB in B subunit (Vrielynck et al. 2016; Stacey et al. 2006). DSBs have preference positions, called DSB hotspots. The DSB hotspots are located at gene promoters in *S. cerevisiae*, while they are enriched in intergenic regions in mice (Smagulova et al. 2011; Baudat and Nicolas 1997). In *Arabidopsis*, the crossover (CO) hotspots can be detected along the entire chromosomes except for the centromere regions where most transposon elements are located with high DNA methylation and H3K9me2 (Salome et al. 2012). The single-strand DNA (ssDNA) is produced after the formation of DSBs (Wang et al. 2020a; Hung et al. 2021), and RAD51 recombinases bind at ssDNA to search for

homologous chromatids sequences (Sung and Robberson 1995; Bishop et al. 1992). Some DSBs can be repaired by using homologous chromosomes as DNA templates, leading to COs formation. Class I COs are ZMM proteins-dependent, firstly identified in *S. cerevisiae*. The ZMM proteins contain Zip1, Zip2, Zip3, Zip4, Msh4, Msh5, Mer3 and Spo16 (Börner, Kleckner, and Hunter 2004). In *Arabidopsis*, *SHOC1/ZIP2*, *ZIP4*, *MSH4*, *MSH5*, *HEI10*, *MER3*, and *PTD* are shown to regulate the formation of class I COs (Mercier et al. 2005; Chelysheva et al. 2012; Higgins et al. 2004; Chelysheva et al. 2007). The class II COs are MUS81- dependent (Higgins et al. 2008).

Most of DSBs with interhomolog invasion are still repaired without reciprocal exchange using sister chromatids as templates. In *Arabidopsis*, around 250 DSBs are formed per meiotic cell; only around 12 recombination events containing 10 class I COs and 2 class II COs are detected. The number of CO per chromosome is usually limited to at least one but does not exceed three, no matter the size of the chromosome, which is called CO interference to inhibit the successive COs (Berchowitz and Copenhaver 2010; Zhang et al. 2014). CO homeostasis is stable even with altered DSBs numbers in *S. cerevisiae* and mice (Martini et al. 2006). However, the study in Maize showed that the increased DSBs could increase the recombination rates (Sidhu et al. 2015).

1.3.4 Histone modifications in meiosis

Histone modifications are involved in the regulation of many meiotic events. For instance, H3K4me3 is enriched at DSB hotspots in yeast (Pan et al. 2011). A similar pattern is also found in mice, indicating the conserved roles of H3K4me3 in the DSB formation (Smagulova et al. 2011). The previous studies in mice show that the PR domain-containing 9 (PRDM9) can tri-methylate H3K4 and H3K36 at the genetic recombination sites to initiate the meiotic recombination in spermatocytes. The positive marks H3K4me3 and H3K36me3 only occur in the recombination regions: hotspots and the sex chromosomes PAR region, indicating their crucial roles in recombination (Powers et al. 2016). In mammals, depletion of G9a, the major H3K9 methyltransferase, impairs H3K9 methylation, and affects synapsis and homologs recombination, leading to the failure of spermatogenesis (Takada et al. 2011; Pan et al. 2011). Suv39h, another H3K9 methyltransferase in mammals, mainly functions during spermatocytes. Loss of *Suv39h* impairs H3K9 methylation at the pericentric

region, leading to abnormal synapsis and chromosomes segregation (Peters et al. 2001). In *Arabidopsis*, loss of H3K9m2 and non-CG methylation in *kyp* and *cmt3* increase the recombination rate near the centromere; however, they are dispensable for chromosome segregation (Underwood et al. 2018).

1.3.5 The cohesin complex in meiosis

The cohesin complex, essential for accurate chromosome segregation, is conserved in eukaryotes (Watrín and Peters 2006; Toyoda and Yanagida 2006; Vass et al. 2003). In *Arabidopsis*, the sister chromatid cohesion is composed of several conserved proteins, forming a ring-shaped structure. The core components of the complex contain four proteins: structural maintenance of chromosome proteins SMC1, SMC3 which form a heterodimer, sister chromatid cohesion protein 1 (SCC1) that REC8/SYN1 replaces in meiosis, and SCC3. These core components can form a tri-partite ring to entrap the sister chromatids together. REC8 is a kleisin cohesion subunit. The C-terminal is shown to bind to SMC1, and the N-terminal bind to SMC3 to close the ring structure (Gruber, Haering, and Nasmyth 2003). Mutation of *REC8* leads to the loss of sister chromatid cohesion. In addition to the core components, the complex also contains the accessory subunits, including precocious dissociation of sisters 5 (PDS5) and wings apart-like (WAPL), which regulate both the association and dissociation between cohesin and chromatin. Pds5 is required for the acetylation of the SMC3 subunit by Chromosome Transmission Fidelity 7 (CTF7) to close the cohesion ring, and also the maintenance of stable interaction between the cohesin complex and chromosomes (Vaur et al. 2012; Rolef Ben-Shahar et al. 2008; Lengronne et al. 2006).

Cohesin is loaded to chromosomes during the G1 phase of the cell cycle by the cohesin loader SCC2-SCC4 complex, which is required for the cohesion establishment but not maintenance after DNA replication (Ciosk et al. 2000; Petela et al. 2018; Watrín et al. 2006). The process of two rounds of chromosome segregation during meiosis relies on both the stepwise release of sister chromatid cohesion and kinetochore orientation. The cohesin complex is released from the chromosome arms by the cohesin dissociation factor WAPL in meiosis I but remains at the pericentromeric region during meiosis I. The Shugoshin-PP2A complex protects the

pericentromeric cohesion until anaphase II to allow the segregation of sister chromatids (Hara et al. 2014; De et al. 2014). In mitosis, Sororin can bind to PDS5 to counteract the release factor Wapl to prevent the premature release of sister chromatid cohesion (Nishiyama et al. 2010; Kueng et al. 2006). SWITCH1 (SWI1) functions as the inhibitor of Wapl during meiosis in *Arabidopsis* (Yang et al. 2019) (Figure 1.7). So, the cohesin complex is essential for chromosome segregation. Besides, the cohesin complex is also involved in DNA break repair, genome stability, chromatin structure, and gene expression (Makrantonis and Marston 2018; Bolanos-Villegas et al. 2017; Litwin, Pilarczyk, and Wysocki 2018; Suja and Barbero 2009). However, whether and how they regulate gene expression during meiosis are not clear in *Arabidopsis*.

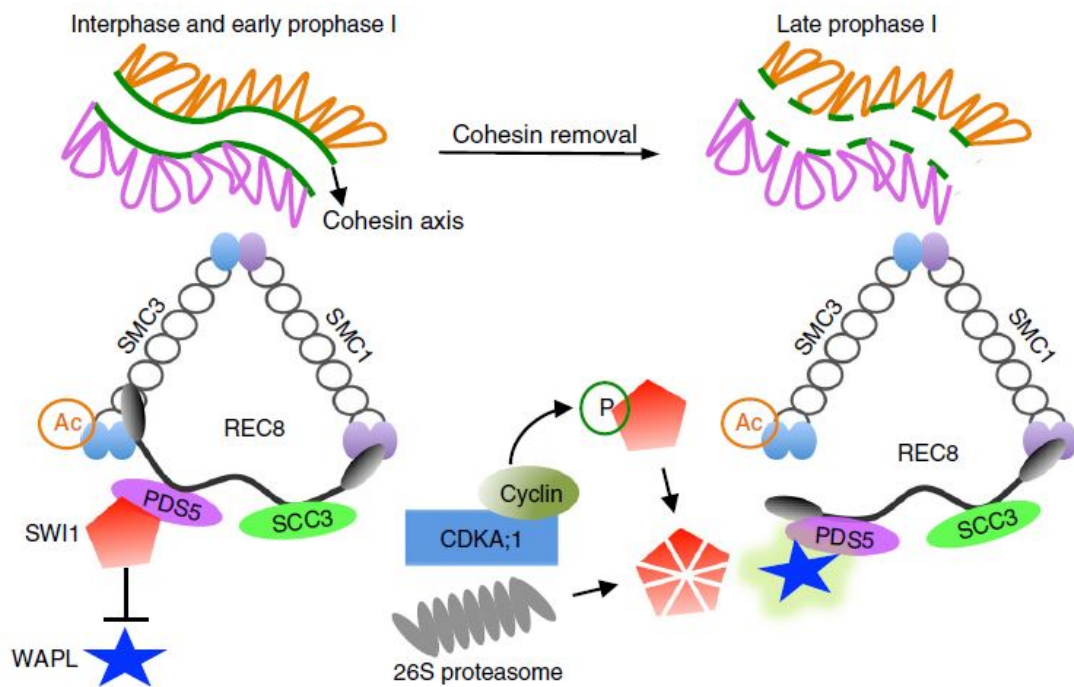


Figure 1.7. The regulation of cohesin during meiosis in *Arabidopsis*. The cohesin core components SMC1, SMC2, and SCC1 in mitosis which is replaced by REC8 in meiosis can form a tri-partite ring. The SMC3 subunit can be acetylated by CTF7 to close the cohesin ring. This complex is loaded to the chromosomes by the SCC2-SCC4 loader to entrap the sister chromatids together. In early prophase I, SWI1, the inhibitor of WAPL, can bind to PDS5 to prevent the release of the cohesin complex. In late prophase I, the ubiquitination of SWI1 leads to its release, allowing the binding of WAPL1 to PDS5. Cohesin dissociation factor WAPL leads to the release of cohesin from chromosome arms (Yang, C *et al.*, 2019).

1.4 Aims of the study

Meiosis is a crucial process for reproduction in eukaryotes. Reduced H3K9me2 levels lead to CO activation at the pericentromeric region during meiosis yet without affecting chromosome segregation and nuclear division, suggesting normal meiosis progression does not rely on correct H3K9me2 deposition. However, it is unclear whether removing H3K9me2 is required for meiosis. So, one of my project aims is to examine the role of eliminating H3K9me2 in *Arabidopsis* meiosis. In this part, I have three main points to address. First, whether H3K9me demethylation is required for the proper meiosis process. Second, as a silencing mark, whether H3K9 methylation is also involved in meiotic gene expression. Third, the downstream of H3K9 demethylation activates gene expression. So, I started with the H3K9 demethylases mutants *ibm1* and *jmj27* to study their functions in *Arabidopsis* male meiosis. After confirming the morphological, cytological, and molecular phenotypes of *ibm1* and *jmj27* in meiosis, I continued to look for the interactors that activate gene expression coupled with histone demethylation. The cohesin complex is involved in DNA repair, condensation, and gene expression in addition to its traditional function in sister chromatid cohesion to hold sister chromatids together until their segregation. However, the exact mechanisms of cohesin regulating gene expression are unknown in *Arabidopsis*. Our results may explain the possible mechanism of how the cohesin complex regulates gene expression in meiosis and mitosis.

In addition to the function of H3K9 demethylation in meiosis, I also want to know whether it is also essential for other reproductive processes. In the second part, I want to address two main questions. First, is H3K9 demethylation required for tapetum development? Second, how are H3K9 demethylases specifically recruited to their substrates? I also used the *ibm1* and *jmj27* mutants for the study. Transcription factors (TFs) are involved in the recruitment of histone methyltransferases and demethylases in many organisms from animals to plants. Here, I will explore whether the TFs are involved in the recruitment of IBM1 and JMJ27 during anther development. Our results will explain how the TF regulates gene expression in more detail.

2 Materials and methods

2.1 Plant Materials and Growth Conditions

The *Arabidopsis thaliana* accession Columbia (Col-0) and WS-2 were used as wild-type references. The T-DNA insertion lines SALK_035608 (*ibm1-4*), SALK_092672 (*jmj27-2*), SALK_152147 (*ams*), SALK_136296 (*msh4*), SAIL_873_C08 (*rad51*), were obtained from Nottingham Arabidopsis Stock Center (NASC), *pds5abce* (PDS5A: SALK_114556, PDS5B: SALK_092843, PDS5C: SALK_013481, PDS5E_SAIL_287_D07) was kindly provided by Prof. Dr. JuanL. Santos, SAIL_807_B08 (*rec8*) was kindly provided by Prof. Dr. Arp Schnittger, Salk_146172 (*spo11-1-3*) and *mus81* were kindly provided by Dr. Stefan Heckman. Seeds were treated at 4°C for three days before sowing on the soil or surface-sterilized in 70% (v/v) ethanol containing 0.1% (v/v) Triton X-100 for 10 minutes, rinsed with 95% ethanol for three times before sowing on the MS plates (½ MS, 1% sucrose, 0.8% plant agar), and kept the plates at 4°C for three days to germinate synchronously before moving them to the light. All plants were cultured in the greenhouse with a 16 h light/8 h dark photoperiod at 22°C with the light intensity of 115 $\mu\text{mol}\cdot\text{m}^{-2}\cdot\text{s}^{-1}$ and humidity of 70%.

2.2 In vivo histone demethylation assay

The protocol used for in vivo histone demethylation assay was previously described by Lu, F *et al.*, (Lu *et al.* 2010). Briefly, vectors containing 35S:JMJ25/JMJ26/JMJ27/JMJ28-GFP were transformed into *Agrobacterium tumefaciens* (*A. tumefaciens*) strain GV3101, and infiltrated into *Nicotiana Benthamian* (*N. Benthamian*) leaves together with *Agrobacterium* cells harboring HC protein plasmids. The *N. Benthamian* leaves were harvested after 48 hours injection and cut into small pieces. The leaves were then fixed in cold 4% paraformaldehyde in Tris-HCl buffer (10mM Tris pH7.5, 10mMEDTA and 100mM NaCl,) for 20 minutes followed by washing with ice-cold Tris-HCl buffer twice for 10 minutes each. Nuclei were isolated by chopping leaves in LB01 buffer (15mMTris-HCl pH7.5, 20mM NaCl, 2mM EDTA, 80mM KCl, 0.5mM spermine, 0.1% TritonX-100) and filtered through a 30- μm Cell Trics filter (Sysmex, Germany). The filtered nuclei were 1:3 diluted with sorting buffer (100mM Tris pH7.5, 50mM KCl, 2mM MgCl_2 2, 0.05% Tween 20, 5% sucrose), and spotted onto microscopy slides to air-dry. The slides can be stored at -20°C or continued to the next step. Post-fixation the slides with 4% paraformaldehyde for 15 min at RT in PBS buffer (10 mM sodium phosphate, pH 7.0,

143 mM NaCl), and wash twice with PBS for 5 minutes each. Blocking the slides with 4% BSA for 30 minutes at 37°C in a moist box following by primary antibody incubation and secondary antibody incubation (all diluted in 1% BSA, 0.1% tween, 1x PBS). After the immune, slides were mounted with 2 µg/ml DAPI. Antibodies used in this experiment: anti-GFP (A11122, Invitrogen, 1:100), anti-H3K9m2 (C15410060, Diagenode, 1:500), anti-GFP nanobody with c-myc was kindly provided by Prof. Dr. Andreas Houben. Alexa Fluor 488 Goat anti-Mouse IgG1 Secondary Antibody (A21121, Invitrogen, 1:100), Alexa Fluor 568 Goat anti-Rabbit IgG (H+L) Secondary Antibody (A-11029, Invitrogen, 1:100). The signals were detected by the confocal microscope, LSM780 (Zeiss).

2.3 Chromatin Immunoprecipitation (ChIP) followed by qRT-PCR or sequencing (ChIP-seq)

Around 0.5 g closed buds were used for one replicate to perform the Chip. To map the IBM1 targets, I used three independent pIBM1:IBM1-GFP/*ibm1-4* transgenic lines that can complement the *ibm1-4* phenotypes for libraries preparation. Chip assay from cross-link to chromatin shearing was previously described by Lambing, et al (Lambing et al. 2020) with minor modifications. Briefly, the closed buds were firstly collected in liquid nitrogen and grind to fine powder. 6 ml of nuclei isolation buffer (1M sucrose, 5mM KCl, 5mM MgCl₂, 5 mM EDTA, 60 mM Hepes pH 8.0, 0.6% Triton X-100, 0.4 mM PMSF, 1 µM pepstatin A, Protease Inhibitor Cocktail (one tablet dissolved in 5 ml H₂O as 20X stock solution)) and 170 µl of 37% formaldehyde solution were added to each sample. Incubating the sample on a Thermo roller mixer (cat number) at 12rpm for 25 min at room temperature, and stop the cross-link by adding 400 µl 2M glycine to a final concentration of 130 mM for another 25 min. When Disuccinimidyl glutarate (DSG) was used, tissue was firstly treated with 2 mM DSG for 25 min and then 1% formaldehyde for another 25 min. After the isolation of nuclei, the chromatin was sonicated firstly with Nuclei lysis buffer (50mMTris–HCl, pH 8.0, 10 mM EDTA, 1% SDS, 0.1 mM PMSF, 1 µM pepstatin A, Protease Inhibitor Cocktail (20X stock solution)) to obtain the desired DNA fragment (size enriched at 300 bp) by a Bioruptor® Plus sonication device. The following procedures were described by Moreno-Romero et al. (Moreno-Romero et al. 2016). After the de-crosslinking, DNA was purified according to the manual of IPure kit v2 Kit (C03010015, Diagenode). For Chip-seq libraries, 2-4 ng purified DNA was used and

the libraries were prepared using NEBNext® Ultra™ II DNA Library Prep Kit (E7645). NEBNext Sample Purification Beads (#E7103) was used to purify the DNA. The antibodies used for Chip-qPCR or Chip-seq: anti-H3 (H9289, Sigma), anti-H3K9me2 (C15410060, Diagenode), and anti-GFP (A11122, Invitrogen).

2.4 RNA extraction followed by qRT-PCR or sequencing (RNA-seq)

Total RNA was isolated using MagMAX™ Plant-RNA-Isolations kit (A33784, Thermo Fisher) for qRT-PCR and RNeasy Plant Mini Kit (74904, Qiagen) for RNA-seq according to manufacturer's instructions. 2 µg total RNA was used to synthesis the second strand DNA using the cDNA Synthesis kit (Thermo Fisher, K1612). Two biological repeats were conducted. 4ng total RNA was used to prepare the RNA-seq libraries using the VAHTS mRNA-seq V3 Library Prep Kit for Illumina kit (NR611-01, Vazyme). Libraries were sequenced at Novogene, UK. Two biological replicates were prepared for each genotype, and at least 15 million reads were produced for each sample. Produced reads were mapped to TAIR10 Col-0 genomes with HISAT2 (Kim et al. 2019). DEGs were analyzed via the Subread (Liao, Smyth, and Shi 2019) and DESeq2 R packages (Love, Huber, and Anders 2014) with a 0.05 false discovery rate (FDR), and 2 log FC cutoff. Volcano plot and heatmap of DEGs were generated by TB tools (Chen et al. 2020).

2.5 Cytological analysis

Chromosome spreading was performed according to the following procedures as described by Wang, et al (Wang et al. 2014). Immunolocalization was performed as previously described (Higgins et al. 2004) with minor modification. Briefly, anthers with appropriate size were digested with digestion buffer for 10 min and squashed with brass rod, the squashed samples were digested again for 10 min. 2% Lipsol solution was used to do the spread preparation. The meiocytes were fixed with 4% paraformaldehyde for 2 h, and immunostaining procedure was performed. The slides were washes in series ethanol 70%, 85%, and 100% ethanol for 2 min each before DAPI was used. Primary antibodies for anti-ASY1 and anti-ZYP1 were used with 1:100 dilution, and these antibodies were kindly provided by Dr. Stefan Heckmann in IPK. Secondary antibodies are the following: goat anti-rab Alexa Fluor 488 (Invitrogen), Alexa Fluor 568 Goat anti-Rabbit IgG (H+L) Secondary Antibody (A-11029, Invitrogen, 1:100). Slides were observed using Zeiss LSM780. Fluorescence in situ hybridization (FISH) was performed according to Lauriane *et al.*, 2018 with minor modifications

(Simon and Probst 2018). The method to release meiotic cells was the same as chromosome spreading, and the cell suspension was covered with cover-slip by 45 degrees. Place the slides in a -80°C refrigerator for at least 10 min, and remove the cover-slip with a razor quickly. Leave the slides to air dry at room temperature before adding 70% formamide (dissolved in 2x SSC). Put the slides on a hot set at 95°C for 5-10 min. Remove the cover-slip and wash the slides with 70%, 90% and 100% ethanol for 5 min each. The slides must be completely dry after the series washing. Dilute the LNA-DNA mixer probe to 1 μ M and add 30 μ L probe to each slide. Heat the slide at 80 °C for 1 min, and incubate the slides in a moist box at 55 °C for 90 min. Wash the slides twice with the following buffer 2x SSC, 0.75x SSC, and 2x SSC-0.1 % Tween 20 for 5 min each. Add 10 μ L DAPI to the slides and observe them with the microscope. The LAN-DNA probe was labelled with FAM that had similar excitation and emission with EGFP and can be detected in the GFP channel. The pictures were processed with image J.

2.6 Yeast two-hybrid assays

For yeast two-hybrid screening, full-length coding sequences of IBM1 and JMJ27 were cloned into TSK108, and the gateway LR reaction was performed to integrate the entry vectors into the pGBKT7-GW terminal vector. The Arabidopsis cDNA library was kindly provided by Prof. Dr. Binglian Zheng. The screening was performed according to the manual of Clontech Matchmaker GAL4 Two-Hybrid System 3 & Libraries. Briefly, the full-length coding sequence of *AMS* was cloned into TSK108, and integrated into the pGADT7 terminal vector by the gateway LR reaction. AD-SSC3, PDS5A, PDS5B, PDS5C, and PDS5E were kindly provided by Prof. Arp Schnittger. Yeast two-hybrid assays were performed according to the Matchmaker GAL4 Two-Hybrid System 3 manual (Clontech). The bait and prey vectors were co-transformed into yeast AH109 strain and incubated on SD/-Leu -Trp solid medium plates for two to three days. The same amount of yeast cells were resuspended in 0.9% NaCl and diluted by 10x, 100x after washing three times. The 1x, 10x, and 100x yeast cells were then plated on SD/-Leu -Trp, and SD/-Leu -Trp -His plates to test the interaction between the bait and prey proteins.

2.7 Pollen viability assay

The pollen viability assay was performed according to the Peterson staining method

(Peterson, Slovin, and Chen 2010). The flower buds were fixed in Carnoy's fixative (3 alcohol: 1 acetic acid) for at least 2 hours. The mature flower buds containing dehiscent anthers were dissected under a binocular and dipped in staining solution (10% ethanol, 0.01% malachite green (dissolved in alcohol), 25% glycerol, 0.05% acid fuchsin, 0.005% orange G, 4% glacial acetic acid). The microscope slide containing the anthers was heated over an alcohol burner to boiling for 90 seconds (Peterson, Slovin, and Chen 2010). The slide was imaged using the light microscope SMZ1500 (Nikon).

2.8 Bimolecular Fluorescence Complementation assay (BiFC)

The BiFC assay was previously described by Martin *et al* (Martin et al. 2009). Briefly, the full-length coding sequences of IBM1 and JM127 were amplified from cDNA and cloned into TSK108, and the gateway LR reaction was performed to integrate them into pSITE-nEYFP-N1. pDONA223-PDS5C and pDONA223-PDS5E were kindly provided by Prof. Dr. Arp Schnittger and were integrated into the pSITE-cEYFP-C1 destination vector through the Gateway LR reaction. *A. tumefaciens* strain GV3101 containing the desired target genes was infiltrated into *N. Benthamian* leaves at a concentration of OD₆₀₀=0.8. The YFP signal was imaged 48 hours after infiltration using Zeiss LSM780. H3.3 was used as the marker protein of the nuclei. The number of nuclei with RFP and GFP signals was calculated.

2.9 Construction and transformation

To complement *ibm1-4*, 1125bp promoter sequence upstream of the translation start site (TSS) of IBM1 and 3084 bp CDS sequences were cloned into TSK108 using the primers listed in Table S1. The artificial microRNAs (amiRNAs) method was used to knock down the expression of IBM1. The primers used to produce the specific miRNA were designed by the WMD3-Web MicroRNA Designer website (<http://wmd3.weigelworld.org/cgi-bin/webapp.cgi?page=Help#procedure>), and the fragments were amplified following the protocol by Rebecca Schwab. The constructs were then integrated into terminal vectors through the gateway LR reaction. The *A. tumefaciens* strain GV3101 containing the desired target genes were transformed into plants by floral dipping (Peterson, Slovin, and Chen 2010). Positive transgenic plants were selected on MS plates with proper antibiotics.

2.10 Co-immunoprecipitation (Co-IP)

35S: IBM1-GFP and 35S:PDS5E-3Flag or 35S:REC8-3Flag are Co-infiltrated into *N.*

Benthamian leaves at a concentration of OD600=0.8. Collect the samples after 72 hours of incubation, and grind the samples in liquid nitrogen. The same amount of tobacco leaves without any injection was used as a control. Homogenize the sample with three volumes of protein IP buffer (50 mM Tris HCl pH 7.5, 150 mM NaCl, 5 mM MgCl₂, 0.1% NP-40, 0.5 mM DTT, 10% glycerol, 1 mM PMSF, 1 µg/µL pepstatin, protease inhibitor cocktail (Roche, 11836145001)), and incubate the samples on ice for 20 min. The samples were centrifuged at 4000 rpm for 10 min at 4 °C, and the supernatant was filtered with miracloth. The Anti-FLAG M2 magnetic beads (M8823, Sigma) was prewashed twice with IP buffer for 5 min each. The supernatant with FLAG antibody was incubated for 3 h at 4°C. Beads were collected and washed five times with IP buffer for 5 min each. Resuspend the beads in PBS and boil at 95 °C for 10 min. Western blotting was performed with anti-GFP(B-2) antibody (SANTA CRUZ sc-9996, 1:50) and anti-FLAG antibody (F1804, Sigma, 1:1000).

2.11 Affinity Purification Mass Spectrometry (AP-MS)

The coding sequence of IBM1 was fused to a C-terminal GS tag by digesting both the fragment and vector with Sall and BamHI for affinity Purification. The AP-MS experiment was performed following the published procedures (Antosz et al. 2017). A protein score of minimum 80 and at least two peptides found with an individual ion score of ≥ 25 were considered as criteria for reliable protein identification. Unfused GS tag bait protein was used as the control to subtract the contaminating proteins. Background proteins were filtered out based on 543 affinity purifications with 115 bait proteins, mainly from PSB-D cells (Van Leene et al. 2015).

3 Results

3.1 H3K9 demethylation is required for meiosis in Arabidopsis

3.1.1 The mutation of *IBM1* leads to enlarged or collapsed pollen

H3K9me₂, a hallmark of heterochromatin, is required at the early stage of meiosis, especially at prophase I. In mammals, loss of H3K9 methylation leads to a disordered progression of synaptonemal complex formation, causing severe defects (Tachibana et al. 2007). In plants, loss of H3K9 methylation in *Arabidopsis* results in the activation of chromosome recombination at pericentromeric regions, but the meiotic progression is largely normal (Underwood et al. 2018), indicating that meiosis is tolerant of losing H3K9me₂ in *Arabidopsis*. In this part, I will use the mutant of an H3K9 demethylase, *ibm1*, to explore the role of H3K9 demethylation in Arabidopsis meiosis.

IBM1, a JmjC domain-containing protein (Figure 1A), is shown to be an active H3K9 demethylase. The mutation of *IBM1* leads to various developmental defects, including narrowed leaves, late flowering, and reduced fertility (Figure 1B) (Miura et al. 2009; Saze et al. 2008). I first confirmed its demethylase activity by immunostaining in *Nicotiana benthamiana* (*N. benthamiana*) leaves. *Agrobacterium tumefaciens* (*A. tumefaciens*) strain GV3101 harboring the 35S:IBM1-GFP plasmid was infiltrated into *N. benthamiana* leaves. Immunostaining was performed after 48 hours of injection. The nuclei with strong IBM1 expression showed weaker H3K9me₂ signals, and vice versa (Figure 1C), indicating the activity of H3K9me₂ removal by IBM1. Pollen size analysis showed that *ibm1* produced collapsed and enlarged pollen that is usually derived from abnormal meiosis (Figure 1D). I further detected the pollen viability of wild type Col-0 and *ibm1* by Alexander staining, in which the viable pollen should be stained with pink whereas the collapsed pollen with green. The pollen in Col-0 were all stained pink, but a lot of pollen were stained with green in *ibm1*, indicating that many pollen were collapsed in *ibm1* (Figure 1E).

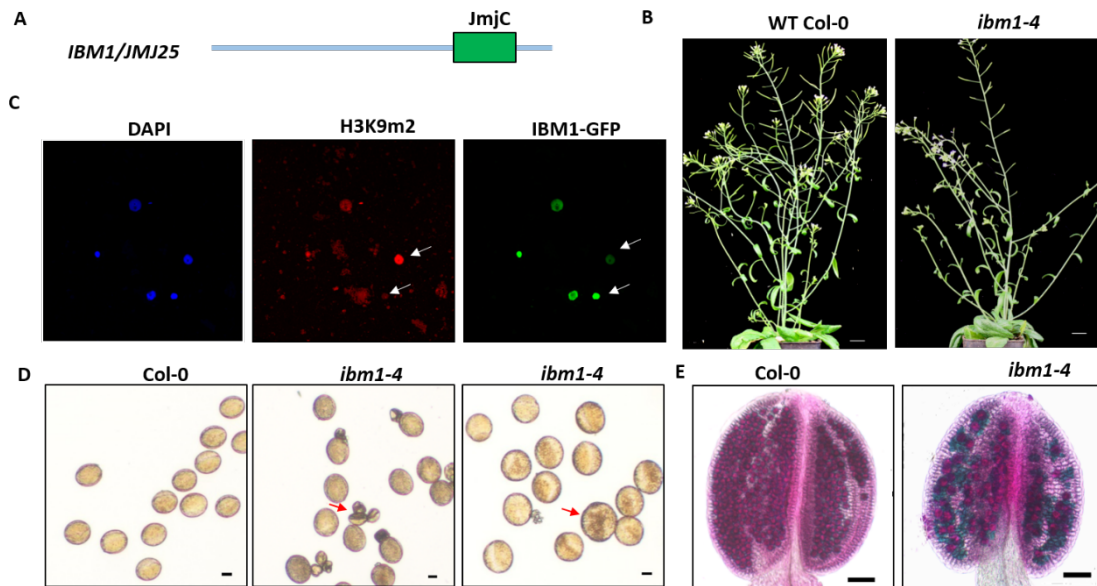


Figure 1. Phenotypes of WT Col-0 and *ibm1* mutants during plant development. (A) A diagram of the *IBM1* protein structure, the box indicates its JmjC domain. (B) Morphology of WT Col-0 and *ibm1-4* 4-week after sowing. Bar, 1 cm. (C) Immunostaining showing the H3K9me2 demethylase activity of IBM1. IBM1-GFP was over-expressed under the control of 35S promoter in *N. benthamiana* leaves. White arrows indicated nuclei that over-expressed the IBM1 protein; yellow arrows indicated the control nuclei without IBM1-GFP expression. DAPI staining (blue) was used to indicate the nuclei, H3K9me2 signal was visualized under RFP channel and IBM1-GFP signal under the GFP channel. (D) Mature pollen of wild type Col-0 and *ibm1*. Red arrows indicated the collapsed or enlarged pollen. Bar, 10 μ m. (E) Alexander staining of WT and *ibm1* mutants. Bar, 50 μ m.

3.1.2 The *ibm1* mutants produced abnormal microspores

To explore whether the meiosis defects led to the production of enlarged pollen in *ibm1*, I further analysed meiotic products at the tetrad stage in Col-0 and *ibm1* by toluidine blue staining. *ibm1* homozygous plants were isolated from the heterozygous F2 population. The *ibm1* mutant produced dyads, triads, and polyads besides tetrads, in contrast to Col-0 that only produced tetrads containing four microspores with equal size (Figure 2A). Quantification analysis showed that the *ibm1* mutant produced around 25% abnormal meiotic products at the tetrad stage (Figure 2B).

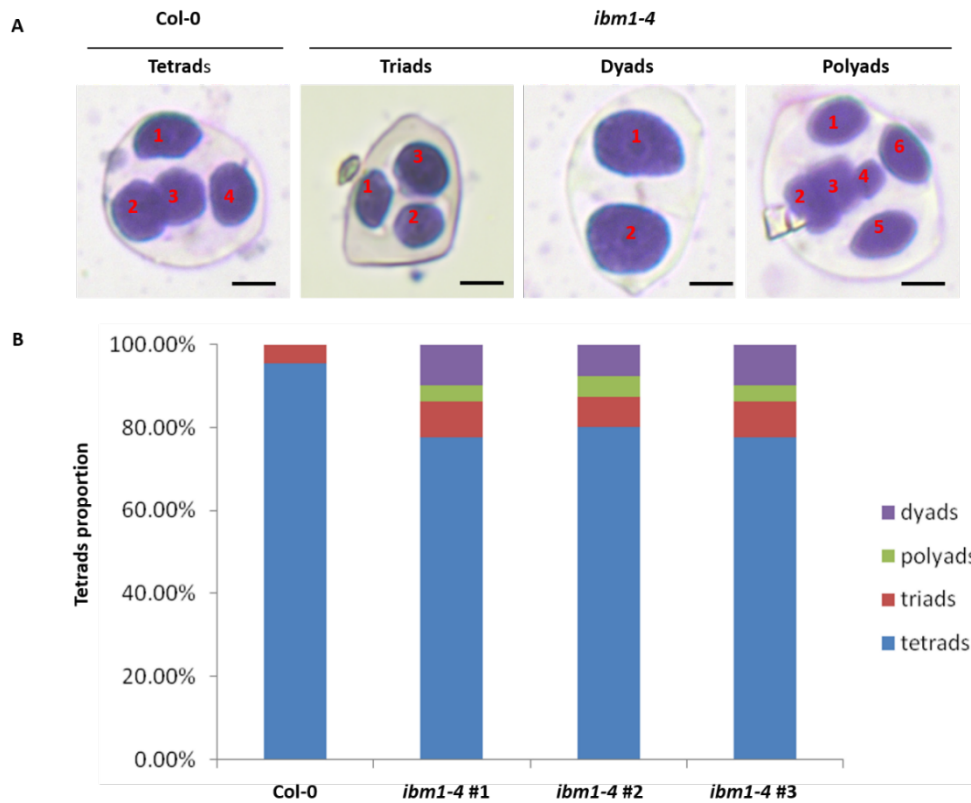


Figure 2. Meiotic products of Col-0 and *ibm1* mutants at the tetrad stage. (A) Toluidine blue staining of microspores at tetrad stage of Col-0 and *ibm1*. Bar, 10 μ m. (B) Quantification of meiotic products at the tetrad stage in A.

The phenotypes of *ibm1* rely on DNA methyltransferase CMT3 and histone methyltransferase KYP, and the mutations of CMT3 and KYP can rescue the developmental defects in *ibm1* (Saze et al. 2008). Therefore, I introduced *kyp* or *cmt3* into *ibm1* to create the double mutants, to test if meiosis defects of *ibm1* were also rescued in the double mutants. The whole development phenotypes of the double mutants were similar to Col-0 (Figure 3A), and meiotic products at the tetrad stage also exhibited a similar phenotype to Col-0 (Figure 3B). These results indicated that ectopic H3K9me2 led to the meiosis defects in *ibm1*.

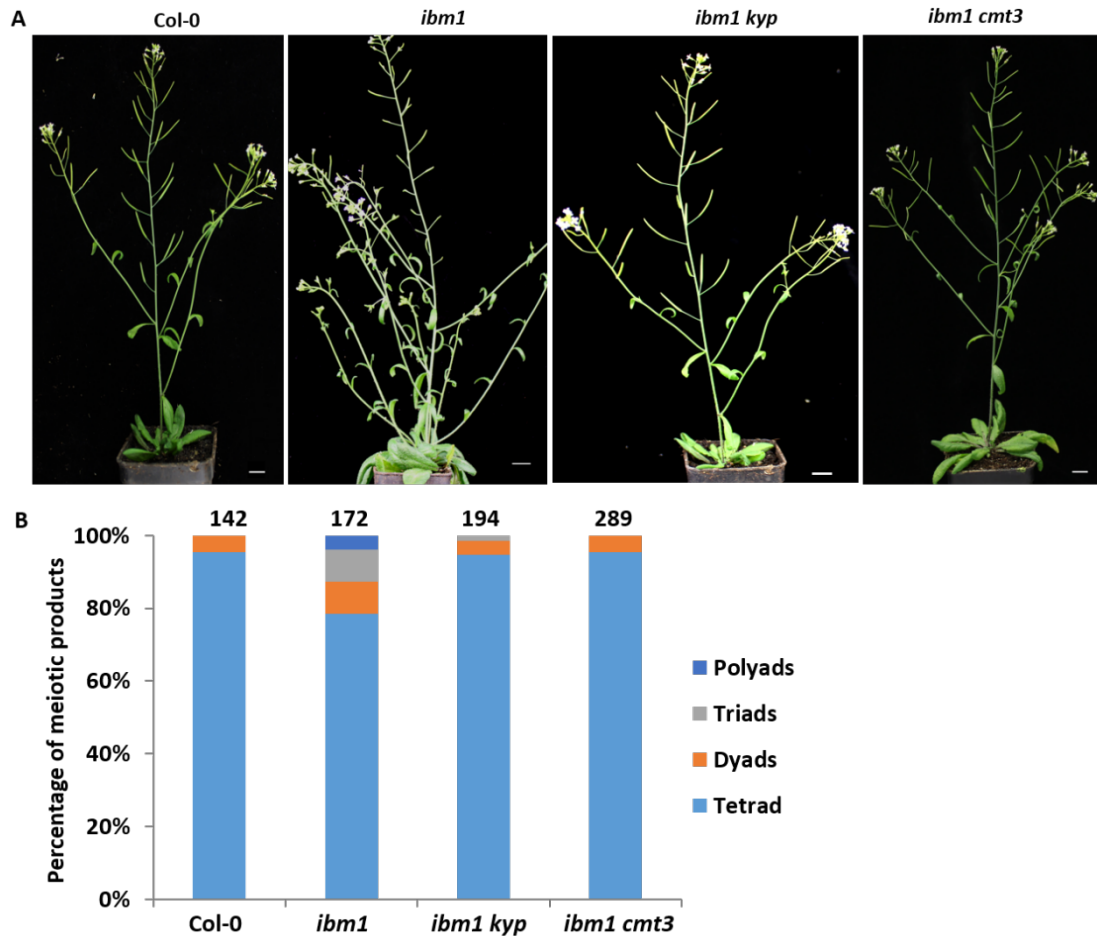


Figure 3. Complementary analysis of the *ibm1 kyp* and *ibm1 cmt3* double mutants. (A) Morphology of Col-0, *ibm1*, and the double mutants 5-week after sowing. Bar, 1 cm. (B) Toluidine blue staining of meiotic products at tetrad stage of Col-0, *ibm1*, and the double mutants.

3.1.3 IBM1 and JMJ27 were functionally redundant

Given that the meiosis defects in *ibm1* were pretty weak, I further tested whether IBM1 is functionally redundant with other H3K9 demethylases. Twenty-one jmjC domain-containing proteins are predicted to function as histone demethylase in *Arabidopsis* (Lu et al. 2008). The KDM3/JHDM2 subgroup, including JMJ24 to JMJ29, is predicted to be H3K9me demethylases. All six proteins contain the JmjC domain, and some of them also harbor the zinc finger domain (Figure 4A). Among them, JMJ24 didn't harbor the cofactors binding sites, so it was shown to be an inactive demethylase (Deng et al. 2016). The demethylase activity of IBM1 and JMJ27 have been confirmed in vitro and/or in vivo (Dutta et al. 2017). Hence, I first detected the demethylase activity of JMJ26, JMJ27, and JMJ28 in *N. benthamiana*. The results

showed that the nuclei with strong JMJ proteins expression showed weak H3K9me2 signals while the nuclei with weak JMJ proteins expression showed strong H3K9me2 signals, indicating these proteins indeed remove H3K9me2 marks (Figure 4B).

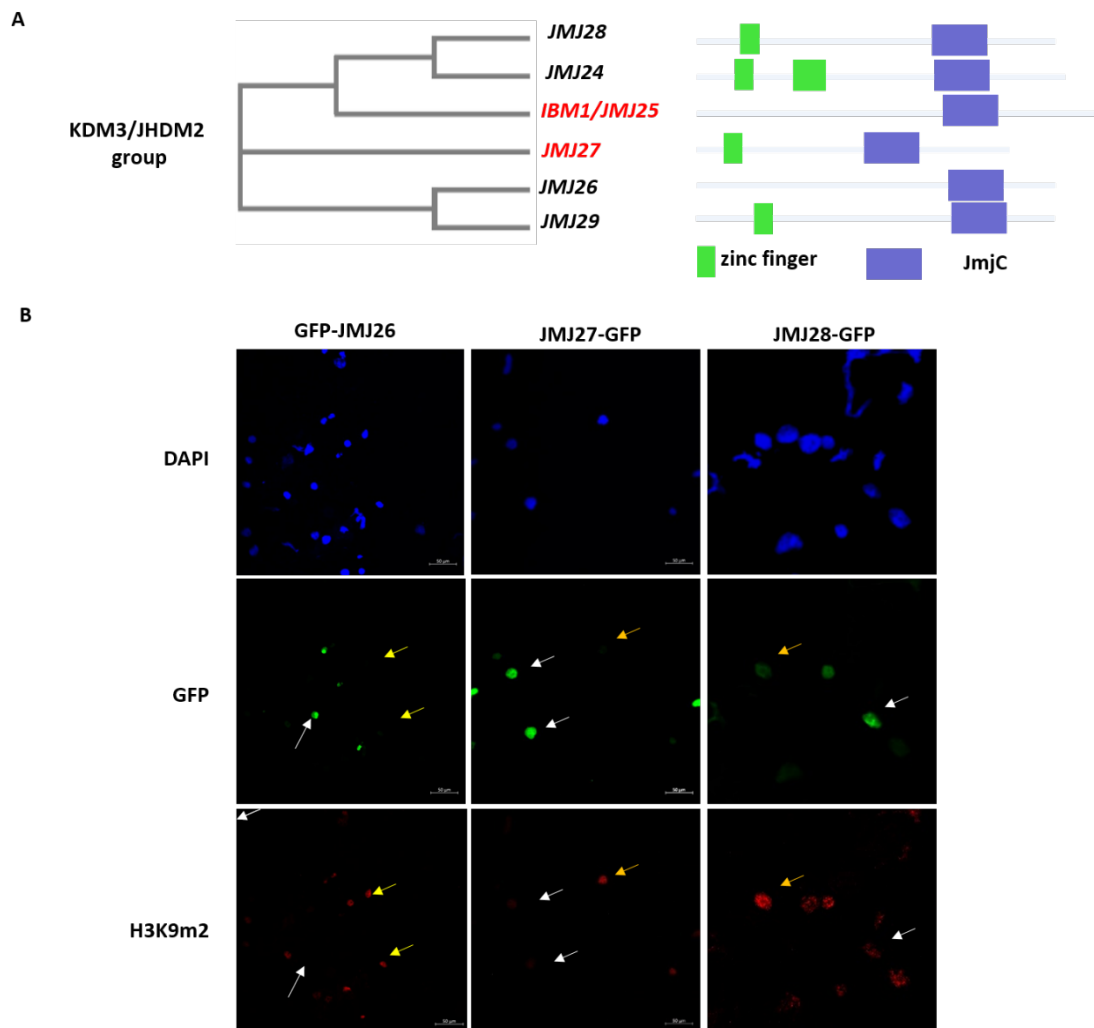


Figure 4. JmjC domain-containing KDM3/JHDM2 group members. (A) Phylogenetic tree of KDM3/JHDM2 group (left) and diagrams of the proteins structure of this group members. (B) Immunostaining of the H3K9m2 demethylase activity of JMJ26/JMJ27/JMJ28. They were over-expressed under the control of 35S promoter in tobacco leaves. White arrows indicate nuclei with robust *JMJ* expression, and yellow arrows indicate nuclei with weak *JMJ* expression. DAPI staining (blue) showed the nuclei, H3K9m2 signal was visualized under the RFP channel, and JMJ26/JMJ27/JMJ28 -GFP signal under the GFP channel.

As JMJ26/JMJ27/JMJ28 also possesses H3K9me demethylase activity. Therefore, I further crossed these mutants with *ibm1* to detect the phenotypes of double mutants. I used the *ibm1 jmj27* mutant in my following study. The *jmj27* mutant is early flowering (Dutta et al., 2017) but WT-like in reproduction (Figure 4). When

jmj27 was introduced into *ibm1*, the double mutant showed more severe phenotypes, including late flowering (not shown), shorter siliques, and completely sterility (Figure 5A-D).

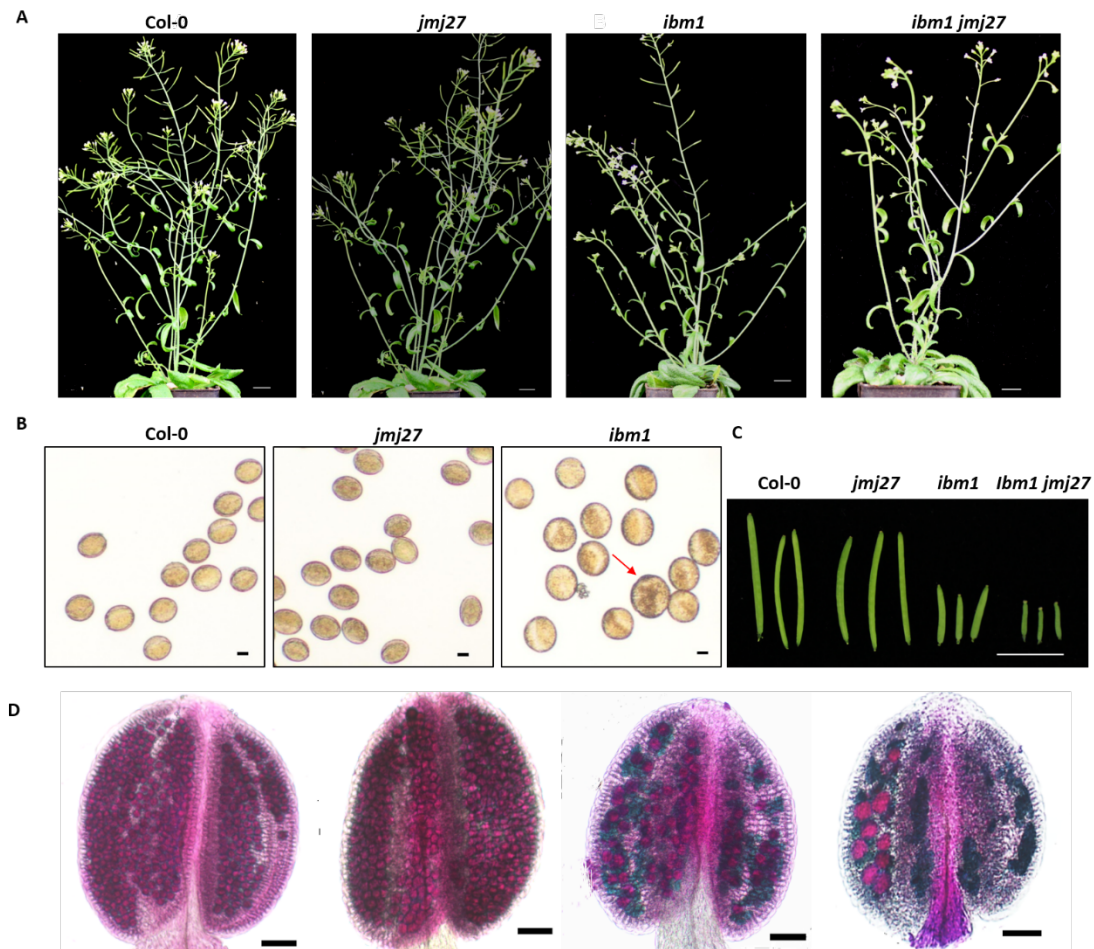


Figure 5. Phenotypes of Col-0, *jmj27*, *ibm1*, and *ibm1jmj27* during plant development. (A) Morphology of Col-0, *jmj27*, *ibm1*, and *ibm1jmj27* 4-week after sowing. Bar, 1 cm. (B) Mature pollen of Col-0, *jmj27*, and *ibm1*. *ibm1jmj27* was sterile. Bar, 10 μ m. (C) Silique morphology of Col-0, *jmj27*, *ibm1*, and *ibm1jmj27*. Bar, 0.1 cm. (D) Alexander staining of Col-0, *jmj27*, *ibm1*, and *ibm1jmj27*. Bar, 50 μ m.

I further detected the meiotic product of *ibm1 jmj27* at the tetrad stage. Most of the meiotic products in *ibm1 jmj27* are polyads, indicating more severe meiosis defects in *ibm1 jmj27* (Figure 6A-B).

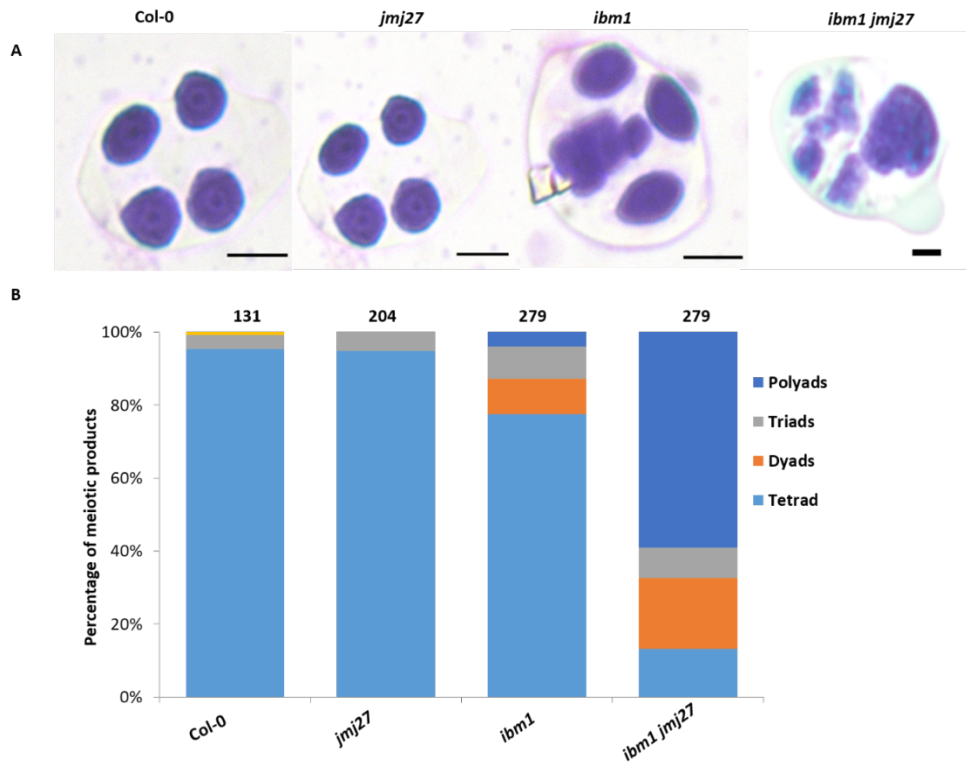


Figure 6. Microspores of Col-0, *jmj27*, *ibm1*, and *ibm1 jmj27* at tetrad stage. (A) Toluidine blue staining of microspores at tetrad stage of Col-0, *jmj27*, *ibm1*, and *ibm1 jmj27* plants. Bar, 10 μ m. (B) Quantifications of the microspores at the tetrad stage in A.

To confirm whether the mutation of *IBM1* and *JMJ27* caused the meiotic phenotypes, I performed the complementation analysis with the full-length coding sequence of *IBM1* fused with a GFP-tag driven by the native promoter (*ProIBM1:IBM1-GFP*). *ProIBM1:IBM1-GFP* rescued the reduced fertility and abnormal meiotic products in both the *ibm1* and *ibm1 jmj27* backgrounds (Figure 7A and B). *IBM1* expression was nearly undetectable in *ibm1* but was recovered to Col-0 levels in the transgenic plants (Figure 7C). Toluidine blue staining results showed both *ProIBM1:IBM1-GFP/ibm1* and *ProIBM1:IBM1-GFP/ibm1 jmj27* meiotic products at tetrad stages were recovered (Figure 7D). These results validated that the mutation in *IBM1* was the cause of the meiosis defects.

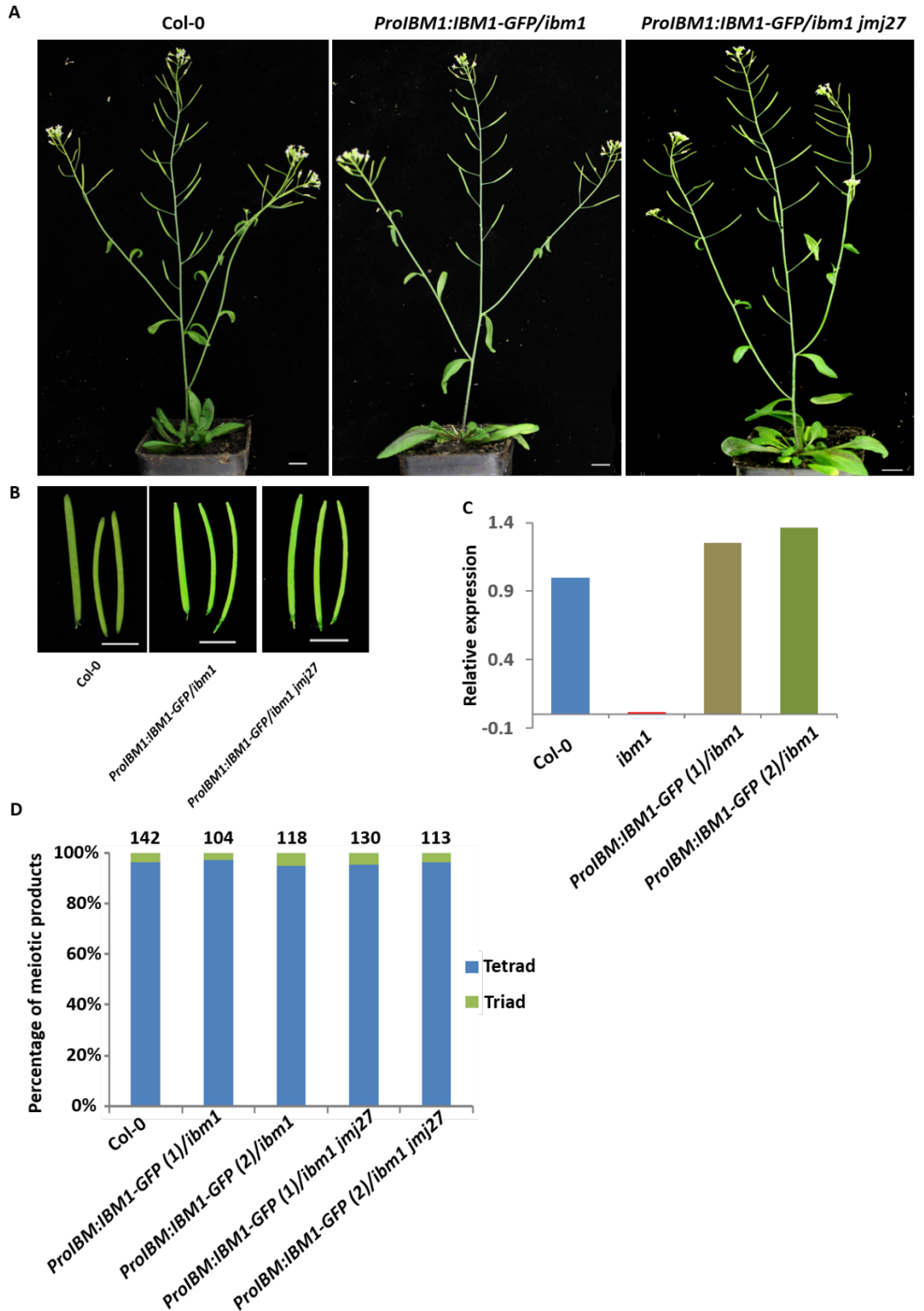


Figure 7. Phenotypes of *ibm1* and *ibm1 jmj27* rescued lines. (A) Morphology of Col-0 and rescued lines of *ibm1* and *ibm1-4 jmj27* driven by the native *IBM1* promoter (*ProIBM1:IBM1-GFP/ibm1* and *ProIBM1:IBM1-GFP/ibm1 jmj27*) 4-week after sowing. Bar, 1 cm. (B) Silique morphology of Col-0 and rescued lines. Bar, 0.1 cm. (C) qRT-PCR to detect the relative

expression of *IBM1* in *ibm1* and rescued lines. (D) Toluidine blue staining of microspores at tetrad stage of Col-0 and rescued lines. *ProIBM1:IBM1-GFP* (1) and *ProIBM1:IBM1-GFP* (2) represent two independent transgenic lines.

Considering that IBM1 and JMJ27 are H3K9me demethylases, I hypothesized that the loss of IBM1 and JMJ27 led to increased H3K9me2 levels, resulting in severe meiosis defects. If this is the case, removal of H3K9me2 in *ibm1 jmj27* may rescue the meiosis defects. Therefore, I introduced *kyp* and *cmt3* into *ibm1 jmj27*. The results showed that only *cmt3* could rescue the phenotypes of *ibm1 jmj27* (Figure 8). There are another two H3K9 methyltransferases, SUVH5 and SUVH6, in *Arabidopsis* (Stroud et al. 2013). Therefore, SUVH5 and SUVH6 maybe also function in this phenotype. Our results are consistent with the previous study showing that the mutation of *KYP* cannot rescue the phenotype of *jmj27* responding to drought stress (Wang et al. 2021).

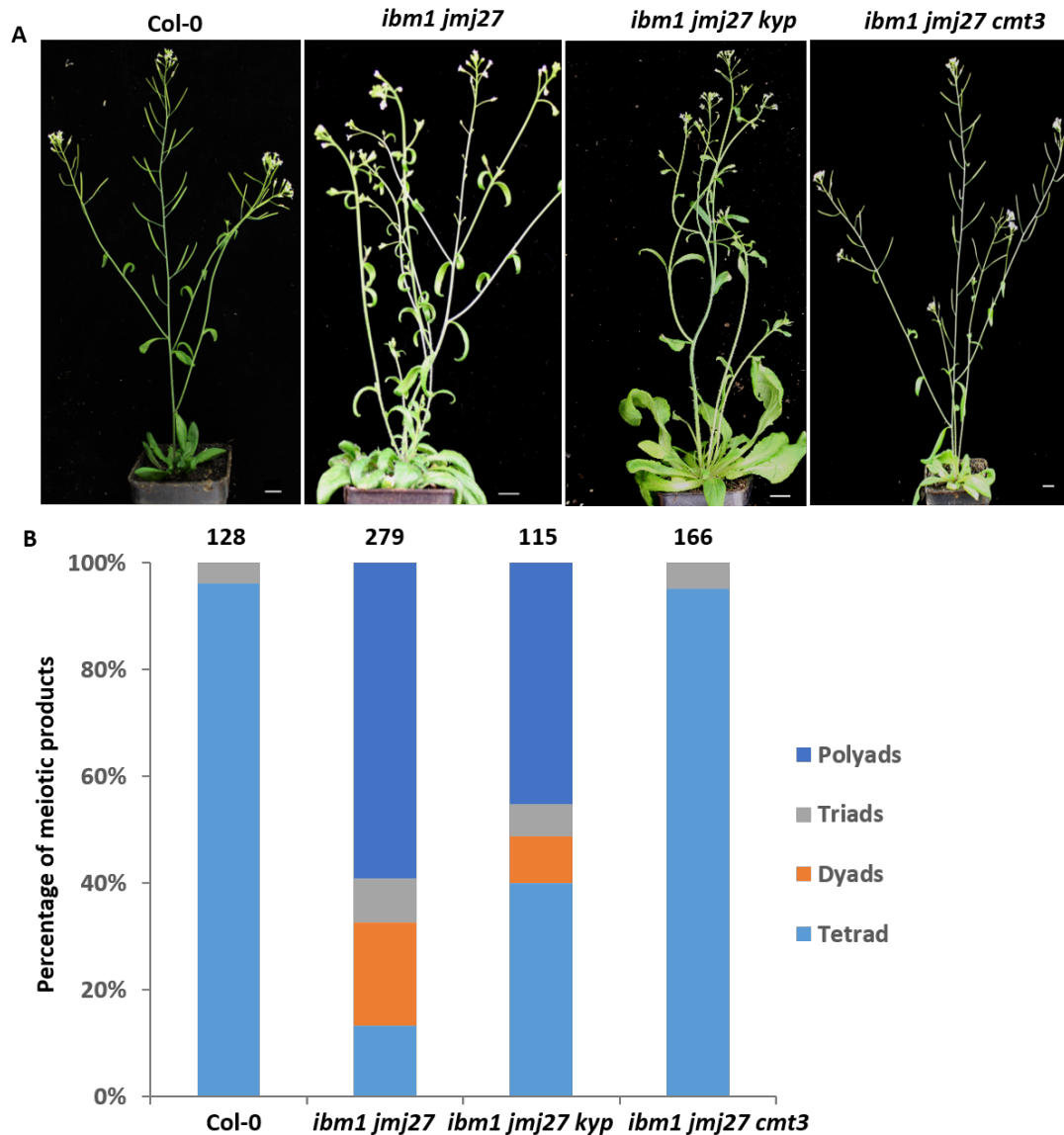


Figure 8. Phenotypes of *ibm1 jmj27 kyp* and *ibm1 jmj27 cmt3* triple mutants. (A) Morphology of Col-0, *ibm1 jmj27*, and the triple mutants *ibm1-4 jmj27 kyp* and *ibm1-4 jmj27 cmt3* 4-week after sowing. Bar, 1 cm. (B) Toluidine blue staining of microspores at tetrad stage of Col-0, *ibm1 jmj27*, and the triple mutants *ibm1-4 jmj27 kyp* and *ibm1-4 jmj27 cmt3*.

3.1.4 The *ibm1* and *ibm1 jmj27* mutants showed multiple defects in meiosis

I further performed chromosome spreads from Col-0 and *ibm1* pollen mother cells (PMCs) stained with 4', 6-diamidino-2-phenylindole (DAPI) to investigate the defects of *ibm1* in meiosis. In Col, homologs pair at early prophase I, and the homologs synapsis finishes at pachytene, forming thick thread-like structures (Figure 9A). Five pairs of highly condensed bivalents were observed at diakinesis (Figure 9B). The

paired homologous chromosomes were kept together through chiasmata at crossover sites until their segregation at anaphase I (Figure 9C and D). The chromosome behavior was similar between Col and *ibm1* at the early stage (Figure 9E and F). However, some homologs were segregated earlier at metaphase I in *ibm1* (Figure 9G). Besides the univalent formation at metaphase I in *ibm1*, the chiasmata number was also affected. Chiasmata, a structure formed after crossover occurs, were reduced from 9.3 per cell in Col-0 to 5.9 per cell in *ibm1* (Figure 9Q and R), indicating that crossover was inhibited or redistributed in *ibm1*. The homologs were segregated to opposite poles in Col anaphase I (Figure 9D). However, the segregation was partially disordered in *ibm1*, and chromosome lagging occurred (Figure 10H). Sister chromatids in Col segregated in meiosis II, forming four equal-sized microspores (Figure 10 I-L). In contrast, the *ibm1* meiocytes showed chromosome lagging at metaphase II (Figure 9N), and more than four microspores were produced (Figure 9P), suggesting that IBM1 is required for the proper meiotic process.

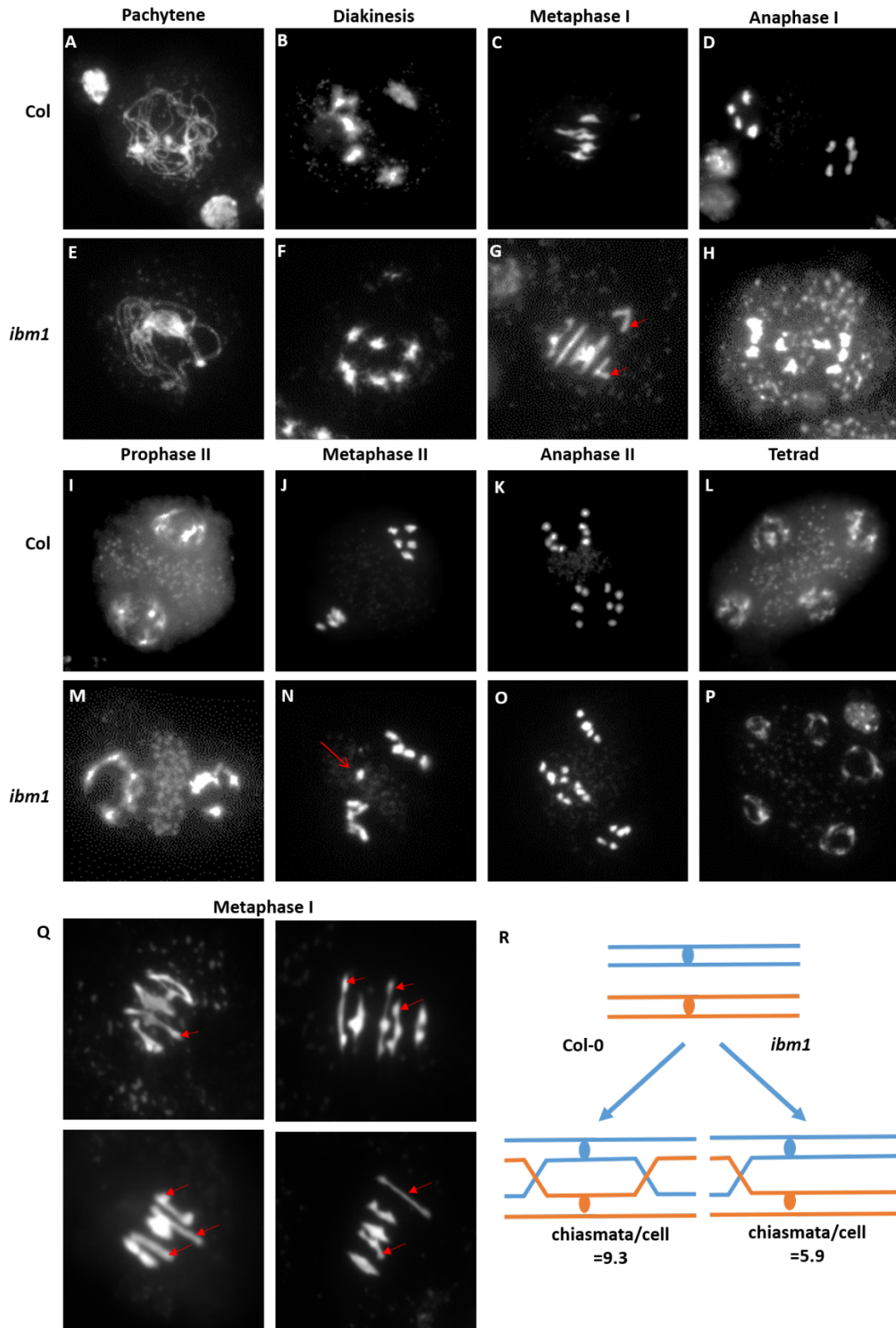


Figure 9. Chromosome morphology of *Col-0*, *ibm1*, and *ibm1 jmj27* male meiocytes. Chromosome spreads of *Col-0* and *ibm1* male meiocytes. Red arrows indicate the defects in synaptic, chromosomal fragments or univalent in *ibm1*. (Q) Homologous chromosomes at

metaphase I in *ibm1*. (R) Chiasmata number in Col-0 and *ibm1*.

I further observed the meiotic process in *ibm1 jmj27*. At pachytene, the chromosome behaved similarly in *ibm1 jmj27* and Col-0 (Figure 10A). However, univalent was observed frequently at diakinesis in *ibm1 jmj27* (Figure 10B) compared to Col that only formed five bivalents (Figure 9B). Subsequently, chromosome alignment at metaphase I and segregation at anaphase I were disordered in *ibm1 jmj27* (Figure 10C and D). I performed fluorescence in situ hybridization (FISH) with a 180 bp centromeric repeat probe to confirm the phenotype of chromosome segregation in meiosis I. At pachytene, I observed five centromeric signals in Col-0 (Figure 10E and I), while more than five but less than ten in *ibm1 jmj27* (Figure 10M and Q). Subsequently, unpaired centromeric signals were observed in *ibm1 jmj27* (Figure 10N and R), which were different from five pairs of centromeric signals at diakinesis in Col-0 (Figure 10F and J). At metaphase I and anaphase I, centromere signals were located at opposite poles in Col-0 (Figure 10G, H, K, and L), while centromeric signals were retained at the equatorial region in *ibm1 jmj27* (Figure 10O, P, S and T). Therefore, *IBM1* and *JMJ27* are required for bivalent formation in male meiosis.

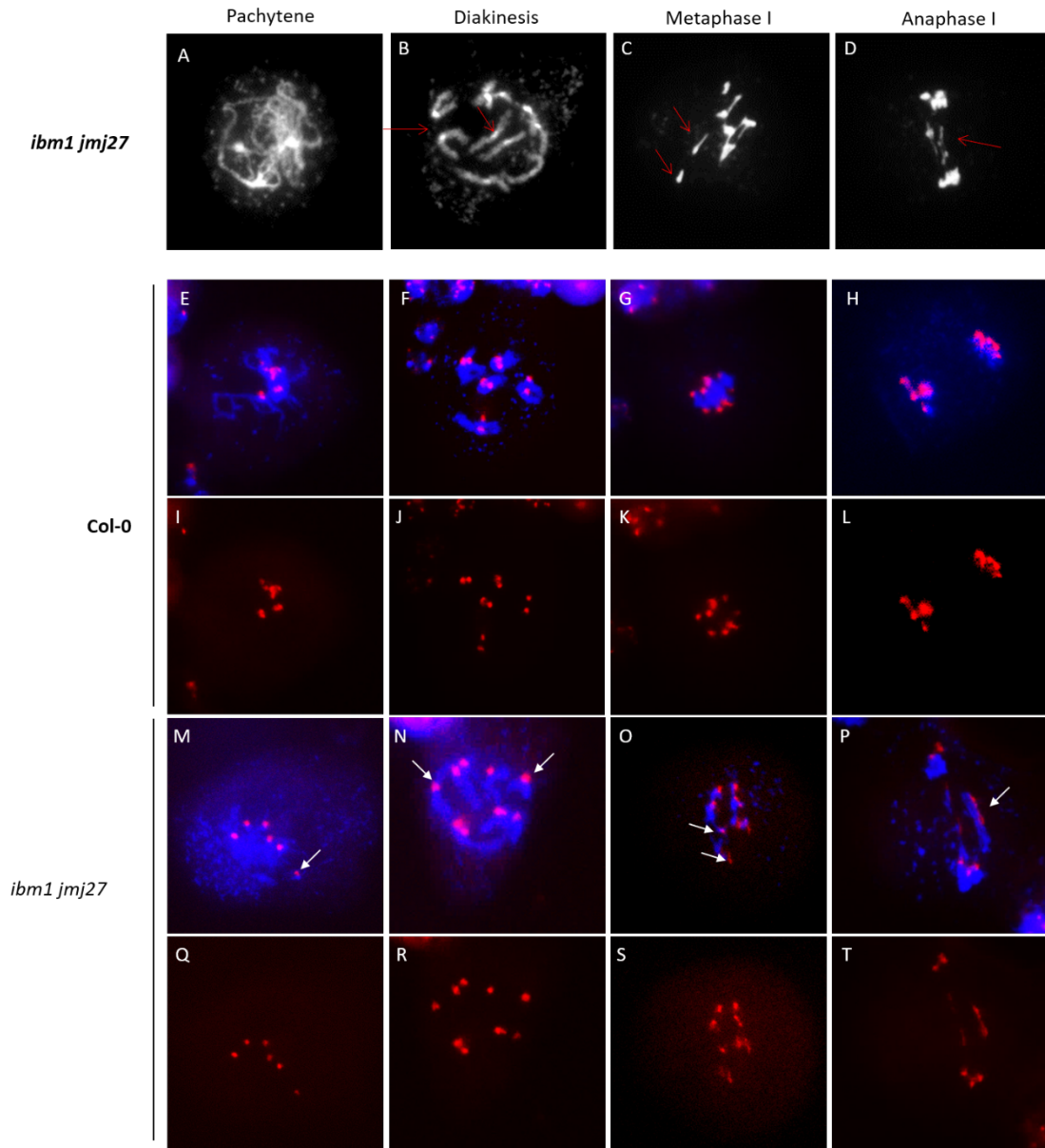


Figure 10. Chromosome morphology of *ibm1 jmj27* male meiocytes. (A-D) Chromosome spreads of *ibm1 jmj27* male meiocytes in meiosis I. Red arrows indicated the univalent or chromosomal fragments in *ibm1 jmj27*. (E-T) Fluorescence in situ hybridization (FISH) of Col-0 (E-L) and *ibm1 jmj27* (M-T) using a centromere 180 repeat probe. White arrows indicated the univalent or chromosomal fragments in *ibm1 jmj27*.

To explore the meiosis-specific function of IBM1 and JMJ27, I used an artificial miRNA (amiRNA) strategy to knockdown their expression in meiotic cells and explore their function in meiosis. First, I examined the amiRNA efficiency by expressing the amiRNA driven by the UBQ promoter, and 23 positive transformants were obtained for further analysis. Eight lines were randomly selected to test the relative expression

of *IBM1* in the transgenic plants using qRT-PCR. Most of the lines reduced the expression level of *IBM1* to around 30% (Figure 11A). Among them, line 1 and line 18 showed the lowest *IBM1* expression levels, and both of them showed poor fertility like the *ibm1* mutant (Figure 11B). I replaced the UBQ promoter with different meiosis-specific promoters, including *DMC1*, *SWI1*, and *REC8*. As a positive control, I knocked down *REC8* with amiRNA driven by the native promoter. After transformation, more than 40 transformants for each line were generated. However, all four lines showed normal fertility (Figure 11C). The toluidine blue staining of the microspores at the tetrad stage also showed the same results as the WT (data not shown), in contrast to the complete sterility in the *rec8* mutant (Bai et al., 1999). Thus, amiRNAs are probably not sufficient to specifically knockdown genes in meiotic cells.

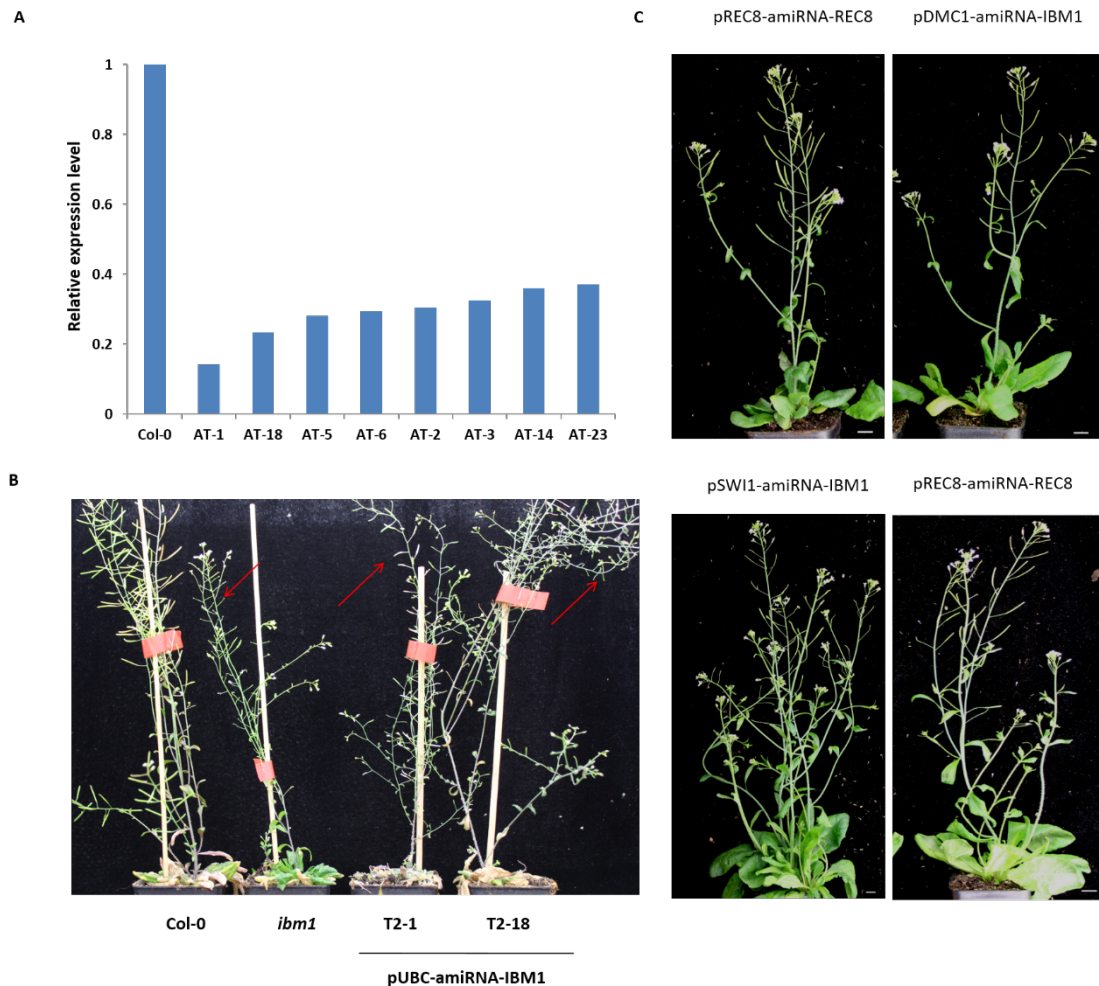


Figure 11. Morphology of the *IBM1* knockdown transgenic plants. (A) The relative expression level of *IBM1* in different transgenic lines. (B) Phenotypes of Col-0, *ibm1*, and amiRNA-*IBM1* transgenic T2 lines 4-week after sowing. (C) Phenotypes of amiRNA-*IBM1* transgenic plants that

were driven by various meiosis-specific promoters. T2 lines were analysed 4-week after sowing.

3.1.5 Many genes obtained ectopic H3K9me2 in *ibm1 jmj27*

Mutation of IBM1 leads to ectopic deposition of H3K9me2 at numerous gene bodies in leaf (Inagaki et al. 2017). To explore whether the mutations of IBM1 and JMJ27 also lead to increased H3K9me2 genome-wide in reproductive tissues, I performed ChIP-seq with the antibody against H3K9me2. Closed buds with enriched meiocytes were used for each sample with two replicates. The regions with increased H3K9me2 were mainly located at euchromatin in both *ibm1* and *ibm1 jmj27*, whereas the regions with decreased H3K9me2 were mainly located at heterochromatin (Figure 12A), in line with the fact that IBM1 mainly removes H3K9me2 from the gene body (Miura et al. 2009). I compared the distribution of increased H3K9me2 regions between *ibm1* and *ibm1 jmj27*. 1444 and 8424 regions with significantly increased H3K9me2 were identified in *ibm1* and *ibm1 jmj27* ($P < 0.05$). 56.4 % (815 out of 1431) and 61.4 % (5174 out of 8424) of these regions located at gene body in *ibm1* and *ibm1 jmj27*, 25.6 % (369 out of 1431) and 36.4 % (3069 out of 8424) of these regions located at the promoter region, and only 18.0% (260 out of 1431) and 2.2% (181 out of 8424) of them located at transposable elements (TEs) region, indicating that gene body was the main targets of IBM1 and JMJ27 (Figure 12B). The previous result indicates that longer genes are more severely affected by IBM1 (Miura et al. 2009), so I examined if it is similar in *ibm1 jmj27*. Around 10% of genes in Col-0 were longer than 4 Kb, while about 70% in *ibm1* and 40% in *ibm1 jmj27* (Figure 12C). Hence, longer genes were more affected in both *ibm1* and *ibm1 jmj27*.

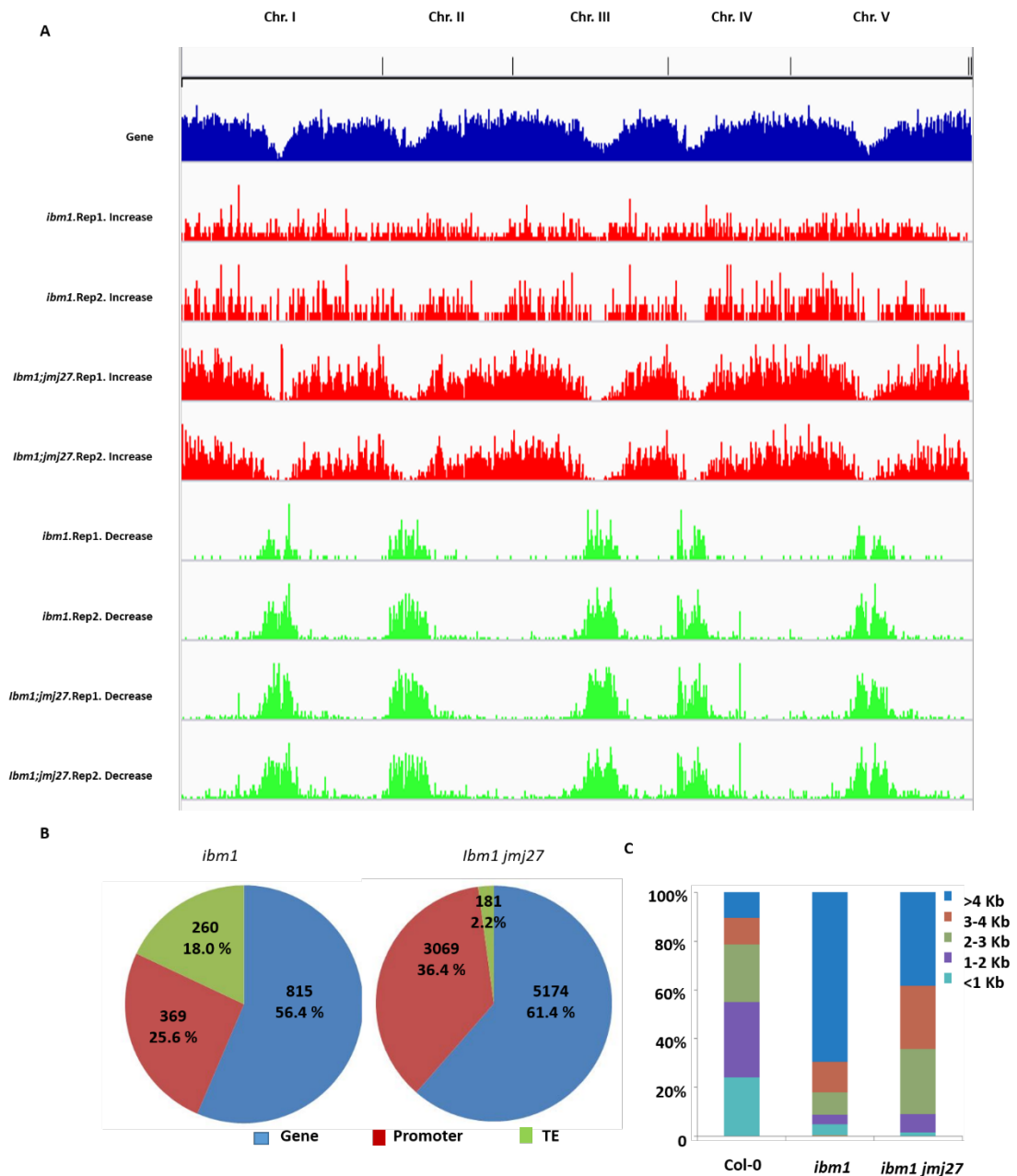


Figure 12. H3K9me2 ChIP-seq analysis. (A) Genome browser views of *ibm1* and *ibm1 jmj27* hypermethylated regions and hypomethylated regions. Each sample had two replicates. (B) Pie charts show the distribution of hypermethylated regions at genes, promoters, and TEs in *ibm1* (left) and *ibm1 jmj27* (right). Numbers and percentage of each category were indicated. (C) The distribution of length of all genes in Col-0 (left), and hypermethylated genes in *ibm1* (middle) and *ibm1 jmj27* (right).

As IBM1 and JMJ27 are functionally redundant in meiosis, I further explored whether H3K9me2 was enhanced in *ibm1 jmj27* compared to *ibm1*. *ibm1 jmj27* acquired 8659 hypermethylated genes, higher than 912 in *ibm1* (Figure 13). These genes showed

higher H3K9me2 levels in *ibm1 jmj27* compared to *ibm1* (Figure 13C and D).

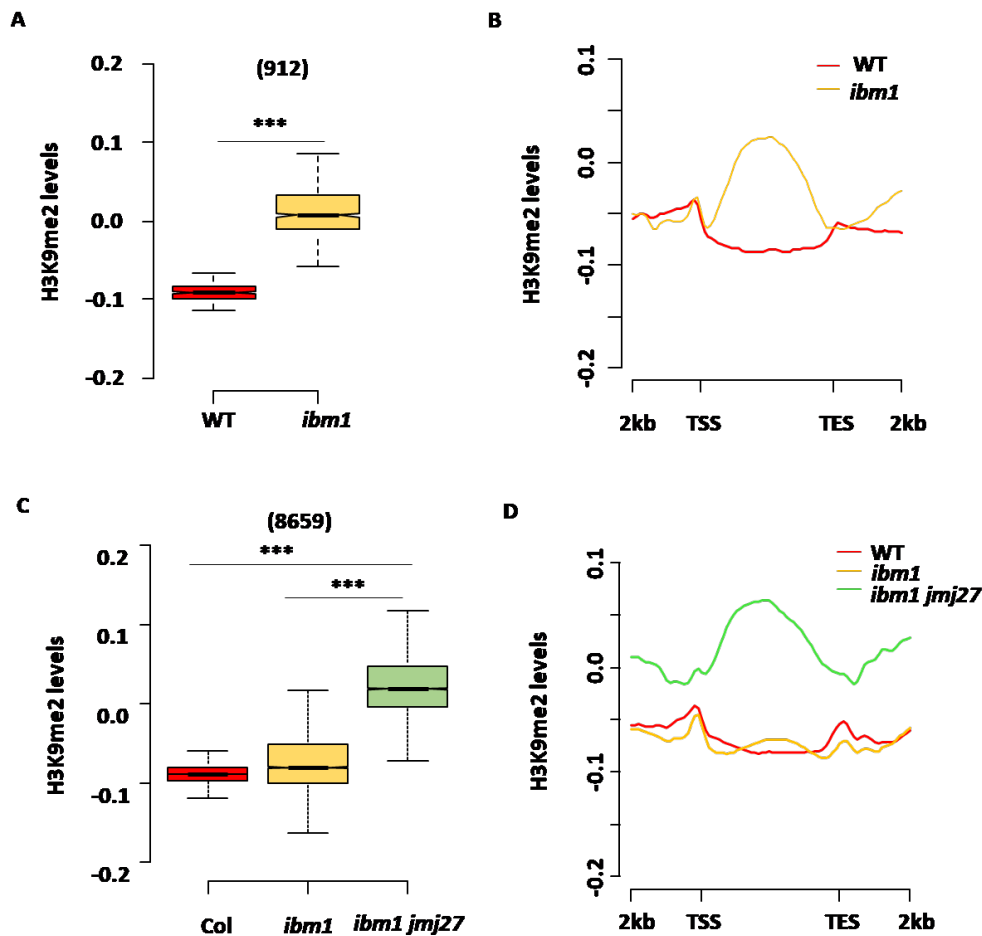


Figure 13. H3K9me2 levels in *ibm1* and *ibm1 jmj27*. (A) Box plot (right) showing H3K9me2 levels of *ibm1* hypermethylated in Col-0 and *ibm1*. (B) Metagene plots showing z-score normalized H3K9me2 in Col-0 and *ibm1*. (C) Box plot (right) showing H3K9me2 levels of *ibm1 jmj27* hypermethylated in Col-0, *ibm1*, and *ibm1 jmj27*. (D) Metagene plots showing z-score normalized H3K9me2 in Col-0, *ibm1*, and *ibm1 jmj27*. *** $P < 0.001$.

In addition to hypermethylated genes, we also identified 4706 transposable elements (TEs) losing H3K9me2 in *ibm1 jmj27* (Figure 14A). Genes essential for RNA-directed DNA methylation (RdDM) are silenced in *ibm1* seedlings (Fan et al. 2012). Thus, it is possible that the loss of DNA methylation was further enhanced in *ibm1 jmj27* closed buds, leading to the decreased H3K9me2 levels through the feedback loop between CHG methylation and H3K9me2 (Du et al. 2015). Indeed, the expression levels of multiple genes required for DNA methylation, *CLSY1*, *CLSY4*, *DCL3*, and *MET1* were reduced in *ibm1 jmj27* (Figure 14B), indicating the indirect effect of *IBM1* and *JMJ27*

mutations on the decreased H3K9me2.

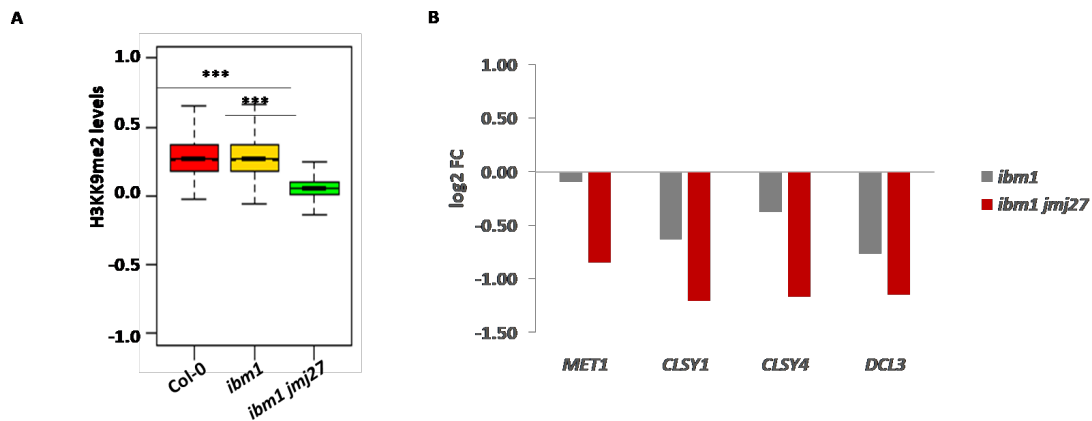


Figure 14. IBM1 and JMJ27 indirect targets. (A) Box plots showing the H3K9me2 levels of *ibm1 jmj27* hypomethylated TEs in Col-0, *ibm1*, and *ibm1 jmj27*. (B) Relative expression levels of genes required for DNA methylation in *ibm1* and *ibm1 jmj27*. *** $P < 0.001$.

3.1.6 IBM1 directly bind at targets to remove H3K9me2

To test whether these hypermethylated genes were targeted by IBM1 directly, I conducted IBM1-GFP ChIP-seq using *Pro: IBM1-IBM1-GFP/ibm1* transgenic T2 lines. Two replicates were performed using two independent T2 lines (Figure 15A). More than 7000 regions were identified as IBM1-occupied regions at genes (Figure 15B). I further compared IBM1 binding regions at genes, hypermethylated genes in *ibm1*, and hypermethylated genes in *ibm1 jmj27*. Group 1 genes were occupied by IBM1, obtaining ectopic H3K9me2 in *ibm1*, and the increased H3K9me2 levels were further enhanced in *ibm1 jmj27*, while the group 2 genes only gained ectopic H3K9me2 in *ibm1 jmj27* (Figure 15C and D). In addition, around 3000 genes belonging to group 3 were occupied by IBM1 without obtaining ectopic H3K9me2, suggesting that IBM1 acts together with other H3K9 demethylases except JMJ27 to regulate these regions (Figure 15C and D).

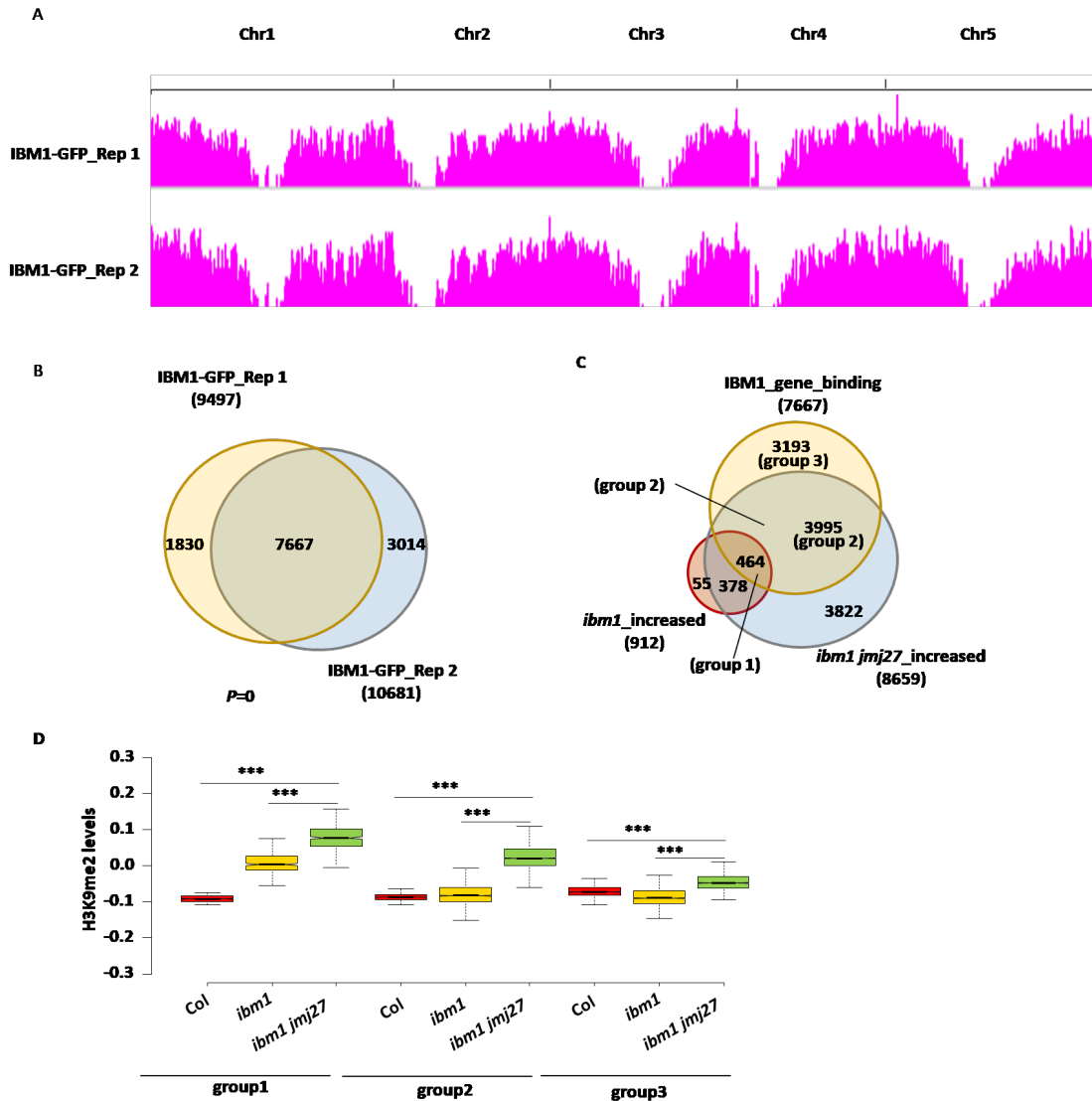


Figure 15. IBM1 binding sites in the genome. (A) Screenshot of genome-wide IBM1 binding sites. (B) Venn diagram showing the overlap of IBM1-occupied genes between two independent replicates.. Numbers of each category were indicated. (C) Venn diagrams showing the overlap between IBM1 binding regions in genes, hypermethylated genes in *ibm1*, and hypermethylated genes in *ibm1 jmj27*. Numbers of each category were indicated. (D) Box plot showing the H3K9me2 levels in each group genes indicated in 15C. *** $P < 0.001$.

3.1.7 Genes with ectopic H3K9me2 were downregulated in *ibm1 jmj27*

I further performed RNA-seq to investigate whether H3K9 hypermethylation led to gene silencing. Closed buds were used to extract total RNA, and two biological replicates for each genotype were performed. Numerous differentially expressed genes (DEGs) were identified in the mutants, represented by volcano plots (Figure

16A). The *ibm1 jmj27* mutant showed more DEGs compared to *ibm1* (Figure 16A). 3133 downregulated genes (DGs) were identified in *ibm1* and 3661 in *ibm1 jmj27*. These DEGs were significantly overlapped between *ibm1* and *ibm1 jmj27* (Figure 16B). There were also many upregulated genes in *ibm1* and *ibm1 jmj27* (Figure 16A), and IBM1 is shown to regulate the expression of *RDR2* and *DCL3* that are the critical components of the RNA-directed DNA methylation (RdDM) pathway (Fan et al. 2012), suggesting that these upregulated genes (UGs) in *ibm1 jmj27* were not directly regulated by IBM1 and JMJ27.

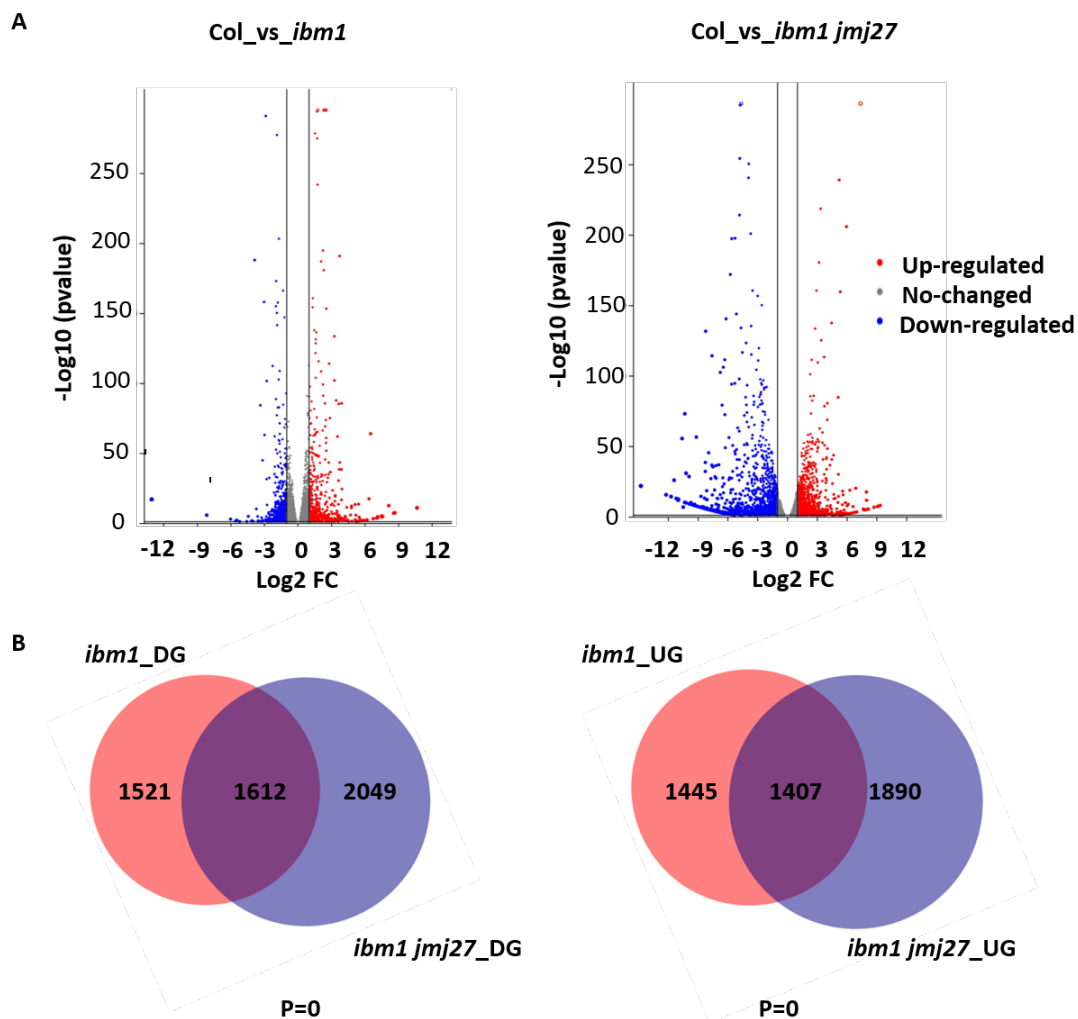


Figure 16. RNA-seq analysis. (A) Volcano plots of DEGs in *ibm1* (left) and *ibm1 jmj27* (right). The X-axis and Y-axis represent log₂FC and the statistical significance as the negative log₁₀ (*p*-value). The red dots represent significantly upregulated genes; the blue dots represent the significantly downregulated genes, and no-changed genes with grey dots. (B) Venn diagrams showing the overlap of downregulated genes (DGs) between *ibm1* and *ibm1 jmj27* (upper) and upregulated

genes (UGs) between *ibm1* and *ibm1 jmj27* (lower).

To explore whether silenced genes obtained ectopic H3K9me2 in the mutants, I analysed the overlap between the genes with differential H3K9me2 levels and the genes with differential expression in *ibm1* and *ibm1 jmj27*. Hypermethylated genes were significantly overlapped with downregulated genes in both *ibm1* and *ibm1 jmj27* (Figure 17A and C). However, there was no overlap between hypomethylated genes and upregulated genes in both *ibm1* and *ibm1 jmj27* (Figure 17B and D), indicating that these upregulated genes were not the direct targets of IBM1 and JMJ27. These results were coincident with the functions of IBM1/JMJ27 in H3K9me2 removal to protect genes from silencing.

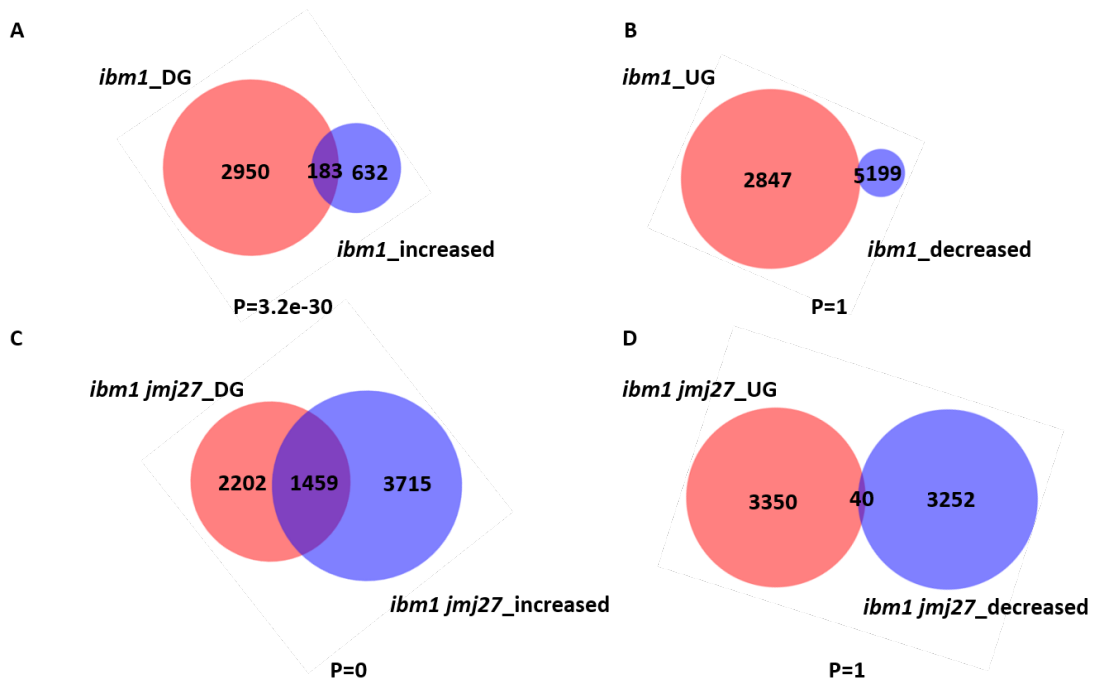


Figure 17. Overlap between H3K9me2 methylation and gene expression. (A, C) Venn diagrams showing the overlap between hypermethylated gene regions and downregulated genes in *ibm1* (A) and *ibm1 jmj27* (C). (B, D) Venn diagrams showing the overlap between hypomethylated genes and upregulated genes in *ibm1* (B) and *ibm1 jmj27* (D). The *P*-value was calculated by the hypergeometric test, and the sample size of $n=33547$ (the number of annotated protein-coding genes in the Arabidopsis genome) was used.

3.1.8 Meiosis essential genes were downregulated with increased H3K9me2 levels in *ibm1 jmj27*

To explore whether H3K9 hypermethylation silenced meiosis-essential genes, leading to meiosis defects in *ibm1* and *ibm1 jmj27*, I further analysed the expression levels of meiosis-essential genes. Many meiosis essential genes were silenced in *ibm1 jmj27* and/or *ibm1* (Figure 18A), including *ZYP1a*, *ZYP1b*, *ZIP4*, *ASY1*, and *SHOC1* critical for chromosome synapsis and crossover formation (Macaisne et al. 2008; Higgins et al. 2005; Chelysheva et al. 2007; Caryl et al. 2000). The functions of these silenced meiotic genes were listed in Table 1. Our RNA-seq and H3K9me2 ChIP-seq showed that these five meiosis essential genes were silenced with increased H3K9me2 level, suggesting that these genes were directly targeted by IBM1 (Figure 18). To further confirm that IBM1 directly regulated these genes, I examined the IBM1-GFP occupied profiles. The ChIP-seq results showed that IBM1 was enriched at these loci (Figure 18B-F), supporting the notion that IBM1 directly bonds at these target genes.

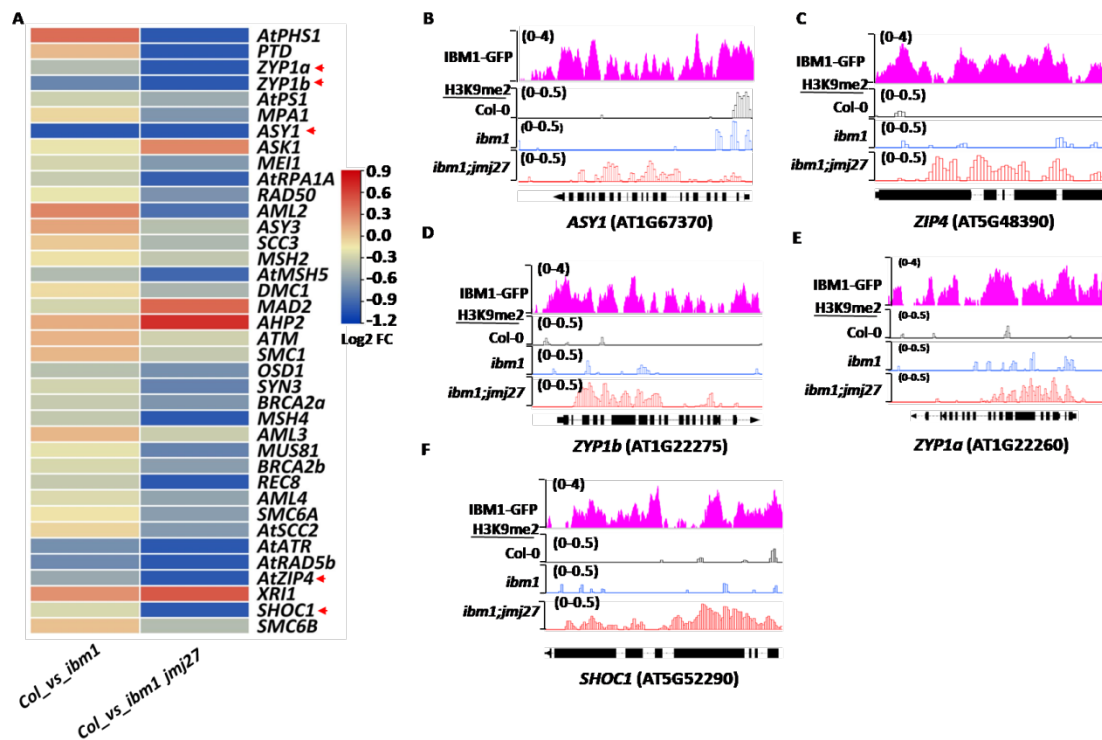


Figure 18. Relative expression level and H3K9me2 level of meiosis genes. (A) Heat map showing the relative expression levels of indicated meiosis genes in *ibm1* and *ibm1 jmj27*. Fold change value (FC) was used. (B) Chip-seq analysis of IBM1 binding regions and H3K9me2 levels in the indicated gene regions in *ibm1* and *ibm1 jmj27*. H3K9me2 levels in Col-0 (black color), *ibm1* (blue color), and *ibm1 jmj27* (red color) at indicated genes were shown. The values of H3K9me2 minus H3 to obtain the enrichment levels of H3K9me2.

I have further performed ChIP-qPCR to examine the levels of H3K9me2 at these gene

loci. Two regions of each candidate, except *ASY1*, were chosen for testing. The results showed that the levels of H3K9me2 were increased at these loci in the *ibm1 jmj27* mutant (Figure 19A and B). Hence, hypermethylation of H3K9me2 at these genes led to the downregulation of these genes, which is coincident with the meiosis defects in *ibm1 jmj27*. Taken together, our results indicated that IBM1 is required for removing H3K9me2 at target genes to activate their expression and ensure meiotic progression.

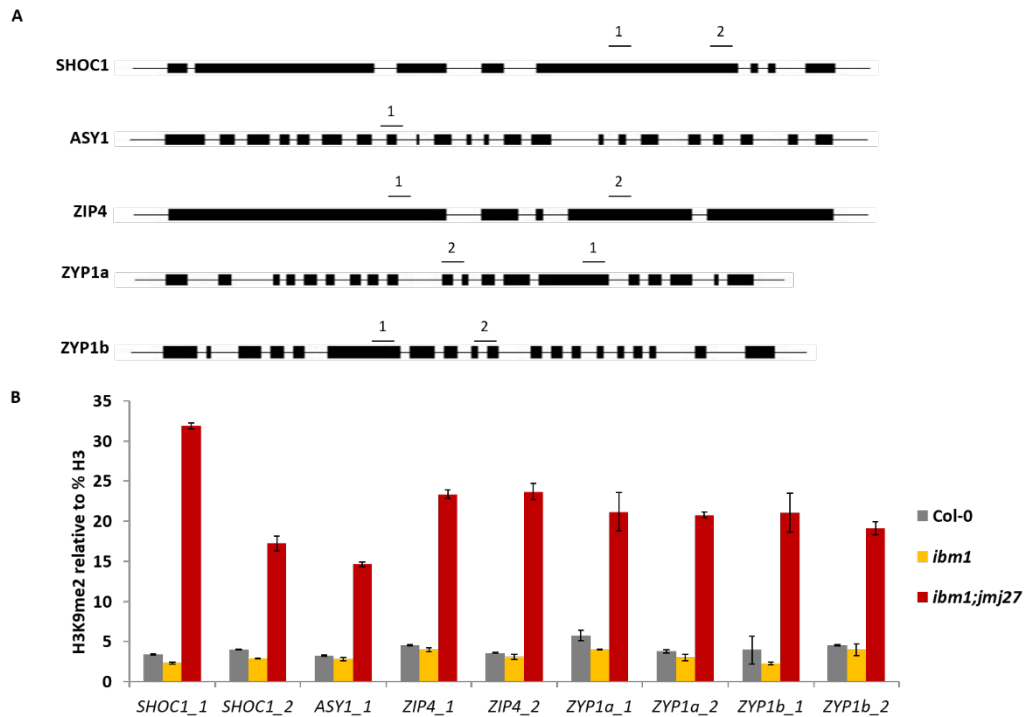


Figure 19. Chip-qPCR analysis of the H3K9me2 levels in *ibm1* and *ibm1 jmj27*. (A) The schematic diagram of indicated genes. Gene regions were indicated by the dotted lines and numbers. (B) The enrichment of H3K9me2 at the indicated genes. H3K9me2 levels were normalized to percentage H3.

To further confirm whether these meiotic genes were exactly silenced in meiotic cells, I performed immunolocalization of ZYP1 in Col-0 and *ibm1 jmj27* male meiocytes. Synapsis is accomplished by pachytene and the ZYP1 signals extended the entire lengths of fully synapsed homologs (Figure 20). However, the ZYP1 signals were much weaker compared to the Col-0, and its localization was also not the entire homologs (Figure 20), indicating that ZYP1 was silenced in the mutant.

pachytene

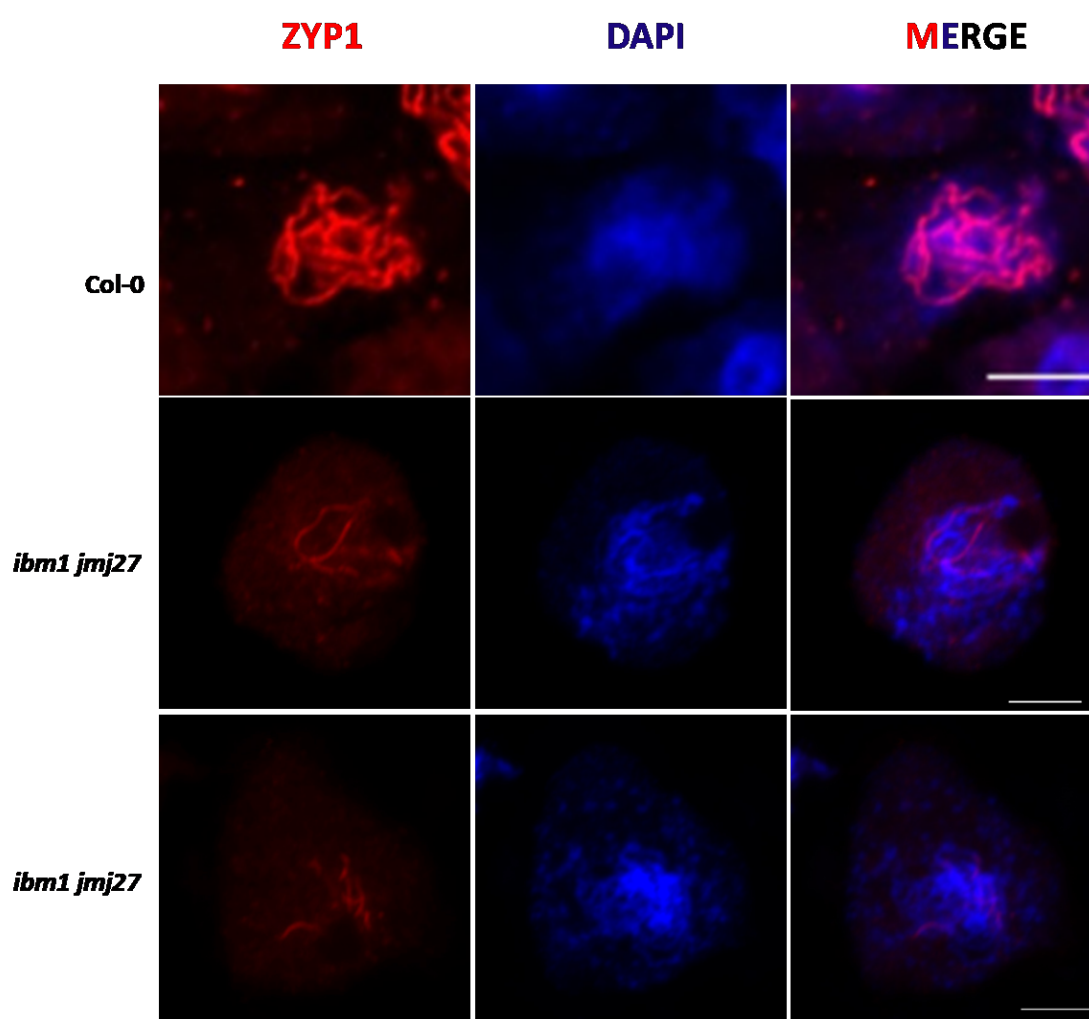


Figure 20. Immunolocalization of ZYP1 protein at pachytene. ZYP1 signals (red) and DAPI (blue) in Col-0 and *ibm1 jmj27* male meiocytes. Bar, 5 μ m.

Table 1: Functions of meiosis genes in Arabidopsis

Gene symbol	ID	Function	References
<i>ZYP1a</i>	AT1G22260	Synapsis, meiotic progression	Higgins et al., 2005
<i>ASY1</i>	AT1G67370	Synapsis	Azumi et al., 2002
<i>RAD50</i>	AT2G31970	synapsis, recombination	Gallego et al., 2001
<i>MSH2</i>	AT3G18524	Inhibit recombination	Emmanuel et al., 2006
<i>AtZIP4</i>	AT5G48390	Class I CO pathway	Chelysheva et al., 2007
<i>SHOC1</i>	AT5G52290	Class I CO pathway	Macaisne et al., 2008
<i>AtMSH5</i>	AT3G20475	Class I CO pathway	Higgins et al., 2008
<i>MUS81</i>	AT4G30870	Class II CO pathway	Higgins et al., 2008
<i>DMC1</i>	AT3G22880	Meiotic recombination	Doutriaux et al., 1998
<i>BRCA2a</i>	AT4G00020	Meiotic recombination	Siaud et al., 2004

<i>BRCA2b</i>	AT5G01630	Meiotic recombination	Siaud et al., 2004
<i>SMC6A</i>	AT5G07660	Homologous Recombination	Watanabe et al., 2009
<i>AtSCC2</i>	AT5G15540	axis formation	Sebastian et al., 2009
<i>SMC6B</i>	AT5G61460	Homologous Recombination	Watanabe et al., 2009
<i>MEI1</i>	AT1G77320	DNA repair	Grelon et al., 2003
<i>ATM</i>	AT3G48190	Regulation of DNA repair	Garcia et al., 2000, 2003
<i>SYN3</i>	AT3G59550	expressed in dividing cells	Dong et al., 2001

3.1.9 IBM1 interacts with PDS5 family proteins

To explore how IBM1 and JM127 protect genes from silencing, I cooperated with Prof. Klaus Grasser (University of Regensburg) to perform affinity purification mass spectrometry (AP-MS) in suspension cells to identify the proteins interacting with IBM1. Table 2 shows some key candidates obtained by AP-MS. The PDS5 family proteins, including PDS5A, PDS5C, and PDS5E, are considered as critical interacting proteins with high scores in three replicates. PDS5 proteins function as cohesion cofactors to be involved in chromosome segregation, DNA repair, and gene transcription in many organisms (Onn et al. 2008; Dorsett 2007; Barbero 2009). In *Arabidopsis*, PDS5s are required for chromosome segregation and DNA repair (Pradillo et al. 2015b). However, their function in gene regulation is unknown.

Table 2. The interaction candidates of IBM1 by IP-MS

Protein	Annotation	Score	Replicate
<i>IBM1</i>	AT3G07610	8813.1	3
<i>PDS5E</i>	AT1G15940	2815.9	3
<i>PDS5C</i>	AT4G31880	2039	3
<i>HTB6</i>	AT3G53650	1678	3
<i>PRPL5</i>	AT4G01310	1656	3
<i>HD2C</i>	AT5G03740	1487	3
<i>ALY4</i>	AT5G37720	1180	3
<i>RFC1</i>	AT5G22010	942	3
<i>PDS5A</i>	AT5G47690	582.6	3
<i>RFC2</i>	AT1G63160	688	3

I first confirmed the interaction between IBM1 and PDS5 by yeast two-hybrid (Y2H). Four of five PDS5 family proteins, including PDS5A, PDS5B, PDS5C, and PDS5E, interact with IBM1 in yeast (Figure 21 A). I also tested if other components or cofactors of the cohesin complex interacted with IBM1. Another cohesin component REC8 and the cofactor SCC3 also interact with IBM1 in yeast, whereas the

interactions were weaker than PDS5s (Figure 22B). The interaction between PDS5C and PDS5E with IBM1 have been further confirmed by bimolecular fluorescence complementation (BiFC) assay (Figure 21B), and H3.3-GFP was used to indicate nuclei. There was no YFP signal in the control combinations, but co-transformation of PDS5 and IBM1 resulted in a very strong YFP signal in nuclei (Figure 21B), indicating that IBM1 interacted with PDS5 family proteins in *N. benthamiana*. Quantification of the nuclei with YFP signals and nuclei with RFP signals was performed to analyze the interaction intensity. Around 80% of nuclei with RFP signal also showed GFP signal in the co-transformation of PDS5 with IBM1, indicating strong interactions (Figure 21D). Co-immunoprecipitation assay (Co-IP) was also performed to further confirm the interaction. Tobacco leaves without any injection and combined injection of IBM1/REC8 were used as the control. The result showed that IBM1-GFP and PDS5E-3xFlag were co-precipitated (Figure 21C). These data indicated that IBM1 interacted with PDS5s in plants.

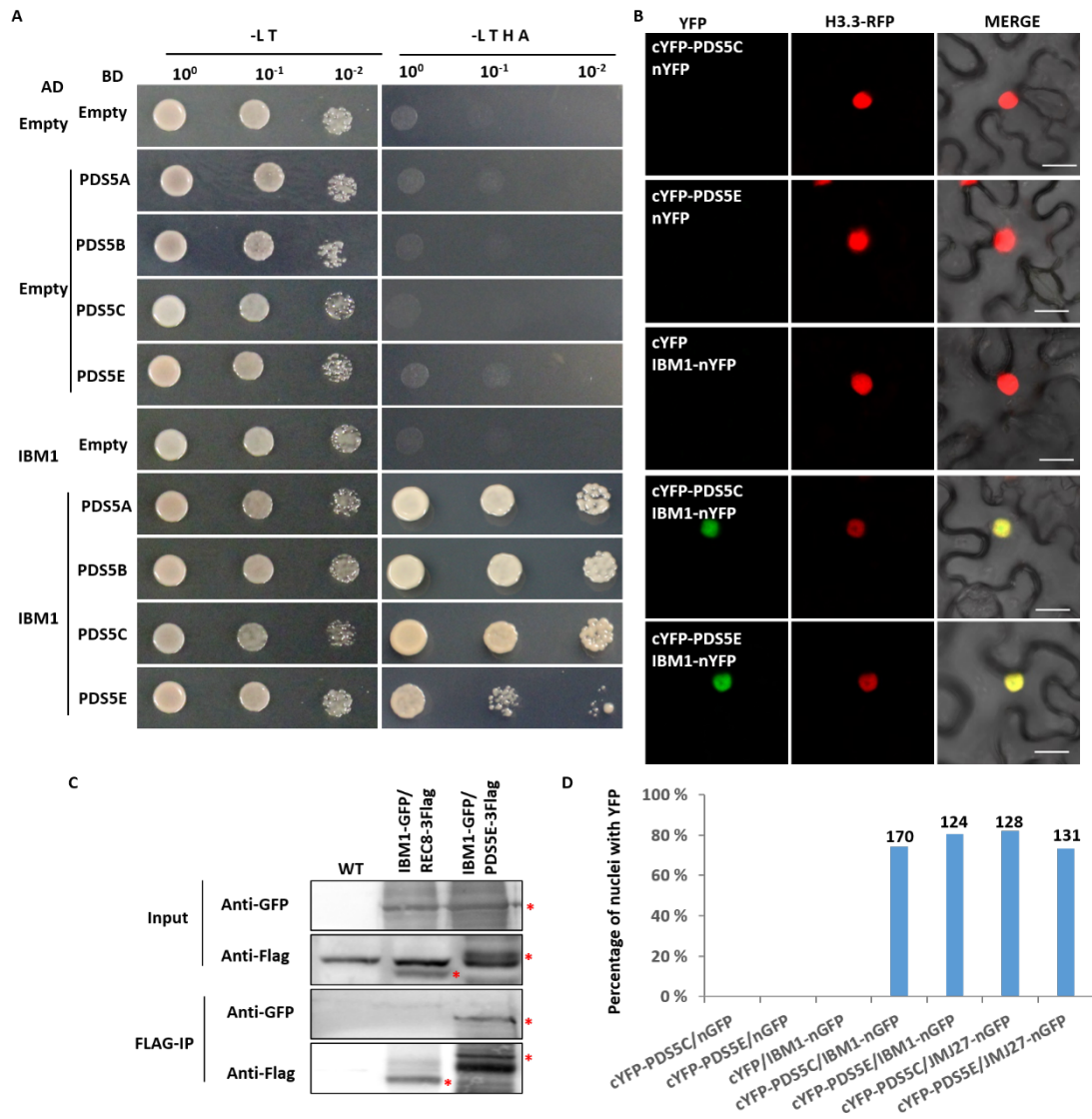


Figure 21. IBM1 physically interacted with PDS5 proteins in vitro and in vivo. (A) Yeast two-hybrid assay to test the interaction between IBM1 and PDS5. Yeast cells containing both the AD (activating domain) and BD (binding domain) vectors were grown on Synthetic Defined (SD) medium supplied with D-Glucose in the absence of Leu and Trp (SD/ -L T, left panel) as control and on SD medium in the absence of Leu, Trp, His and Adenine (SD/ -LTHA, right panel) for the interaction test. Yeast cells were diluted 10- and 100- fold after cultured to specific OD. (B) Bimolecular fluorescence complementation (BiFC) assays to test the interaction between IBM1 and PDS5 proteins. YFP was split into cYFP and nYFP and YFP signal indicated the interaction of the tested proteins. H3.3-RFP was used to indicate the nuclei. (C) Co-immunoprecipitation assay to test the interaction between IBM1 and PDS5E in tobacco. Tobacco leaves without any injection and combined injection of IBM1/REC8 were used as genitive control. All of these assays were repeated with similar results. Asterisks indicate targeted proteins. (D) Quantification of the nuclei

with YFP signals to nuclei with RFP signals. The scored numbers of nuclei were shown above the bar.

Given that IBM1 and JMJ27 were functionally redundant, I further explored if JMJ27 interacted with PDS5s by BiFC assay. Similar to IBM1, JMJ27 also interacted with PDS5C and PDS5E (Figure 22A). Quantification of the nuclei with YFP signals to nuclei with RFP signals was also performed to analyze the interaction intensity. Similarly, 80% of nuclei with RFP signal also showed GFP signal in the co-transformation of PDS5 with JMJ27 (Figure 21D). Therefore, our results indicate that both IBM1 and JMJ27 interacted with PDS5s. Moreover, our BiFC result also showed that IBM1 and JMJ27 interacted with each other (Figure 22C), and their interaction may benefit their histone demethylases activity.

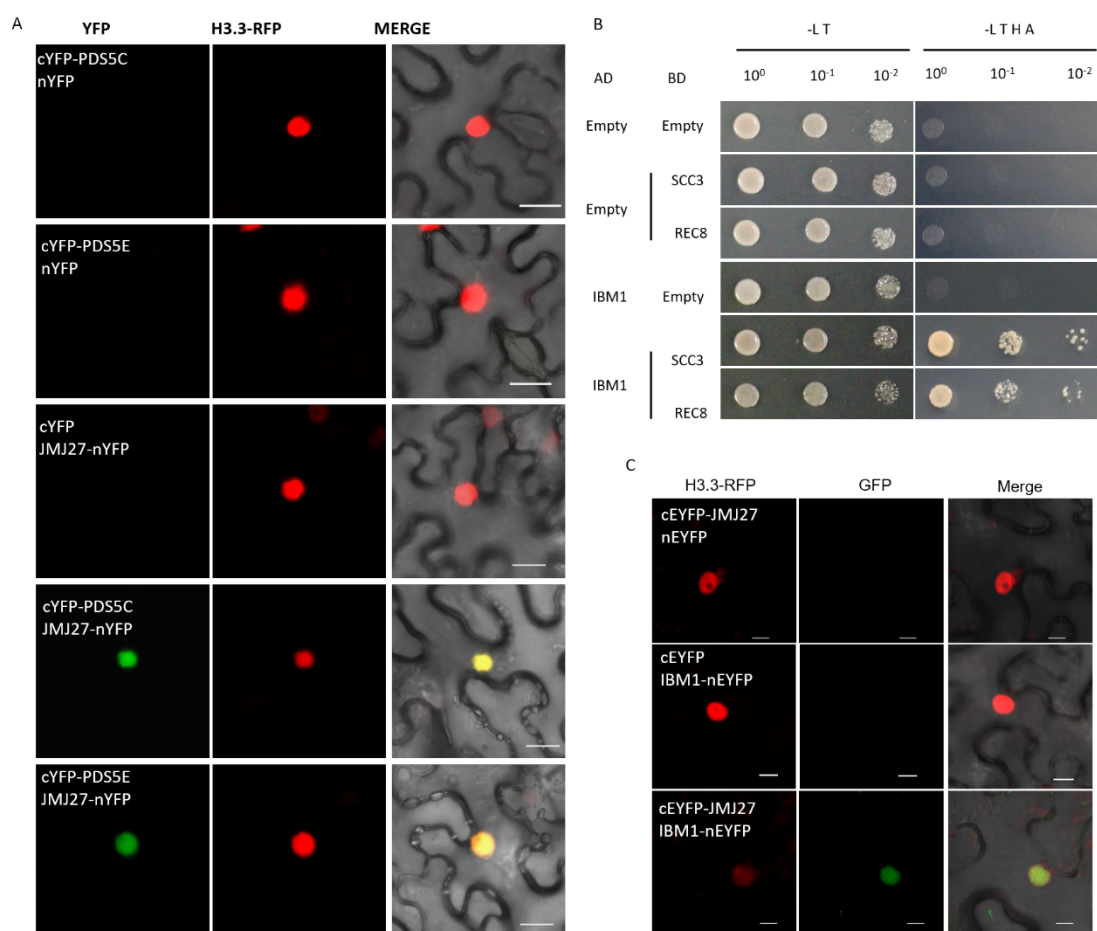


Figure 22. JMJ27 interacts with PDS5 proteins. (A) Bimolecular fluorescence complementation (BiFC) assays to test the interaction of JMJ27 and PDS5 proteins. YFP was split into cYFP and nYFP and YFP signal indicated the interaction of the tested proteins. H3.3-RFP was used to indicate the nuclei. (B) Yeast two-hybrid assay to test the interaction between IBM1 and cohesin factors.

Yeast cells containing both the AD (activating domain) and BD (binding domain) vectors were grown on Synthetic Defined (SD) medium supplied with D-Glucose in the absence of Leu and Trp (SD/ -L T, left panel) as control and on SD medium in the absence of Leu, Trp, His and Adenine (SD/ -LTHA, right panel) for the interaction test. Yeast cells were diluted 10- and 100- fold after cultured to specific OD. (C) Bimolecular fluorescence complementation (BiFC) assays to test the interaction of IBM1 and JMJ27. YFP was split into cYFP and nYFP and YFP signal indicated the interaction of the tested proteins. H3.3-RFP was used to indicate the nuclei.

3.1.10 PDS5s act downstream of H3K9 demethylation to activate gene expression

I hypothesized that PDS5s act with IBM1 and JMJ27 by two mechanisms: (1) PDS5s act downstream of IBM1 and JMJ27 and are required for gene activating. (2) PDS5s recruit IBM1 and JMJ27 and are required for H3K9me2 demethylation. To examine the hypothesis 1, I conducted RNA-seq with *pds5* closed buds. Downregulated genes (DGs) and upregulated genes (UGs) were significantly overlapped between *ibm1 jmj27* and *pds5* (Figure 23A). However, the altered levels of these DEG were lower in *pds5* compared to *ibm1 jmj27* (Figure 23B). When I further compared meiosis essential genes between *ibm1 jmj27* and *pds5*, multiple genes essential for chromosome pairing, crossover, such as *ASY1*, *ZYP1a*, *ZYP1b*, *AtZIP4*, and *SHOC1*, were also silenced in *pds5* (Figure 23C). However, the reduction in *pds5* was weaker than in *ibm1 jmj27* (Figure 23C), in line with weak meiosis defects in *pds5* (Pradillo et al. 2015a). A similar gene expression pattern between *ibm1 jmj27* and *pds5* indicated that PDS5s are functional in H3K9 demethylation-mediated gene activation. To further know PDS5 act up- or down-stream of IBM1 and JMJ27, I further conducted H3K9me2 ChIP-seq. The H3K9me2 levels in *pds5* were similar to Col-0, and hypermethylation only occurred in *ibm1* and *ibm1 jmj27* (Figure 23D-G), indicating that PDS5 was not required for H3K9me2 removal. Hence, PDS5s act downstream of H3K9 demethylation and are required for activating the expression of meiosis essential genes.

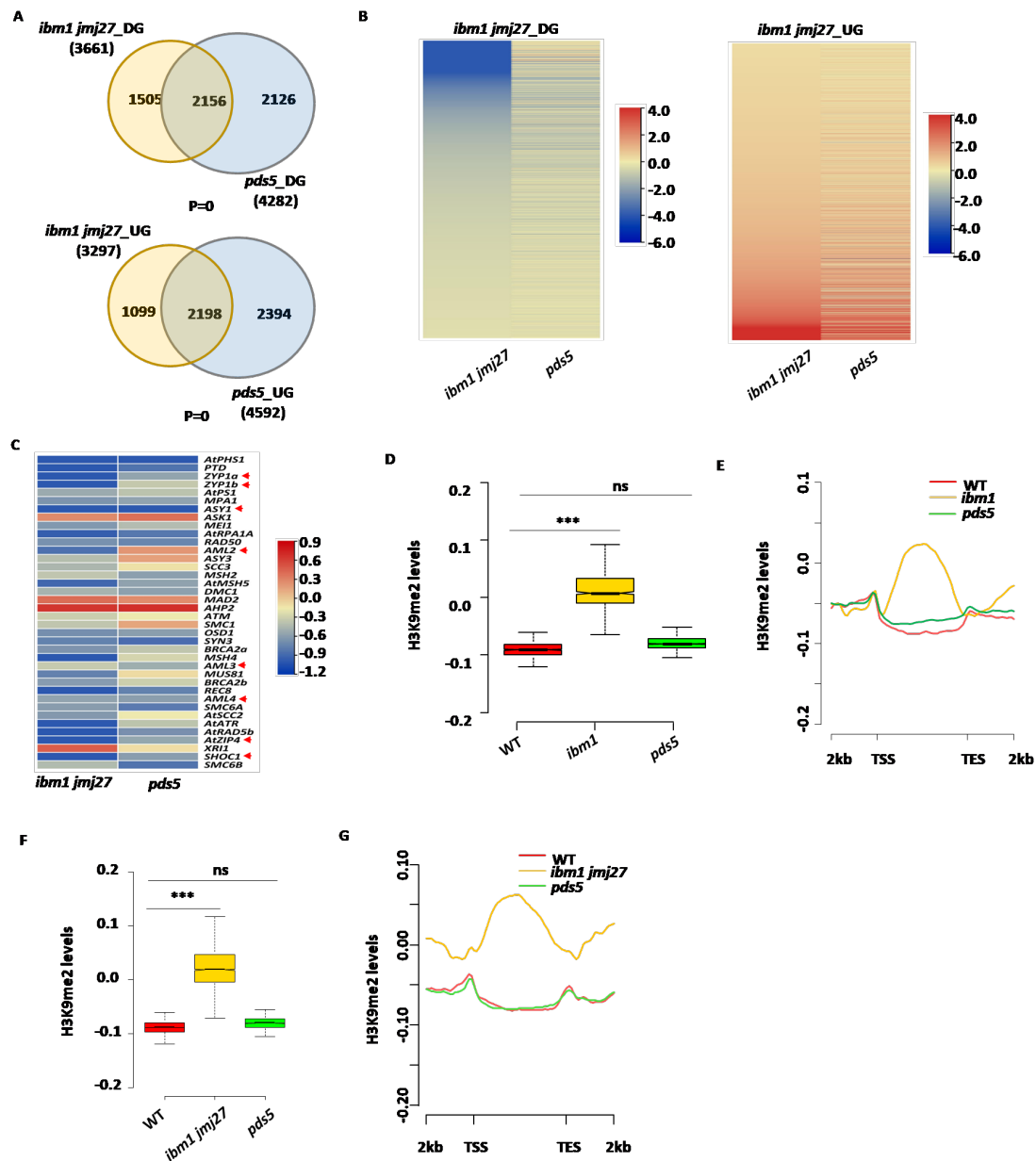


Figure 23. PDS5s act downstream of H3K9 demethylation in reproduction tissue. (A) Venn diagrams showing the overlap of downregulated genes (DG) (upper) and upregulated genes (UG) (lower) between *ibm1 jmj27* and *pds5*. Numbers of each category were indicated. (B) Heatmaps showing relative expression levels of *ibm1 jmj27* DG genes (left) and UG genes (right) in *ibm1 jmj27* and *pds5*. (C) Heat map showing the relative mRNA expression levels of indicated meiotic genes in *ibm1 jmj27* and *pds5*. (D) Box plots showing median values of z-score-normalized H3K9me2 levels in Col-0, *ibm1*, and *pds5*. (E) Metagene plots showing H3K9me2 levels in Col-0, *ibm1*, and *pds5*. (F) Box plots showing median values of z-score-normalized H3K9me2 levels in Col-0, *ibm1 jmj27*, and *pds5*. (G) Metagene plots showing H3K9me2 levels in Col-0, *ibm1 jmj27*, and *pds5*.

I further examined whether the deposition of H3K9me2 was altered at these meiotic essential genes. Screenshots from our H3K9me2 Chip-seq profiles showed that the ectopic deposition of H3K9me2 at indicated meiotic genes only occurs in *ibm1 jmj27* but not in *pds5* (Figure 24).

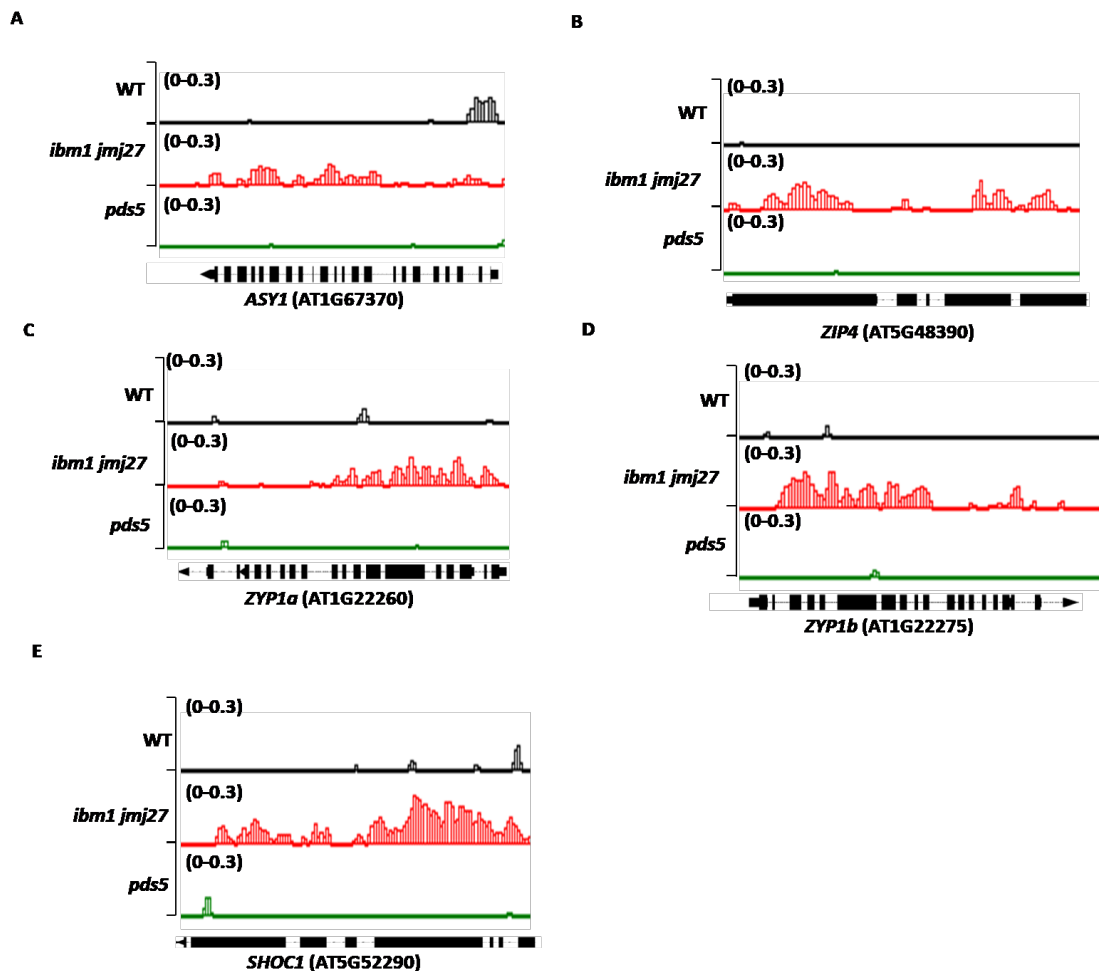


Figure 24. Meiotic genes did not obtain ectopic H3K9me2 in *pds5*. (A-E) H3K9me2 levels at the indicated gene loci in Col-0, *ibm1 jmj27*, and *pds5*.

PDS5s, the cohesin cofactors, are functional in both meiosis and mitosis. To test whether H3K9me2-mediated gene activation coupled with PDS5s was exactly functional in meiosis, I first generated the transcriptome profile of *rec8*, a meiosis-specific component of the cohesin complex. Indeed, both the DGs and UGs were significantly overlapped between *ibm1 jmj27* and *rec8* (Figure 25A). I have also performed qRT-PCR to confirm the relative expression levels of meiosis-essential genes that were silenced in *ibm1 jmj27*. These silenced genes in *ibm1 jmj27* also have reduced expression levels in *rec8*, including *SHOC1*, *ZYP1*, and *ASY1* (Figure 25B).

Hence, the meiotic cohesin complex is required for H3K9me2-mediated gene activation in meiosis.

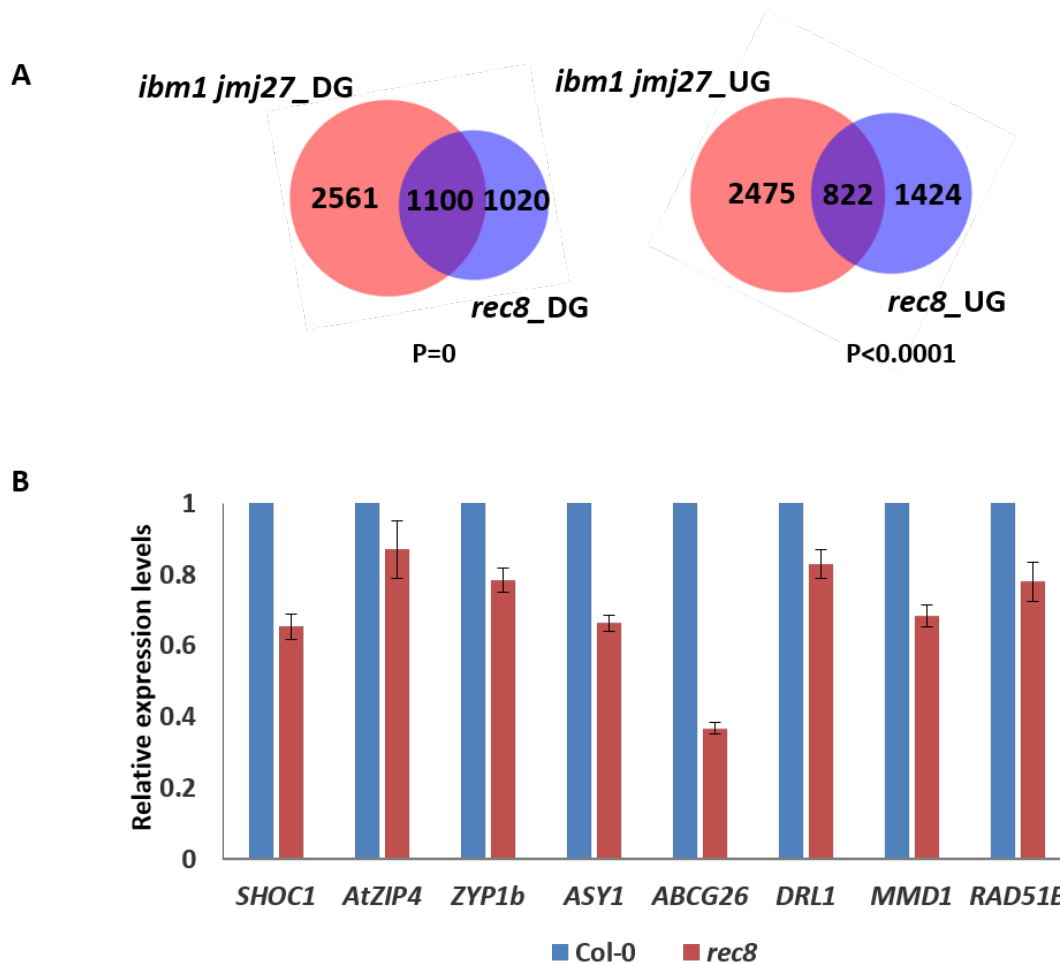


Figure 25. *ibm1 jmj27* and *rec8* RNA-seq analysis. (A) Venn diagrams showing the overlap between DGs in *ibm1 jmj27* and *rec8*. The *P*-value were calculated by hypergeometric test and sample size of $n=33547$ (the number of annotated protein-coding genes in the Arabidopsis genome) was used. (B) Quantitative reverse transcription PCR (RT-qPCR) showing the relative expression of the indicated genes in *ibm1 jmj27* and *rec8*. The values were normalized to *GAPDH* and shown as the means \pm SEMs. Two biological replicates were performed.

As mentioned before, PDS5s function in both mitosis and meiosis, so I further examined whether PDS5s were also required to activate gene expression in vegetative stage. I generated the expression profiles for *ibm1 jmj27* and *pds5* in 18-day seedlings. Both DGs and UGs were significantly overlapped in *ibm1 jmj27* and *pds5* (Figure 26A). Relative expression of DGs and UGs in *ibm1 jmj27* and *pds5* were shown in heatmap (Figure 26B). Similar to the results of closed buds, these silenced

genes acquired ectopic H3K9me2 in *ibm1 jmj27* but not in *pds5* (Figure 26C). Our results indicated that PDS5s, IBM1, and JMJ27 cooperatively activate gene expression in both vegetative and reproductive stages.

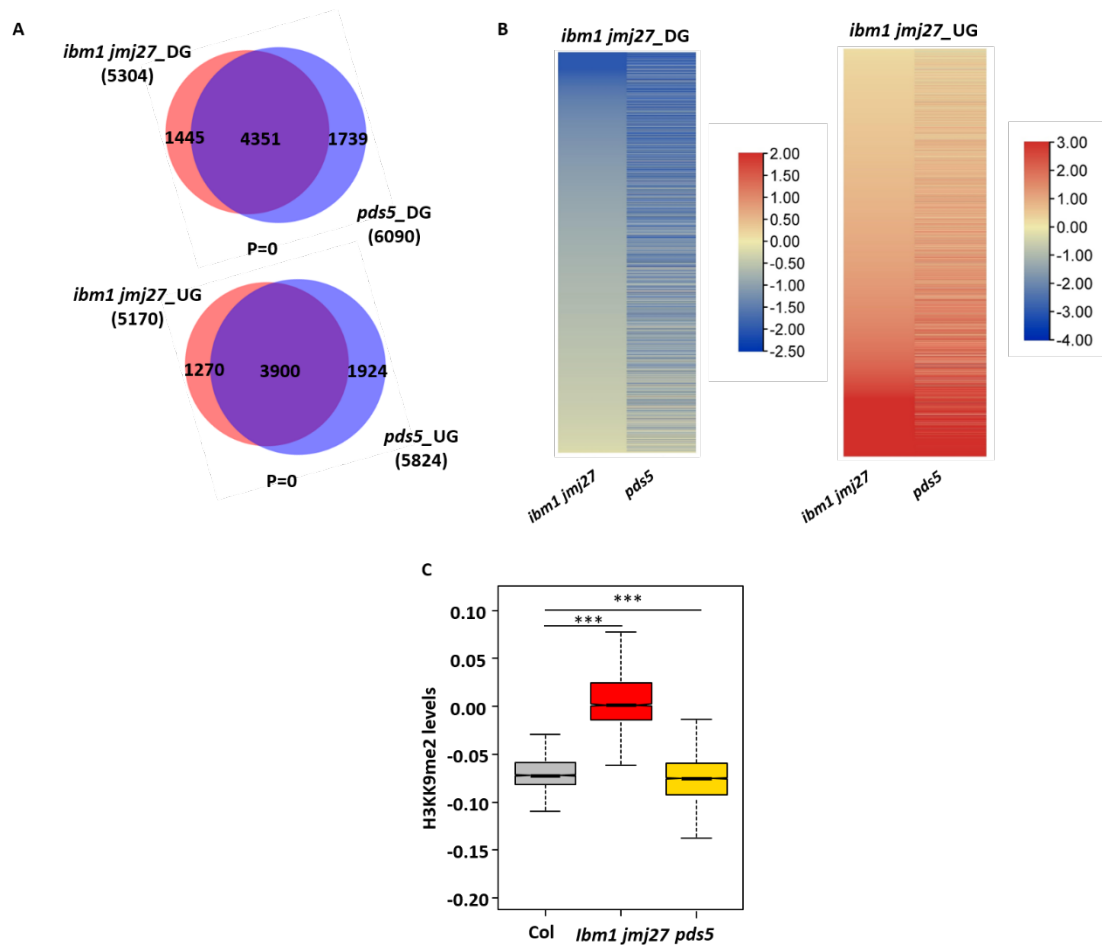


Figure 26. PDS5s also act downstream of H3K9 demethylation in leaf. (A) Venn diagrams showing the overlap of downregulated genes (DGs) (upper) and upregulated genes (UGs) (lower) between *ibm1 jmj27* and *pds5* in seedling. Numbers of each category were indicated. (B) Heatmaps showing relative expression levels of *ibm1 jmj27* DGs and UGs (right) in *ibm1 jmj27* and *pds5* in seedling. (C) Box plots showing median values of z-score-normalized H3K9me2 levels in Col-0, *ibm1 jmj27* and *pds5* seedling.

To further examine whether IBM1 and JMJ27 were required for PDS5s recruitment to activate meiotic genes expression, I performed Chip-qPCR using antibody anti-PDS5E which was shown to have strong interaction with IBM1 and JMJ27 (Figure 21 and 22). PDS5E binding at promoter and gene bodies were detected (for example, *pZIP4* indicated the promoter region, and *ZIP4_1* and *ZIP4_2* indicated gene bodies). The enrichment of PDS5E at these indicated loci was reduced in *ibm1 jmj27* compared to

Col-0 (Figure 27A), indicating that IBM1 and JMJ27 were required for the recruitment of PDS5s to activate gene expression in meiosis.

In summary, my results showed that histone demethylases IBM1 and JMJ27 were required for male meiosis. IBM1 and JMJ27 removed the silencing mark H3K9me2 from numerous gene bodies. Meanwhile, IBM1 and JMJ27 directly bind at meiosis-related genes to remove H3K9me2, coupled with the cohesin cofactor PDS5s, and activate the expression of meiotic-related genes to ensure the meiotic progression (Figure 27B).

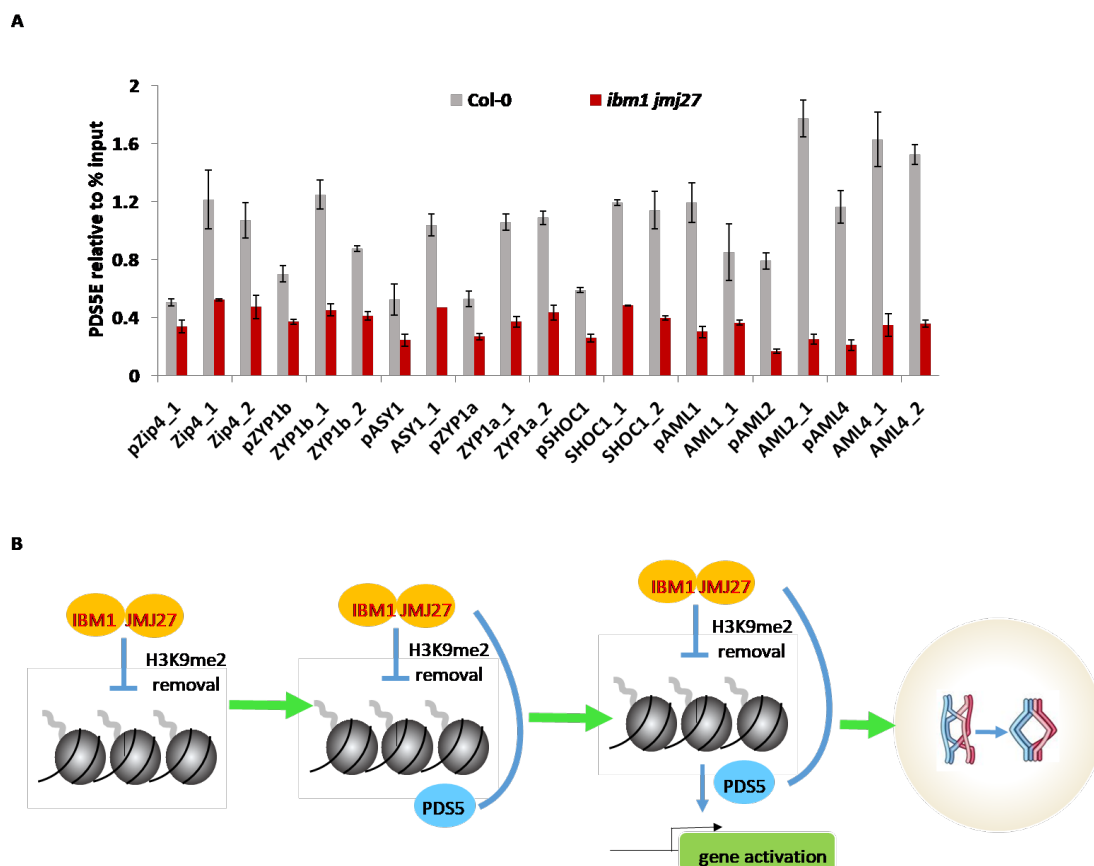


Figure 27. IBM1 was required for the recruitment of PDS5s. (A) Chip-qPCR to examine PDS5E enrichment at these meiotic loci in *ibm1 jmj27* closed buds. PDS5E enrichment levels were normalized to percentage input. (B) Model for histone demethylation-mediated gene activation. In wild type plants, Histone demethylases IBM1 and JMJ27 work together to remove the H3K9me2 mark from the gene locus. At the same time, IBM1 and JMJ27 recruit cohesin cofactors PDS5 proteins to the target locus. The hypomethylation coupled with PDS5 proteins further activate the meiosis-essential genes expression.

3.2 H3K9 demethylation is required for pollen wall formation

3.2.1 H3K9 demethylation is required for exine formation

ibm1 produced around 25% abnormal meiotic products at the tetrad stage (Figure 2), but most of the pollen in *ibm1* was collapsed, indicating defective pollen development. Tapetum is the innermost somatic cell layer surrounding the male gametophyte and provides materials for pollen development (Ariizumi and Toriyama 2011). I first examined the tapetum development in the mutants. Cross-sections of wild type and *ibm1* were detected from stage 6 to 12. The structures of tapetum and pollen were similar between wild type and *ibm1* from stage 6 to stage 10. At stage 12, *ibm1* produced collapsed or enlarged pollen, differing from pollen grains in wild type (Figure 28). No viable pollen was found in *ibm1 jmj27* at stage 10 (data not shown).

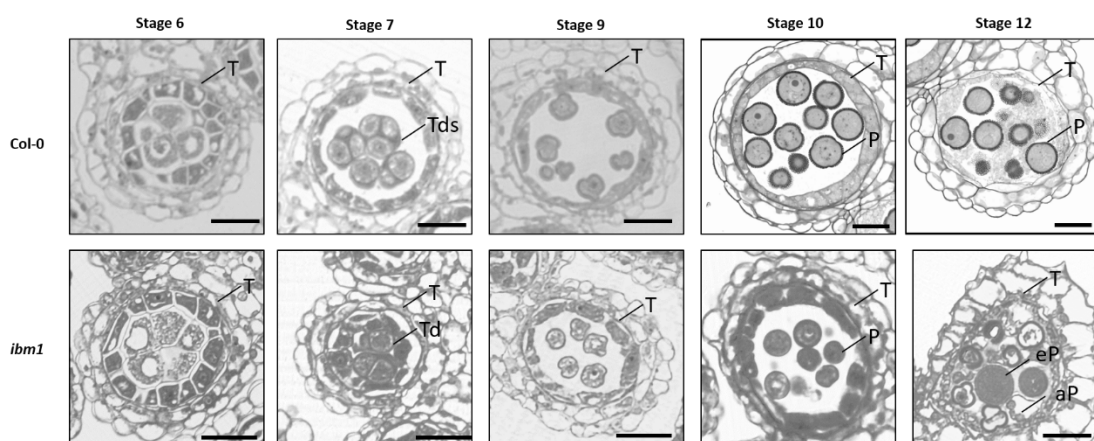


Figure 28. Mutations of IBM1 and JMJ27 lead to defective pollen development. Cross-sections of wild type, *ibm1*, *ibm1 jmj27*, showed the anther development from stage 6 to stage 12. T, tapetum; Tds, tetrads; P, pollen; Ep, enlarged pollen; ap, aborted pollen. Scale bars, 20 μ m.

To further examine the reason leading to collapsed pollen in *ibm1* and *ibm1 jmj27*, I performed transmission electron microscopy (TEM) analysis by collaborating with Dr. Michael Melzer (IPK, Gatersleben). The nexine layer presented at stage 8 and became thicker at later stages in wild type (Figure 29), but this structure was abnormal in *ibm1* and completely absent in the *ibm1 jmj27* mutant (Figure 29).

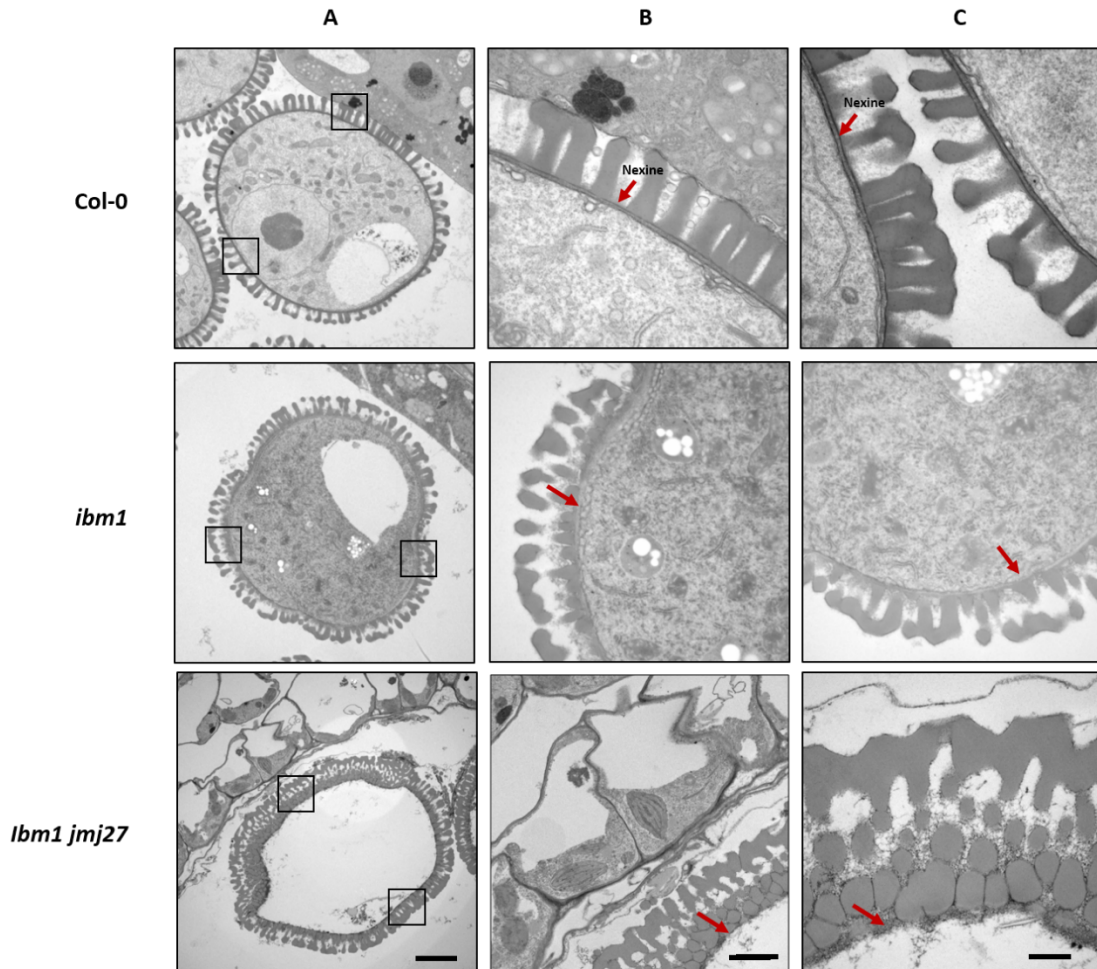


Figure 29. TEM images of pollen wall development. (A) Pollen wall structure in Col-0, *ibm1*, and *ibm1 jmj27*. B (left side) and C (right side) are the higher magnification view of B. X bar in A, 2 μ m; B and C, 500nm.

I also examined whether exine pattern was affected in *ibm1* and *ibm1 jmj27*. The regular structure of exine, including nexine, bacula, tectum, were observed in wild type (Figure 30A). However, bacula was abnormally deposited in *ibm1* (Figure 30B) and absent in *ibm1 jmj27* (Figure 28C). The bacula structure was abnormal in *ibm1 jmj27* (Figure 30B and C). CYP98A8 and CYP98A9 are required for proper pollen wall pattern, and the double mutant shows an abnormal exine layer with irregular baculum and tectum and disordered tryphine deposition (Xu et al. 2014). So, I examined their expression in *ibm1* and *ibm1 jmj27*. RNA-seq showed that they were downregulated in *ibm1* and *ibm1 jmj27* (Figure 33B), and these genes also acquired H3K9me2 in *ibm1 jmj27* compared to *ibm1* and wild type (Figure 30B), indicating that IBM1 and JMJ27 control pollen wall pattern by regulating the expression of CYP98A8

and *CYP98A9*. Our results indicated that IBM1 and JMJ27 are required for nexine formation.

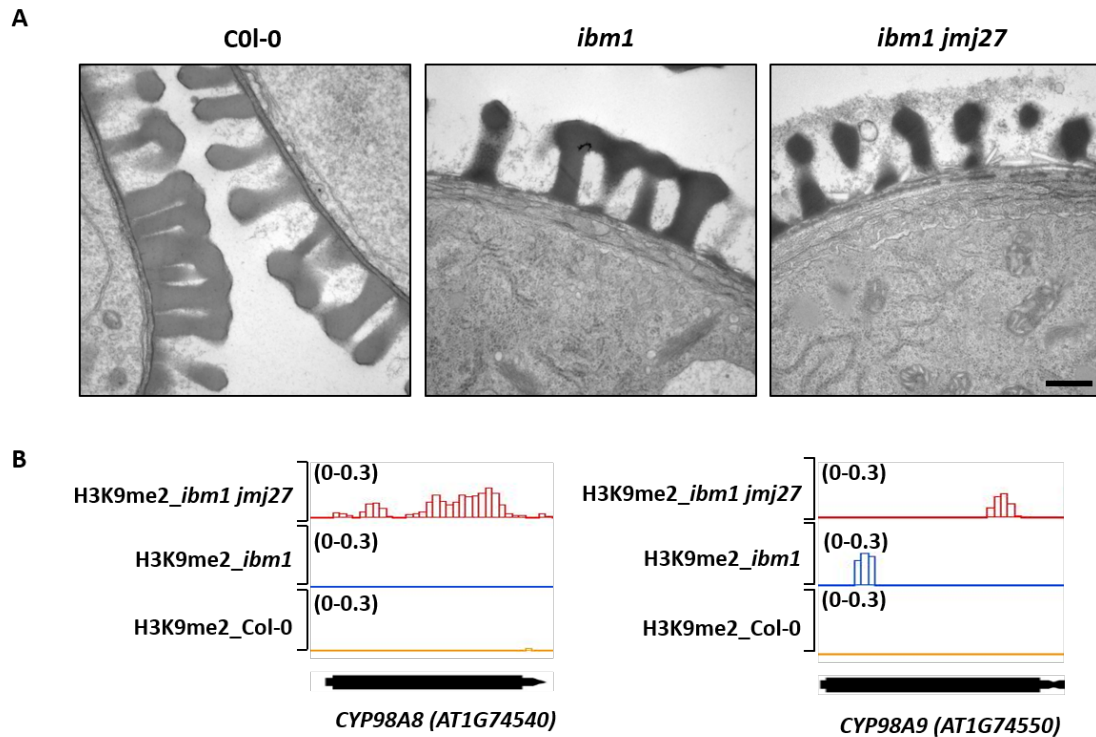


Figure 30. Pollen wall pattern in Col-0, *ibm1* and *ibm1 jmj27*. (A) The pollen wall structure in Col-0 (left), *ibm1* (middle) and *ibm1 jmj27* (right) by TEM. Bar, 500 nm (B) Chip-seq analysis of the H3K9me2 levels at the indicated gene regions in the *ibm1* and *ibm1 jmj27* mutants. H3K9me2 levels in Col-0 (yellow), *ibm1* (blue), and *ibm1 jmj27* (red) at indicated genes were shown. The values of H3K9me2 minus H3 and obtained the enrichment levels of H3K9me2.

3.2.2 AMS interacts with IBM1

IBM1 and JMJ27 are required for pollen wall formation, so I hypothesized that IBM1 and JMJ27 bind at the targets to activate genes required for pollen wall formation. It is unknown how IBM1 and JMJ27 are recruited to their targets. Given that transcription factors (TFs) play important roles in recruiting histone modifiers (Bulut-Karslioglu et al. 2012), I tested whether TFs were also required for recruiting IBM1 and JMJ27. To address this question, I first tested the interaction between IBM1 and all TFs in Arabidopsis by collaborating with Nobutaka Mitsuda (National Institute of Advanced Industrial Science and Technology, Japan). After two rounds of screening, we identified 78 TFs showing strong interaction with IBM1, belonging to twenty different TF families (Figure 31). AMS, a bHLH family protein required for

tapetum and microspores development (Xu et al. 2014; Sorensen et al. 2003), was the key candidate.

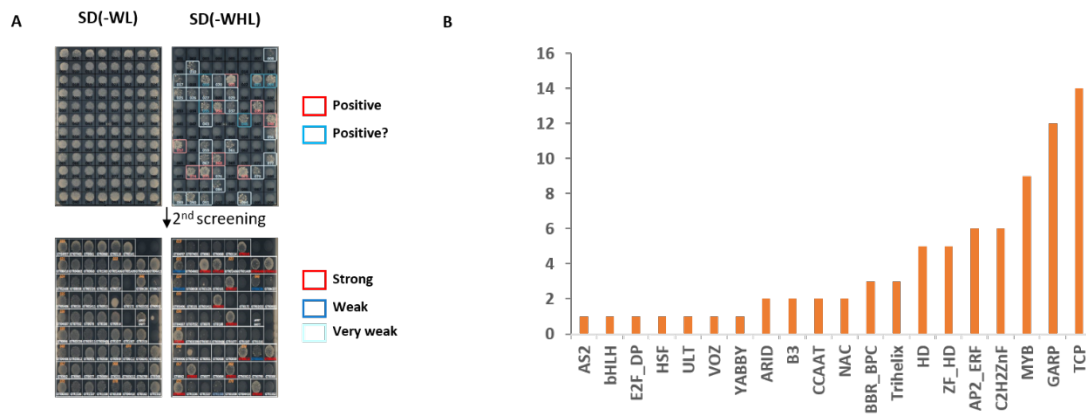


Figure 31. Candidates of IBM1/JMJ27 interactor. (A) Yeast two-hybrid screening assay to test the interaction between IBM1 and transcription factors in Arabidopsis. IBM1 was used as he bait. Synthetic Defined (SD) medium supplied with D-Glucose in the absence of Leu, Trp, His (SD/ -WHL) was used to select the positive interaction. Two rounds of selection were performed. (B) The number of selected candidates in the indicated TF families from A.

I confirmed the interaction between IBM1/JMJ27 and AMS by Y2H and BiFC assays. Y2H results showed that AMS interacted with both IBM1 and MJJ27 (Figure 32A), and BiFC assay also showed that co-transformation of AMS and IBM1 or MJJ27 resulted in YFP signals in the nuclei (Figure 32B). No YFP signal in the control combinations was detected (Figure 32B). Around 30-40% of the nuclei with RFP signal also showed GFP signal in the co-transformation of AMS with IBM1 or MJJ27 (Figure 32C). Therefore, our results demonstrated that AMS interacts with both IBM1 and MJJ27.

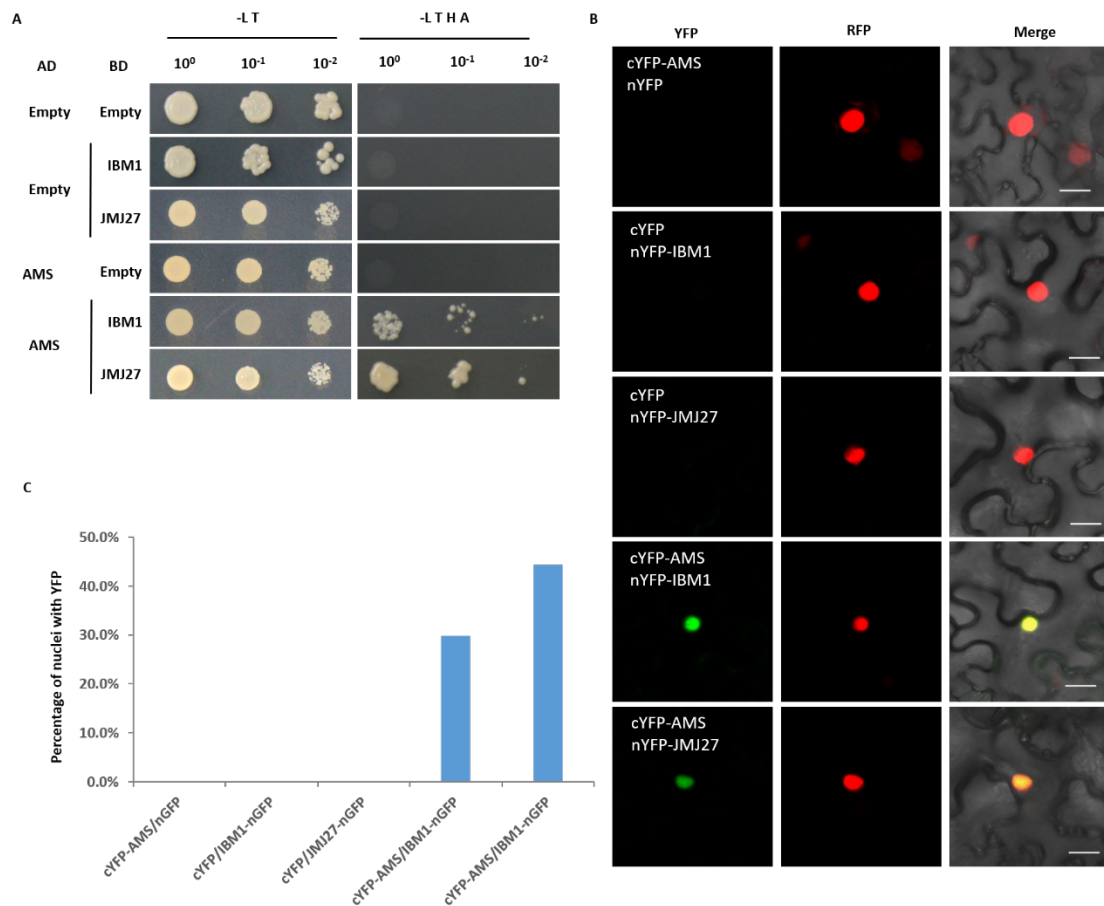


Figure 32. AMS interacts with IBM1 and JMJ27. (A) Yeast two-hybrid assay to test the interaction between AMS and IBM1, and JMJ27. Yeast cells (AH109 strain) containing both AD (activating domain) and BD (binding domain) vectors were grown on Synthetic Defined (SD) medium supplied with D-Glucose in the absence of Leu and Trp (SD/ -L T, left panel) as control, and on SD medium in the absence of Leu, Trp, His and Adenine (SD/ -LTHA, right panel) for the interaction test. (B) Bimolecular fluorescence complementation (BiFC) assays to test the interaction between AMS and IBM1, and JMJ27. YFP was split into cYFP and nYFP, and YFP signal indicated the interaction of the tested proteins. H3.3-RFP was used to indicate the nuclei. (C) Quantification of the nuclei with YFP signals to nuclei with RFP signals. The numbers of scored nuclei were shown above the bar.

3.2.3 IBM1 and JMJ27 activate *TEK* expression to regulate nexine formation

Given that AMS interacts with IBM1 and JMJ27, and TFs function in recruiting histone demethylases (Hung et al. 2020; Hung et al. 2021), I hypothesized that AMS is required for recruiting IBM1 and JMJ27 to remove H3K9me2. To test this hypothesis, I first compared gene expression between *ibm1 jmj27* and *ams*. Half of the downregulated genes in *ams* (Xu et al. 2014) were also silenced in *ibm1 jmj27* (Figure

33A). 24 genes required for pollen wall formation (listed in Table 2) have been confirmed as AMS targets (Xu et al. 2014). We have also checked the relative expression of these genes in *ibm1* and *ibm1 jmj27*. 17 out of 24 genes were silenced in *ibm1* and *ibm1 jmj27*, especially in *ibm1 jmj27* (Figure 33B). I further examined whether these downregulated genes also obtained H3K9me2. Indeed, 34 silenced genes obtained H3K9me2 in *ibm1 jmj27* (Figure 33C). *KCS7*, *KCS15*, and *TEK* are required for nexine layer formation (Xu et al. 2014; Lou et al. 2014), so I have further examined H3K9me2 levels at these gene regions. Indeed, *KCS7*, *KCS15*, and *TEK* obtained H3K9me2 in *ibm1 jmj27* (Figure 33D), indicating that *IBM1* and *JMJ27* control pollen wall formation by removing H3K9me2 from these loci.

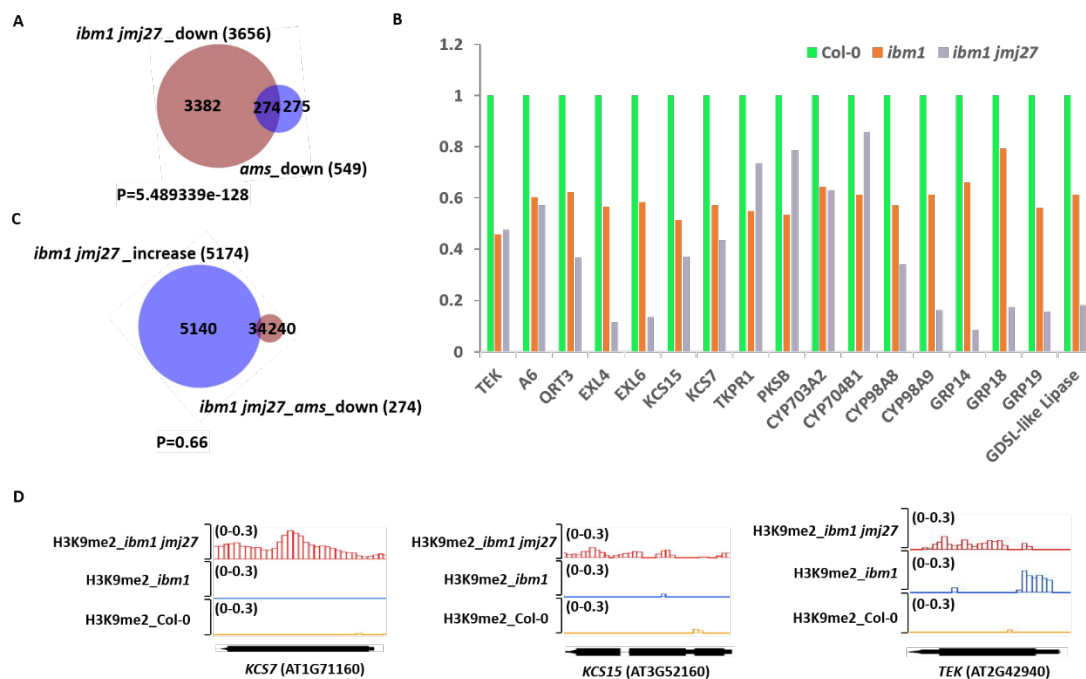


Figure 33. AMS targets were also downregulated with increased H3K9me2 levels in *ibm1 jmj27*.

(A) Venn diagram showing the overlap between downregulated gene in *ibm1 jmj27* and *ams*, the numbers in each category are indicated. (B) RNA-seq showing the relative expression level of AMS targets in *ibm1* and *ibm1 jmj27*, indicated by fold change value (Log FC). (C) Venn diagram showing the overlap between increased H3K9me2 genes and downregulated genes in *ibm1 jmj27* and *ams*. The numbers in each category are indicated. The *P*-value in A and C were calculated using hypergeometric test, sample size of $n=33547$ (the number of annotated protein-coding genes in Arabidopsis genome) was used. (D) ChIP-seq analysis of H3K9me2 levels in *ibm1* and *ibm1 jmj27*, and IBM1 enrichment at the indicated gene regions. H3K9me2 levels in wild type (black), *ibm1* (blue), *ibm1 jmj27* (red) at the indicated genes are shown. The values of H3K9me2 minus H3 represent the enrichment levels of H3K9me2.

Table 2: Genes directly regulated by AMS

Gene ID	Gene Name	Description	Reference
<i>AT1G75920</i>	<i>EXL5</i>	Family Ilextracellular lipase 5	Xu et al. (2010)
<i>AT1G75910</i>	<i>EXL4</i>	Family Ilextracellular lipase 4	Xu et al. (2014)
<i>AT1G75930</i>	<i>EXL6</i>	Family Ilextracellular lipase 6	Xu et al. (2014)
<i>AT1G69500</i>	<i>CYP704B1</i>	Cytochrome P450 704B1	Xu et al. (2014)
<i>AT1G01280</i>	<i>CYP703A2</i>	Cytochrome P450 703A2	Xu et al. (2014)
<i>AT1G74540</i>	<i>CYP98A8</i>	Cytochrome P450 98A8	Xu et al. (2014)
<i>AT1G74550</i>	<i>CYP98A9</i>	Cytochrome P450 98A9	Xu et al. (2014)
<i>AT1G13140</i>	<i>CYP86C3</i>	Cytochrome P450 CYP86C3	Xu et al. (2010)
<i>AT3G52160</i>	<i>KCS15</i>	β -Ketoacyl-CoA synthase 15	Xu et al. (2014)
<i>AT5G49070</i>	<i>KCS21</i>	β -Ketoacyl-CoA synthase 21	Xu et al. (2010)
<i>AT1G71160</i>	<i>KCS7</i>	β -Ketoacyl-CoA synthase 7	Xu et al. (2014)
<i>AT4G14080</i>	<i>A6</i>	Anther-specific protein 6	Xu et al. (2014)
<i>AT4G20050</i>	<i>QRT3</i>	Quartet 3	Xu et al. (2014)
<i>AT3G51590</i>	<i>LTP12</i>	Lipid transfer protein 12	Xu et al. (2010)
<i>AT1G66850</i>		LTP family protein	Xu et al. (2010)
<i>AT5G62080</i>		LTP family protein	Xu et al. (2014)
<i>AT3G13220</i>	<i>WBC27</i>	ABC transporter	Xu et al. (2010)
<i>AT4G34850</i>	<i>PKSB/LAP5</i>	Polyketide synthase B/Less adhesive pollen 5	Xu et al. (2014)
<i>AT4G35420</i>	<i>TKPR1/DRL1</i>	Tetraketide a-pyrone reductase	Xu et al. (2014)
<i>AT4G00040</i>	<i>CHS</i>	Chalcone synthase	Xu et al. (2010)
<i>AT1G06990</i>	<i>GDSL-like</i>	lipase/Extracellular lipase	Xu et al. (2014)
<i>AT5G07520</i>	<i>GRP18</i>	Glycine-rich protein18	Xu et al. (2014)
<i>AT5G07550</i>	<i>GRP19</i>	Glycine-rich protein19	Xu et al. (2014)
<i>AT2G42940</i>	<i>TEK/AHL16</i>	AT-HOOK motif nuclear-localized protein 16	Lou et al. (2014)

The table 2 is modified from Xu et al, 2014.

AGPs are directly regulated by *TEK* (Figure 34A) (Lou et al. 2014), and our data showed that *TEK* directly targeted by *IBM1/JMJ27*. Accordingly, *AGPs* should also be silenced in *ibm1* and *ibm1 jmj27*. Indeed, these *AGPs*, including *AGP6*, *AGP11*, *AGP23*, *AGP24*, and *AGP40*, were all silenced without increased H3K9me2 levels (Figure 34B and C), supporting the idea that *IBM1* and *JMJ27* directly regulate *TEK* expression, resulting in *AGPs* silencing indirectly.

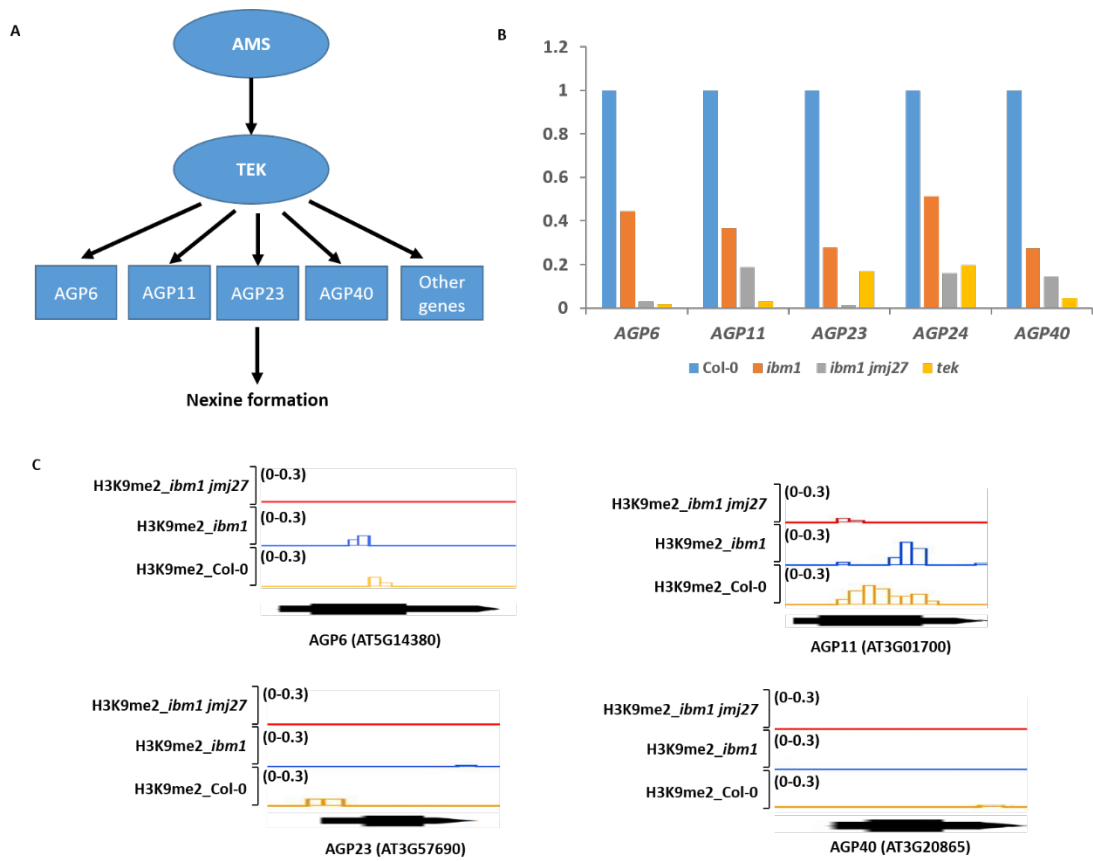


Figure 34. (A) Simplified regulatory network of nexine formation. (B) Gene expression of *TEK* target genes in the *ibm1* and *ibm1 jmj27* mutants by RNA-seq. (C) Chip-seq analysis of the H3K9me2 levels at the indicated gene regions in the *ibm1* and *ibm1 jmj27* mutants. H3K9me2 levels in Col-0 (yellow color), *ibm1* (blue color), and *ibm1 jmj27* (red color) at indicated genes were shown. The values of H3K9me2 minus H3 and obtained the enrichment levels of H3K9me2.

4 Discussion

Diploid sporophyte cells undergo meiosis to produce haploid spores. In flowering plants, haploid spores further develop into haploid gametes by two rounds of mitotic divisions. Genetic exchanges occur between parental genomes through meiotic recombination at prophase in meiosis I. In *Arabidopsis*, loss of H3K9 methylation results in the activation of chromosome recombination at the pericentromeric region, but the meiotic progression is largely normal. Our study showed that the H3K9 demethylases, IBM1 and JMJ27, are required for H3K9me2 removal from meiotic genes to activate their expression and ensure the meiotic progression.

Microspores produced through male meiosis finally develop into mature pollen. Pollen development has been well studied in both *Arabidopsis* and crop species (Wilson and Zhang 2009). This process, including anther wall and pollen wall formation, is essential for producing viable pollen grains. The pollen wall is composed of intine and exine, and exine is further divided into nexine and sexine. The *DYT1-TDF1-AMS-TEK* pathway regulates the nexine formation, while the *DYT1-TDF1-AMS-MS188* pathway regulates the sexine formation (Zhang et al. 2007; Xu et al. 2010; Lou et al. 2014; Dickinson and Heslop-Harrison 1968). As a transcription factor, AMS controls sexine formation by directly regulating the expression of *TEK* (Lou et al. 2014). Our present study further indicated that AMS recruits IBM1 and JMJ27 to the *TEK* loci, removing H3K9me2 and activating *TEK* expression. Hence, our results uncover a novel role of AMS in transcriptional regulation and exine formation.

4.1 Cooperation of H3K9 demethylases in plant development

There are 21 JmjC domain-containing proteins in *Arabidopsis*, which are grouped into five subgroups according to their substrate specificity. JMJ24 to JMJ29 are predicted to be H3K9 demethylases (Lu et al. 2008). Their roles in regulating flowering time have been well studied (Dutta et al. 2017; Hung et al. 2021). The *ibm1* and *jmj28* mutants show a late flowering phenotype (*ibm1* from this study, data not shown), while *jmj27* flowers earlier, indicating their different roles in regulating flowering time. The *jmj27* and *jmj28* mutants are all wild type like except for the flowering phenotypes while *ibm1* exhibits multiple developmental defects (Dutta et al. 2017; Saze et al. 2008; Hung et al. 2021). As mentioned above, *ibm1* mutant exhibits

reduced fertility, indicating a possible role of *IBM1* in reproductive. This study has elucidated the roles of histone demethylases *IBM1* and *JMJ27* in male meiosis.

H3K9 methylation is required for proper meiotic progression. In mammals, loss of H3K9 methylation leads to disordered progression of synaptonemal complex formation, causing severe meiosis defects (Tachibana et al. 2007). In *Arabidopsis*, loss of H3K9 methylation and CHG result in the activation of chromosome recombination at pericentromeric region, indicating the roles of histone methylation in meiosis. Whether histone demethylation is also functional in meiosis is unknown. By detecting mature pollen in *ibm1* with compromised *IBM1* demethylase activity, enlarged pollen was observed in the mutant (Figure 1). Missegregation of chromosomes often results in differential size of pollen grains (De Storme, Copenhaver, and Geelen 2012). Chromosome segregation occurs in meiosis to produce haploid pollen. Hence, tetrad analysis were performed to examine the meiotic products at tetrad stage. Around 25% abnormal meiotic products, including dyads, triads, polyads, were observed (Figure 2). Further cytological analysis showed that homologs pairing was abnormal in *ibm1* (Figure 9), indicating that H3K9 demethylation is required to ensure meiotic progression.

Recent studies demonstrate that *IBM1*, *JMJ27*, *JMJ28* and *JMJ29* have demethylase activity (Dutta et al. 2017; Saze et al. 2008; Hung et al. 2021; Hung et al. 2020). An interesting point is whether these H3K9 demethylases are functionally redundant in meiosis. To address this question, I first generated *ibm1 jmj27* double mutant. *ibm1 jmj27* was sterile with higher polyads frequency (Figure 5 and 6). The double mutants also exhibited more severe cytological meiosis defects (Figure 10) compared to the single mutants. Our results indicate that H3K9 demethylases can cooperatively regulate meiotic progression. Apart from *IBM1* and *JMJ27*, we found that the other H3K9 demethylases, at least *JMJ26* and *JMJ29*, are also functionally redundant. *ibm1 jmj26* and *ibm1 jmj29* showed similar developmental phenotypes to *ibm1 jmj27*, and both of them exhibited reduced fertility (data not shown), further study is needed to determine whether they are also functional in meiosis. These similar phenotypes indicate that their coordination is probably widespread. The overlap between the genome profiles of *IBM1*-occupied regions and increased H3K9me2 levels in *ibm1*, and *ibm1 jmj27* also indicates the widespread coordination of these H3K9

demethylases. Our data showed that 3193 genes are occupied by IBM1 without elevated H3K9me2 levels in both *ibm1* and *ibm1 jmj27*, suggesting that these regions need both IBM1 and other H3K9 demethylases to remove H3K9, and activate their expression. Collectively, our study indicates a role of H3K9 demethylases in meiosis, and also their coordination to regulate plant development.

Similar to H3K9 demethylases, *elf6* and *ref6*, two H3K27 demethylases mutants, also exhibit opposite flowering phenotypes. ELF6 activate *FLC* expression to repress flowering (Noh et al. 2004), while REF6 positively regulates flowering (Lu et al. 2011). Although they regulate flowering time in different ways, they are shown to set restriction boundary of H3K27me3 spatially and temporally together, allowing tissue-specific gene activation (Yan et al. 2018). Our results are consistent with the finding of H3K27 demethylases, indicating widespread coordination of histone demethylases.

4.2 H3K9m2 removal is required for Arabidopsis meiosis

Meiosis is under genetic and epigenetic control to ensure proper chromosomes segregation. Genes required for meiosis must be precisely regulated to ensure the proper meiotic progression. Until now, around 80 genes have been documented to function in *Arabidopsis* meiosis, and more than half of them are essential for proper meiotic progression (Yang et al. 2011; Ma 2006; Crismani and Mercier 2013). For instance, the kinetochore must be inactivated at prophase I to prevent the chromosomes from early separating. In the later stage, the kinetochores must be activated to allow the segregation of chromosomes and produce the daughter cells. Activation and inactivation of kinetochore are controlled by the relative expression level of Ndc80 protein (Chen et al. 2017). In this study, we found that IBM1 and JMJ27 regulate meiotic crucial genes expression through H3K9me2 removal. In wild type, homologs are held together until anaphase I, while they were separated at diakinesis and metaphase I in *ibm1*, and the phenotypes were enhanced in *ibm1 jmj27*, subsequently affecting chromosomes segregation in later stages (Figure 9 and 10). Meiosis crucial genes including *ZYP1*, *ASY1* required for chromosome synapsis, and *SHOC1*, *ZIP4* for crossover (Macaisne et al. 2008; Higgins et al. 2005; Chelysheva et al. 2007; Caryl et al. 2000) were silenced due to increased H3K9me2 levels in *ibm1 jmj27* (Figure 18), indicating that IBM1 and JMJ27 are required to activate these

meiosis crucial genes expression to ensure meiotic progression. In contrast, G9a, a histone H3K9 mono- and di- methyltransferase, is required for chromosome synapsis in mice. Gene expression is altered minimally in G9a which is thought to not cause meiosis defects (Tachibana et al. 2007), indicating the different mechanisms in regulating meiosis in plant and animal by histone methyltransferase and demethylase. We also found that IBM1 directly binds to these meiotic genes. We reasoned that IBM1 and/or JMJ27 can directly bind to the meiotic gene loci to remove H3K9me2 and activate their expression.

Chromosomes are three-dimensionally organized in the nucleus of eukaryotes (Sexton et al. 2012; Jin et al. 2013; Feng et al. 2014; Dixon et al. 2012). Different chromosome regions can interact with each other during the chromosome folding to participate in many important biological processes, including genome integrity maintenance, regulation of gene expression, and silent chromatin formation (Sexton et al. 2012; Jin et al. 2013; Dixon et al. 2012). Chromatin interaction can form the interactive domains, termed topologically associated domains (TAD). These domains are all highly related with epigenetic modifications (Sexton et al. 2012; Dixon et al. 2012). CTCF transcription factors, a key player in TAD establishment and chromatin loops formation in animals, are absent in Arabidopsis. However, similar chromatin loop is also observed in Arabidopsis. Mutation of *CLF*, a H3K27 methyltransferase, leads to the interaction between H3K27me3-loss regions and H3K9ac-marked regions (Huang et al. 2021). H3K9me2, a repressive mark, is mainly deposited at pericentromeric region but eliminated from gene body. Mutations of IBM1 and JMJ27, two H3K9 demethylases, lead to ectopic deposition of H3K9me2 at numerous gene body (Figure 12), leading to the redistribution of H3K9me2. Growing evidence shows that histone modifications alter chromatin condensation, which will affect genome topology and chromatin conformation, and these changes will ultimately regulate gene expression by modulating the accessibility of the transcriptional machinery to the gene locus (Huang et al. 2020; Rodriguez-Granados et al. 2016). Even many silenced genes obtain ectopic H3K9me2, there are still many genes that are silenced without increased H3K9me2 (Figure 17), indicating that these silenced

genes are not targeted directly by IBM1 and JMJ27. H3K27me3 is speculated to repress gene expression through inhibiting the interaction between H3K27me3-enriched regions and H3K9ac-marked regions. Thus, H3K9me2 is possible to regulate some of these genes in a similar way. In mammals, the DNA binding protein CTCF can recruit the cohesin to targets, promoting the loop formation between enhancers and promoters, which will further activate gene expression (Hansen et al. 2017). The interaction between IBM1 and JMJ27, and PDS5s also indicate the possible mechanisms that H3K9me2 regulate gene expression through chromatin conformation. To address this question, ATAC-seq (Assay for Transposase-Accessible Chromatin using sequencing) and Hi-C (High-throughput chromosome conformation capture) is required to test whether the chromatin structure is also affected in our mutants.

Crossover usually occurs at chromosome arms but absent in centromere (Lambing, Franklin, and Wang 2017; Choi and Henderson 2015) which is linked to enriched DNA methylation and histone methylation at pericentromeric region. In Arabidopsis, mutation of IBM leads to reduced chiasmata numbers (Figure 9), indicating the inhibition of crossover formation or redistribution of crossover. H3K9me2 is eliminated from euchromatin but enriched in heterochromatin in wild type Arabidopsis, and mutations of IBM1 and JMJ27 lead to the deposition of H3K9me2 along chromosome arms. It is possible that increased H3K9me2 levels along chromosome arms directly repress the recombination, leading to reduced crossovers formation. Therefore, in addition to regulate the expression of meiosis essential genes, our data also suggests a possible role of histone demethylases in regulating meiosis through H3K9me2 redistribution on chromosome arms.

In summary, our results indicate that IBM1 and JMJ27 may regulate meiotic progression in three ways: 1) IBM1 and/or JMJ27 directly bind at meiotic genes to remove H3K9me2 and activate their expression. 2) Removal of H3K9me2 can also alter chromatin structure to further affect meiotic gene expression. 3) Removal of H3K9 affects essential meiotic progression, such as crossover formation, without altering gene expression.

4.3 PDS5s act downstream of H3K9me2 to regulate meiotic gene expression

The roles of cohesin are highly conserved in eukaryotes (Anderson et al. 2002; Sumara et al. 2000). The complex is critical to ensure the correct chromosome segregation in both mitosis and meiosis (Doutriaux et al. 1998; Pradillo et al. 2015b; Grelon et al. 2001). The cohesin complex is also involved in gene regulation (Wendt et al. 2008; Stedman et al. 2008; Schuldiner et al. 2008; Pauli et al. 2008; Parelho et al. 2008; Lengronne et al. 2004; Glynn et al. 2004). In yeast, remodeling the structure of chromatin (RSC) provides nucleosome-free regions for the cohesin loading, making the DNA accessible to transcription factors (Clapier et al. 2017). In *Drosophila*, Nipped-B, the ortholog of SCC2, affects the interaction between enhancer and promoter to regulate gene expression (Rollins, Morcillo, and Dorsett 1999). A recent study in mice shows that tissue-specific transcription factors can recruit the cohesin complex to targets, maintaining promoter-enhancer loops to regulate gene expression (Liu et al. 2021). In this study, a possible mechanism of how the cohesin complex regulates gene expression in Arabidopsis is elucidated. IBM1 and JMJ27 interact with the cohesin cofactors PDS5 proteins, including PDS5A, PDS5C, and PDS5E (Figure 20, 21 and Table 2). The mutation of *IBM1* and *JMJ27*, and *PDS5s* showed similar gene expression pattern (Figure 22). However, H3K9me2 levels were not altered in *pds5* (Figure 22), indicating that the cohesin cofactors PDS5s are required for meiotic gene activation but not the deposition of H3K9me2. So, PDS5s act downstream of H3K9me2 demethylation to activate meiotic genes expression. The abolishment of *REC8*, meiosis-specific cohesin factor that is replaced by SCC1 in mitosis, also leads to slightly reduced the expression of meiosis crucial genes, which were also silenced in *ibm1 jmj27* (Figure 23).

In yeast, PDS5 is required for homologs pairing and crossover formation (Song et al. 2021; Jin, Guacci, and Yu 2009). There are five PDS5 proteins in Arabidopsis, mutation of four PDS5s just leads to a weak meiosis defect (Pradillo et al. 2015b), possibly because another PDS5, PDS5D, is still functional. Meanwhile, *ibm1 jmj27* exhibits stronger homologs pairing and crossover defects (Figure 10), which is comparable to phenotypes in yeast *pds5*, suggesting that PDS5s are involved in meiotic progression acting downstream of IBM1 and JMJ27 in Arabidopsis. In addition, the loading of the cohesin needs SCC2-SCC4 loader complex. SCC2-SCC4

complex together with PDS5s are required for stable chromosome binding of cohesin at highly transcribed gene regions (Bhardwaj et al. 2016). However, our preliminary results showed that IBM1 and JMJ27 had no direct interaction with both SCC2 and SCC4, and chromosome spread results of *ibm1 jmj27* did not show abnormal sister chromatids segregation in the early stage (Figure 10), indicating that the cohesin loading is correct in the *ibm1 jmj27* mutant.

Collectively, possible mechanisms of how the histone demethylases regulate meiotic progression and also how the cohesin regulates gene expression are elucidated or hypothesized according to our preliminary results in this study. Mutations of IBM1 and JMJ27 lead to increased H3K9me2 levels along the chromosome arms which will probably repress the recombination at chromosome arms. Indeed, chiasmata numbers were reduced in *ibm1* (Figure 9), and the reduced chiasmata further affect chromosomes segregation in late stages. In addition, meiosis-crucial genes were silenced in *ibm1* and *ibm1 jmj27*. Gene silencing is possibly mediated by IBM1, JMJ27, and PDS5s in at least two ways. 1) IBM1 and JMJ27 remove the H3K9me2 from meiotic gene bodies, and PDS5s are recruited to the targets at the same time to activate their expression. 2) IBM1, JMJ27, and PDS5s affect the chromatin structure together without altering H3K9me2 levels at some loci, affected chromatin structure further activate meiotic genes expression. Together, they regulate gene expression by directly H3K9me2 removal or indirectly, such as affecting the chromatin structure or regulate upstream gene expression.

4.4 H3K9me2 removal is required for pollen wall development mediated by AMS recruitment

The pollen wall is composed of intine and exine, and exine is further divided into nexine and sexine. *DYT1-TDF1-AMS-TEK* pathway regulates nexine formation (Zhang et al. 2007; Xu et al. 2010; Lou et al. 2014; Dickinson and Heslop-Harrison 1968). AMS directly targets to *TEK* to regulate the nexine formation (Lou et al. 2014). In this study, we found that IBM1 and JMJ27 are required for nexine formation, and the nexine formation is defective in *ibm1* and *ibm1 jmj27* which is comparable to *tek* (Figure 27). *tek* is silenced with increased H3K9me2 levels in the *ibm1 jmj27* mutant (Figure 31). In general, the histone demethylases target to its targets via its DNA binding domain or its interactors. For example, C2H2 zinc-finger domains, which can

recognize the CTCTGYTY motifs (Y is equal to C/T), is required for the binding of REF6 to specific targets sites (Cui et al. 2016). JMJ28 regulates flowering time through its interactor FLOWERING BHLH (FBH) transcription factors (Hung et al. 2021). In this study, we found that IBM1 and JMJ27 interact with AMS, the bHLH transcription factor family protein required for extensive anther-expressed genes expression and pollen wall formation (Figure 30). IBM1-occupied regions are enriched with bHLH family binding motif G-box (CACGTG) (Toledo-Ortiz, Huq, and Quail 2003), indicating that AMS is probably required for IBM1 and JMJ27 targeting to their targets. The identification of IBM1 and JMJ27 interaction proteins further elucidate the mechanism of how nexine related genes are activated by AMS and TEK. Whether the mutation of *AMS* will lead to the abolishment of IBM1 binding at *TEK* still needs to be confirmed. In addition to *TEK*, many other genes that are required for pollen wall formation, including *KCS7*, *KCS15*, *CYP86C3*, *CYP98A8*, *CYP98A9* were also downregulated (Figure 31). Sporopollenin, consisting of complex biopolymers derived mainly from phenolic compounds and long-chain fatty acids, is the main component of the pollen wall (Bubert et al. 2002). *CYP98A8* and *CYP98A9* are the enzymes required for the production of phenolic precursors, and *KCS7*, *KCS15* are required for fatty acid elongation. All these four genes were also silenced with elevated H3K9me levels in *ibm1* and *ibm1 jmj27*. Besides, they are also the direct targets of AMS. Similar to *TEK*, these genes are also possibly the targets of IBM1 and JMJ27 mediated by AMS recruitment. Together, these results indicate a possible mechanism that AMS recruit IBM1 and JMJ27 to the targets to active their expression, and regulate pollen wall formation.

5 Summary

Histone methylation is involved in many important processes in eukaryotes, and its function in meiosis have been studied in mammals. In *Arabidopsis*, loss of H3K9me2 or non-CG methylation leads to the activation of crossover (CO) near centromere without affecting plant fertility. H3K9me2 is a silencing mark which is mainly enriched at the pericentromeric region to silence TEs and other repeat sequences to keep the genome stability. It is eliminated at most active gene regions to protect them from silencing in wild-type *Arabidopsis*. Mutation of IBM1, a member of the JmjC domain-containing family, results in ectopic deposition of H3K9me2 at thousands of gene bodies, leading to pleiotropic development defects. However, its function in meiosis is unknown.

In my recent study, I first analysed the phenotypes of *ibm1* at the meiotic stage, as *ibm1* exhibits reduced fertility. Tetrad formation analysis showed that the *ibm1* mutant produces around 25% abnormal meiotic products, including dyads, triads and polyads. I also found that JMJ27, another H3K9me demethylase, was functionally redundant with IBM1. The *ibm1 jmj27* double mutant showed much stronger phenotypes compared to the *ibm1* single mutant. Further cytological analysis showed that the mutants showed bivalent formation defects during meiosis, indicating that IBM1 and JMJ27 are required for the bivalent formation. To test the hypothesis, I firstly performed Chip-seq with antibody against anti-H3K9me2. Genome-wide analysis showed that thousands of genes obtained ectopic H3K9me2, and many meiotic genes are among them. H3K9me2 is a silencing mark, I further examined whether the increase in H3K9me2 resulted in gene silencing. RNA-seq results showed that numerous genes were downregulated, and most of the downregulated genes also obtained ectopic H3K9me2, indicating that gene silencing was caused by increased H3K9me2 levels. Meiotic genes that were required for the proper bivalent formation, including *ZYP1*, *ASY1* required for chromosome synapsis, and *SHOC1*, *ZIP4* for crossover (Macaisne et al. 2008; Higgins et al. 2005; Chelysheva et al. 2007; Caryl et al. 2000). The direct binding of IBM1 to these loci have been confirmed by Chip-seq with antibody against anti-GFP using *proIBM1-IBM1-GFP/ibm1* lines. These results indicated that IBM1 and JMJ27 directly bind to these meiotic genes to remove H3K9me2 and active gene expression, which

is required for proper meiotic process.

To identify the interactors of IBM1 and JMJ27 that are required for H3K9me2-mediated gene silencing, I performed AP-MS and around 300 candidates have been identified. Several PDS5 proteins, including PDS5A, PDS5D, and PDS5E are among them with very high scores, indicating their strong interaction. PDS5 proteins are the cohesin cofactors required to load and unload the cohesin to the chromosomes. We found that *ibm1 jmj27* and *pds5* exhibited similar gene expression pattern, but without ectopic H3K9me2 deposition in *pds5*, indicating that PDS5s act downstream of H3K9 demethylation to activate gene expression. Our results explain a possible mechanism of how the cohesin regulate gene expression in Arabidopsis.

Besides, I have found that H3K9 demethylation-mediated gene activation is cell-type dependent. During the anther development, a bHLH transcription factor AMS is required for the recruitment of IBM1 and JMJ27. The interaction between IBM1, JMJ27 and AMS leads to the recruitment of IBM1 and JMJ27 to the targets, which is required for gene activation to regulate nexine formation. The *ibm1 jmj27* mutant showed defective nexine formation, indicating their function during pollen wall formation.

Taken together, my results demonstrated the function of H3K9 demethylation at different developmental stages in *Arabidopsis*, including meiosis and anther development. Different factors are required for H3K9 demethylation-mediated gene activation, and they are cell-type dependent. At the same time, our results also explained the mechanisms of how the cohesin complex regulates gene expression in plants.

6 Reference

- Alvarez-Venegas, R., S. Pien, M. Sadler, X. Witmer, U. Grossniklaus, and Z. Avramova. 2003. 'ATX-1, an Arabidopsis homolog of trithorax, activates flower homeotic genes', *Curr Biol*, 13: 627-37.
- Alves-Ferreira, M., F. Wellmer, A. Banhara, V. Kumar, J. L. Riechmann, and E. M. Meyerowitz. 2007. 'Global expression profiling applied to the analysis of Arabidopsis stamen development', *Plant Physiol*, 145: 747-62.
- Anderson, D. E., A. Losada, H. P. Erickson, and T. Hirano. 2002. 'Condensin and cohesin display different arm conformations with characteristic hinge angles', *J Cell Biol*, 156: 419-24.
- Antosz, W., A. Pfab, H. F. Ehrnsberger, P. Holzinger, K. Kollen, S. A. Mortensen, A. Bruckmann, T. Schubert, G. Langst, J. Griesenbeck, V. Schubert, M. Grasser, and K. D. Grasser. 2017. 'The Composition of the Arabidopsis RNA Polymerase II Transcript Elongation Complex Reveals the Interplay between Elongation and mRNA Processing Factors', *Plant Cell*, 29: 854-70.
- Antunez-Sanchez, J., M. Naish, J. S. Ramirez-Prado, S. Ohno, Y. Huang, A. Dawson, K. Opasathian, D. Manza-Mianza, F. Ariel, C. Raynaud, A. Wibowo, J. Daron, M. Ueda, D. Latrasse, R. K. Slotkin, D. Weigel, M. Benhamed, and J. Gutierrez-Marcos. 2020. 'A new role for histone demethylases in the maintenance of plant genome integrity', *Elife*, 9.
- Ariizumi, T., K. Hatakeyama, K. Hinata, S. Sato, T. Kato, S. Tabata, and K. Toriyama. 2003. 'A novel male-sterile mutant of Arabidopsis thaliana, faceless pollen-1, produces pollen with a smooth surface and an acetolysis-sensitive exine', *Plant Mol Biol*, 53: 107-16.
- Ariizumi, T., and K. Toriyama. 2011. 'Genetic regulation of sporopollenin synthesis and pollen exine development', *Annu Rev Plant Biol*, 62: 437-60.
- Armstrong, S. J., and G. H. Jones. 2003. 'Meiotic cytology and chromosome behaviour in wild-type Arabidopsis thaliana', *J Exp Bot*, 54: 1-10.
- Arnaudo, A. M., and B. A. Garcia. 2013. 'Proteomic characterization of novel histone post-translational modifications', *Epigenetics Chromatin*, 6: 24.
- Ballas, N., E. Battaglioli, F. Atouf, M. E. Andres, J. Chenoweth, M. E. Anderson, C. Burger, M. Moniwa, J. R. Davie, W. J. Bowers, H. J. Federoff, D. W. Rose, M. G. Rosenfeld, P. Brehm, and G. Mandel. 2001. 'Regulation of neuronal traits by a novel transcriptional complex', *Neuron*, 31: 353-65.
- Barbero, J. L. 2009. 'Cohesins: chromatin architects in chromosome segregation, control of gene expression and much more', *Cell Mol Life Sci*, 66: 2025-35.
- Barski, A., S. Cuddapah, K. Cui, T. Y. Roh, D. E. Schones, Z. Wang, G. Wei, I. Chepelev, and K. Zhao. 2007. 'High-resolution profiling of histone methylations in the human genome', *Cell*, 129: 823-37.
- Battaglioli, E., M. E. Andres, D. W. Rose, J. G. Chenoweth, M. G. Rosenfeld, M. E. Anderson, and G. Mandel. 2002. 'REST repression of neuronal genes requires components of the hSWI.SNF complex', *J Biol Chem*, 277: 41038-45.
- Baudat, F., and A. Nicolas. 1997. 'Clustering of meiotic double-strand breaks on yeast chromosome III', *Proc Natl Acad Sci U S A*, 94: 5213-8.
- Berchowitz, L. E., and G. P. Copenhaver. 2010. 'Genetic interference: don't stand so close to me', *Curr Genomics*, 11: 91-102.
- Bergerat, A., B. de Massy, D. Gabelle, P. C. Varoutas, A. Nicolas, and P. Forterre. 1997. 'An atypical

- topoisomerase II from Archaea with implications for meiotic recombination', *Nature*, 386: 414-7.
- Bernatavichute, Y. V., X. Zhang, S. Cokus, M. Pellegrini, and S. E. Jacobsen. 2008. 'Genome-wide association of histone H3 lysine nine methylation with CHG DNA methylation in *Arabidopsis thaliana*', *PLoS One*, 3: e3156.
- Bhardwaj, S., M. Schlackow, M. Rabajdova, and M. Gullerova. 2016. 'Transcription facilitates sister chromatid cohesion on chromosomal arms', *Nucleic Acids Res*, 44: 6676-92.
- Bishop, D. K., D. Park, L. Xu, and N. Kleckner. 1992. 'DMC1: a meiosis-specific yeast homolog of *E. coli* recA required for recombination, synaptonemal complex formation, and cell cycle progression', *Cell*, 69: 439-56.
- Black, J. C., C. Van Rechem, and J. R. Whetstone. 2012. 'Histone lysine methylation dynamics: establishment, regulation, and biological impact', *Mol Cell*, 48: 491-507.
- Bolanos-Villegas, P., K. De, M. Pradillo, D. Liu, and C. A. Makaroff. 2017. 'In Favor of Establishment: Regulation of Chromatid Cohesion in Plants', *Front Plant Sci*, 8: 846.
- Börner, G. Valentin, Nancy Kleckner, and Neil Hunter. 2004. 'Crossover/noncrossover differentiation, synaptonemal complex formation, and regulatory surveillance at the leptotene/zygotene transition of meiosis', *Cell*.
- Bubert, H., J. Lambert, S. Steuernagel, F. Ahlers, and R. Wiermann. 2002. 'Continuous decomposition of sporopollenin from pollen of *Typha angustifolia* L. by acidic methanolysis', *Z Naturforsch C J Biosci*, 57: 1035-41.
- Bulut-Karslioglu, A., V. Perrera, M. Scaranaro, I. A. de la Rosa-Velazquez, S. van de Nobelen, N. Shukeir, J. Popow, B. Gerle, S. Opravil, M. Pagani, S. Meidhof, T. Brabletz, T. Manke, M. Lachner, and T. Jenuwein. 2012. 'A transcription factor-based mechanism for mouse heterochromatin formation', *Nat Struct Mol Biol*, 19: 1023-30.
- Burgess, S. M. 2002. 'Homologous chromosome associations and nuclear order in meiotic and mitotically dividing cells of budding yeast', *Adv Genet*, 46: 49-90.
- Capilla-Perez, L., S. Durand, A. Hurel, Q. Lian, A. Chambon, C. Taochy, V. Solier, M. Grelon, and R. Mercier. 2021. 'The synaptonemal complex imposes crossover interference and heterochiasmy in *Arabidopsis*', *Proc Natl Acad Sci U S A*, 118.
- Caryl, A. P., S. J. Armstrong, G. H. Jones, and F. C. Franklin. 2000. 'A homologue of the yeast HOP1 gene is inactivated in the *Arabidopsis* meiotic mutant *asy1*', *Chromosoma*, 109: 62-71.
- Chanvivattana, Y., A. Bishopp, D. Schubert, C. Stock, Y. H. Moon, Z. R. Sung, and J. Goodrich. 2004. 'Interaction of Polycomb-group proteins controlling flowering in *Arabidopsis*', *Development*, 131: 5263-76.
- Chelysheva, L., G. Gendrot, D. Vezon, M. P. Doutriaux, R. Mercier, and M. Grelon. 2007. 'Zip4/Spo22 is required for class I CO formation but not for synapsis completion in *Arabidopsis thaliana*', *PLoS Genet*, 3: e83.
- Chelysheva, L., D. Vezon, A. Chambon, G. Gendrot, L. Pereira, A. Lemhemdi, N. Vrielynck, S. Le Guin, M. Novatchkova, and M. Grelon. 2012. 'The *Arabidopsis* HEI10 is a new ZMM protein related to Zip3', *PLoS Genet*, 8: e1002799.
- Chen, C., H. Chen, Y. Zhang, H. R. Thomas, M. H. Frank, Y. He, and R. Xia. 2020. 'TBtools: An Integrative Toolkit Developed for Interactive Analyses of Big Biological Data', *Mol Plant*, 13: 1194-202.
- Chen, J., A. Tresenrider, M. Chia, D. T. McSwiggen, G. Spedale, V. Jorgensen, H. Liao, F. J. van Werven, and E. Unal. 2017. 'Kinetochores inactivation by expression of a repressive mRNA', *Elife*, 6.

- Chen, W., X. H. Yu, K. Zhang, J. Shi, S. De Oliveira, L. Schreiber, J. Shanklin, and D. Zhang. 2011. 'Male Sterile2 encodes a plastid-localized fatty acyl carrier protein reductase required for pollen exine development in Arabidopsis', *Plant Physiol*, 157: 842-53.
- Chen, Y., Y. Yang, F. Wang, K. Wan, K. Yamane, Y. Zhang, and M. Lei. 2006. 'Crystal structure of human histone lysine-specific demethylase 1 (LSD1)', *Proc Natl Acad Sci U S A*, 103: 13956-61.
- Cheng, J., R. Blum, C. Bowman, D. Hu, A. Shilatifard, S. Shen, and B. D. Dynlacht. 2014. 'A role for H3K4 monomethylation in gene repression and partitioning of chromatin readers', *Mol Cell*, 53: 979-92.
- Choi, H., J. Y. Jin, S. Choi, J. U. Hwang, Y. Y. Kim, M. C. Suh, and Y. Lee. 2011. 'An ABCG/WBC-type ABC transporter is essential for transport of sporopollenin precursors for exine formation in developing pollen', *Plant J*, 65: 181-93.
- Choi, K., and I. R. Henderson. 2015. 'Meiotic recombination hotspots - a comparative view', *Plant J*, 83: 52-61.
- Ciferri, C., G. C. Lander, A. Maiolica, F. Herzog, R. Aebersold, and E. Nogales. 2012. 'Molecular architecture of human polycomb repressive complex 2', *Elife*, 1: e00005.
- Ciosk, R., M. Shirayama, A. Shevchenko, T. Tanaka, A. Toth, A. Shevchenko, and K. Nasmyth. 2000. 'Cohesin's binding to chromosomes depends on a separate complex consisting of Scc2 and Scc4 proteins', *Mol Cell*, 5: 243-54.
- Clapier, C. R., J. Iwasa, B. R. Cairns, and C. L. Peterson. 2017. 'Mechanisms of action and regulation of ATP-dependent chromatin-remodelling complexes', *Nat Rev Mol Cell Biol*, 18: 407-22.
- Clements, A., A. N. Poux, W. S. Lo, L. Pillus, S. L. Berger, and R. Marmorstein. 2003. 'Structural basis for histone and phosphohistone binding by the GCN5 histone acetyltransferase', *Molecular Cell*, 12: 461-73.
- Cokus, S. J., S. Feng, X. Zhang, Z. Chen, B. Merriman, C. D. Haudenschild, S. Pradhan, S. F. Nelson, M. Pellegrini, and S. E. Jacobsen. 2008. 'Shotgun bisulphite sequencing of the Arabidopsis genome reveals DNA methylation patterning', *Nature*, 452: 215-9.
- Crismani, W., and R. Mercier. 2013. 'Identifying meiotic mutants in Arabidopsis thaliana', *Methods Mol Biol*, 990: 227-34.
- Cui, X., F. Lu, Q. Qiu, B. Zhou, L. Gu, S. Zhang, Y. Kang, X. Cui, X. Ma, Q. Yao, J. Ma, X. Zhang, and X. Cao. 2016. 'REF6 recognizes a specific DNA sequence to demethylate H3K27me3 and regulate organ boundary formation in Arabidopsis', *Nature Genetics*, 48: 694-9.
- Dawe, R. K. 1998. 'Meiotic Chromosome Organization and Segregation in Plants', *Annu Rev Plant Physiol Plant Mol Biol*, 49: 371-95.
- De, K., L. Sterle, L. Krueger, X. Yang, and C. A. Makaroff. 2014. 'Arabidopsis thaliana WAPL is essential for the prophase removal of cohesin during meiosis', *PLoS Genet*, 10: e1004497.
- De Storme, N., G. P. Copenhaver, and D. Geelen. 2012. 'Production of diploid male gametes in Arabidopsis by cold-induced destabilization of postmeiotic radial microtubule arrays', *Plant Physiol*, 160: 1808-26.
- Deng, S., I. C. Jang, L. Su, J. Xu, and N. H. Chua. 2016. 'JMJD2 targets CHROMOMETHYLASE3 for proteasomal degradation in Arabidopsis', *Genes Dev*, 30: 251-6.
- Dickinson, H. G., and J. Heslop-Harrison. 1968. 'Common mode of deposition for the sporopollenin of sexine and nexine', *Nature*, 220: 926-7.
- Dindar, G., A. M. Anger, C. Mehlhorn, S. B. Hake, and C. J. Janzen. 2014. 'Structure-guided mutational analysis reveals the functional requirements for product specificity of DOT1 enzymes', *Nat*

- Commun*, 5: 5313.
- Ding, Y., M. Fromm, and Z. Avramova. 2012. 'Multiple exposures to drought 'train' transcriptional responses in Arabidopsis', *Nat Commun*, 3: 740.
- Ding, Y., I. Ndamukong, Z. Xu, H. Lapko, M. Fromm, and Z. Avramova. 2012. 'ATX1-generated H3K4me3 is required for efficient elongation of transcription, not initiation, at ATX1-regulated genes', *PLoS Genet*, 8: e1003111.
- Dixon, J. R., S. Selvaraj, F. Yue, A. Kim, Y. Li, Y. Shen, M. Hu, J. S. Liu, and B. Ren. 2012. 'Topological domains in mammalian genomes identified by analysis of chromatin interactions', *Nature*, 485: 376-80.
- Dong, X., Z. Hong, M. Sivaramakrishnan, M. Mahfouz, and D. P. Verma. 2005. 'Callose synthase (CalS5) is required for exine formation during microgametogenesis and for pollen viability in Arabidopsis', *Plant J*, 42: 315-28.
- Dorsett, D. 2007. 'Roles of the sister chromatid cohesion apparatus in gene expression, development, and human syndromes', *Chromosoma*, 116: 1-13.
- Doutriaux, M. P., F. Couteau, C. Bergounioux, and C. White. 1998. 'Isolation and characterisation of the RAD51 and DMC1 homologs from Arabidopsis thaliana', *Mol Gen Genet*, 257: 283-91.
- Du, J., L. M. Johnson, S. E. Jacobsen, and D. J. Patel. 2015. 'DNA methylation pathways and their crosstalk with histone methylation', *Nat Rev Mol Cell Biol*, 16: 519-32.
- Dutta, A., P. Choudhary, J. Caruana, and R. Raina. 2017. 'JMJ27, an Arabidopsis H3K9 histone demethylase, modulates defense against *Pseudomonas syringae* and flowering time', *Plant J*, 91: 1015-28.
- Ebbs, M. L., and J. Bender. 2006. 'Locus-specific control of DNA methylation by the Arabidopsis SUVH5 histone methyltransferase', *Plant Cell*, 18: 1166-76.
- Eissenberg, J. C., T. C. James, D. M. Foster-Hartnett, T. Hartnett, V. Ngan, and S. C. Elgin. 1990. 'Mutation in a heterochromatin-specific chromosomal protein is associated with suppression of position-effect variegation in *Drosophila melanogaster*', *Proc Natl Acad Sci U S A*, 87: 9923-7.
- Fan, D., Y. Dai, X. Wang, Z. Wang, H. He, H. Yang, Y. Cao, X. W. Deng, and L. Ma. 2012. 'IBM1, a JmjC domain-containing histone demethylase, is involved in the regulation of RNA-directed DNA methylation through the epigenetic control of RDR2 and DCL3 expression in Arabidopsis', *Nucleic Acids Res*, 40: 8905-16.
- Feng, B., D. Lu, X. Ma, Y. Peng, Y. Sun, G. Ning, and H. Ma. 2012. 'Regulation of the Arabidopsis anther transcriptome by DYT1 for pollen development', *Plant J*, 72: 612-24.
- Feng, S., S. J. Cokus, V. Schubert, J. Zhai, M. Pellegrini, and S. E. Jacobsen. 2014. 'Genome-wide Hi-C analyses in wild-type and mutants reveal high-resolution chromatin interactions in Arabidopsis', *Mol Cell*, 55: 694-707.
- Ferguson, A. C., S. Pearce, L. R. Band, C. Yang, I. Ferjentsikova, J. King, Z. Yuan, D. Zhang, and Z. A. Wilson. 2017. 'Biphasic regulation of the transcription factor ABORTED MICROSPORES (AMS) is essential for tapetum and pollen development in Arabidopsis', *New Phytol*, 213: 778-90.
- Fornieris, F., E. Battaglioli, A. Mattevi, and C. Binda. 2009. 'New roles of flavoproteins in molecular cell biology: histone demethylase LSD1 and chromatin', *FEBS J*, 276: 4304-12.
- Fraser, W. T., A. C. Scott, A. E. S. Forbes, I. J. Glasspool, R. E. Plotnick, F. Kenig, and B. H. Lomax. 2012. 'Evolutionary stasis of sporopollenin biochemistry revealed by unaltered Pennsylvanian spores', *New Phytol*, 196: 397-401.

- Friedman, J. R., W. J. Fredericks, D. E. Jensen, D. W. Speicher, X. P. Huang, E. G. Neilson, and F. J. Rauscher, 3rd. 1996. 'KAP-1, a novel corepressor for the highly conserved KRAB repression domain', *Genes Dev*, 10: 2067-78.
- Glynn, E. F., P. C. Megee, H. G. Yu, C. Mistrot, E. Unal, D. E. Koshland, J. L. DeRisi, and J. L. Gerton. 2004. 'Genome-wide mapping of the cohesin complex in the yeast *Saccharomyces cerevisiae*', *PLoS Biol*, 2: E259.
- Goldberg, R. B., T. P. Beals, and P. M. Sanders. 1993. 'Anther development: basic principles and practical applications', *Plant Cell*, 5: 1217-29.
- Grelon, M., D. Vezon, G. Gendrot, and G. Pelletier. 2001. 'AtSPO11-1 is necessary for efficient meiotic recombination in plants', *EMBO J*, 20: 589-600.
- Gruber, S., C. H. Haering, and K. Nasmyth. 2003. 'Chromosomal cohesin forms a ring', *Cell*, 112: 765-77.
- Hahn, P., J. Bose, S. Edler, and A. Lengeling. 2008. 'Genomic structure and expression of Jmjd6 and evolutionary analysis in the context of related JmjC domain containing proteins', *BMC Genomics*, 9: 293.
- Hall, I. M., G. D. Shankaranarayana, K. Noma, N. Ayoub, A. Cohen, and S. I. Grewal. 2002. 'Establishment and maintenance of a heterochromatin domain', *Science*, 297: 2232-7.
- Hansen, A. S., I. Pustova, C. Cattoglio, R. Tjian, and X. Darzacq. 2017. 'CTCF and cohesin regulate chromatin loop stability with distinct dynamics', *Elife*, 6.
- Hara, K., G. Zheng, Q. Qu, H. Liu, Z. Ouyang, Z. Chen, D. R. Tomchick, and H. Yu. 2014. 'Structure of cohesin subcomplex pinpoints direct shugoshin-Wapl antagonism in centromeric cohesion', *Nat Struct Mol Biol*, 21: 864-70.
- Hartung, F., R. Wurzel-Wildersinn, J. Fuchs, I. Schubert, S. Suer, and H. Puchta. 2007. 'The catalytically active tyrosine residues of both SPO11-1 and SPO11-2 are required for meiotic double-strand break induction in Arabidopsis', *Plant Cell*, 19: 3090-9.
- He, Y., S. D. Michaels, and R. M. Amasino. 2003. 'Regulation of flowering time by histone acetylation in Arabidopsis', *Science*, 302: 1751-4.
- Hernandez-Pinzon, I., J. H. Ross, K. A. Barnes, A. P. Damant, and D. J. Murphy. 1999. 'Composition and role of tapetal lipid bodies in the biogenesis of the pollen coat of *Brassica napus*', *Planta*, 208: 588-98.
- Heyting, C. 1996. 'Synaptonemal complexes: Structure and function', *Current Opinion in Cell Biology*, 8: 389-96.
- Higgins, J. D., S. J. Armstrong, F. C. Franklin, and G. H. Jones. 2004. 'The Arabidopsis MutS homolog AtMSH4 functions at an early step in recombination: evidence for two classes of recombination in Arabidopsis', *Genes Dev*, 18: 2557-70.
- Higgins, J. D., E. F. Buckling, F. C. Franklin, and G. H. Jones. 2008. 'Expression and functional analysis of AtMUS81 in Arabidopsis meiosis reveals a role in the second pathway of crossing-over', *Plant J*, 54: 152-62.
- Higgins, J. D., E. Sanchez-Moran, S. J. Armstrong, G. H. Jones, and F. C. Franklin. 2005. 'The Arabidopsis synaptonemal complex protein ZYP1 is required for chromosome synapsis and normal fidelity of crossing over', *Genes Dev*, 19: 2488-500.
- Hsieh, K., and A. H. Huang. 2005. 'Lipid-rich tapetosomes in Brassica tapetum are composed of oleosin-coated oil droplets and vesicles, both assembled in and then detached from the endoplasmic reticulum', *Plant J*, 43: 889-99.

- Huang, Y., N. Y. Rodriguez-Granados, D. Latrasse, C. Raynaud, M. Benhamed, and J. S. Ramirez-Prado. 2020. 'The matrix revolutions: towards the decoding of the plant chromatin three-dimensional reality', *J Exp Bot*, 71: 5129-47.
- Huang, Y., S. Sicar, J. S. Ramirez-Prado, D. Manza-Mianza, J. Antunez-Sanchez, R. Brik-Chaouche, N. Y. Rodriguez-Granados, J. An, C. Bergounioux, M. M. Mahfouz, H. Hirt, M. Crespi, L. Concia, F. Barneche, S. Amiard, A. V. Probst, J. Gutierrez-Marcos, F. Ariel, C. Raynaud, D. Latrasse, and M. Benhamed. 2021. 'Polycomb-dependent differential chromatin compartmentalization determines gene coregulation in Arabidopsis', *Genome Res*.
- Hung, F. Y., J. H. Chen, Y. R. Feng, Y. C. Lai, S. Yang, and K. Wu. 2020. 'Arabidopsis JMJ29 is involved in trichome development by regulating the core trichome initiation gene GLABRA3', *Plant Journal*, 103: 1735-43.
- Hung, F. Y., Y. C. Lai, J. Wang, Y. R. Feng, Y. H. Shih, J. H. Chen, H. C. Sun, S. Yang, C. Li, and K. Wu. 2021. 'The Arabidopsis histone demethylase JMJ28 regulates CONSTANS by interacting with FBH transcription factors', *Plant Cell*.
- Inagaki, S., A. Miura-Kamio, Y. Nakamura, F. Lu, X. Cui, X. Cao, H. Kimura, H. Saze, and T. Kakutani. 2010. 'Autocatalytic differentiation of epigenetic modifications within the Arabidopsis genome', *EMBO J*, 29: 3496-506.
- Inagaki, S., M. Takahashi, A. Hosaka, T. Ito, A. Toyoda, A. Fujiyama, Y. Tarutani, and T. Kakutani. 2017. 'Gene-body chromatin modification dynamics mediate epigenome differentiation in Arabidopsis', *EMBO J*, 36: 970-80.
- Ishihara, H., K. Sugimoto, P. T. Tarr, H. Temman, S. Kadokura, Y. Inui, T. Sakamoto, T. Sasaki, M. Aida, T. Suzuki, S. Inagaki, K. Morohashi, M. Seki, T. Kakutani, E. M. Meyerowitz, and S. Matsunaga. 2019. 'Primed histone demethylation regulates shoot regenerative competency', *Nat Commun*, 10: 1786.
- Ito, T., N. Nagata, Y. Yoshida, M. Ohme-Takagi, H. Ma, and K. Shinozaki. 2007. 'Arabidopsis MALE STERILITY1 encodes a PHD-type transcription factor and regulates pollen and tapetum development', *Plant Cell*, 19: 3549-62.
- Ivanova, A. V., M. J. Bonaduce, S. V. Ivanov, and A. J. Klar. 1998. 'The chromo and SET domains of the Ctr4 protein are essential for silencing in fission yeast', *Nat Genet*, 19: 192-5.
- J, Heslop-Harrison. 1968. 'Tapetal origin of pollen-coat substances in Liliaceae', *New Phytol*
- Jiang, D., N. C. Kong, X. Gu, Z. Li, and Y. He. 2011. 'Arabidopsis COMPASS-like complexes mediate histone H3 lysine-4 trimethylation to control floral transition and plant development', *PLoS Genet*, 7: e1001330.
- Jiang, D., W. Yang, Y. He, and R. M. Amasino. 2007. 'Arabidopsis relatives of the human lysine-specific Demethylase1 repress the expression of FWA and FLOWERING LOCUS C and thus promote the floral transition', *Plant Cell*, 19: 2975-87.
- Jiang, J., Z. Zhang, and J. Cao. 2013. 'Pollen wall development: the associated enzymes and metabolic pathways', *Plant Biol (Stuttg)*, 15: 249-63.
- Jin, F., Y. Li, J. R. Dixon, S. Selvaraj, Z. Ye, A. Y. Lee, C. A. Yen, A. D. Schmitt, C. A. Espinoza, and B. Ren. 2013. 'A high-resolution map of the three-dimensional chromatin interactome in human cells', *Nature*, 503: 290-4.
- Jin, H., V. Guacci, and H. G. Yu. 2009. 'Pds5 is required for homologue pairing and inhibits synapsis of sister chromatids during yeast meiosis', *J Cell Biol*, 186: 713-25.
- Johnson, L. M., M. Bostick, X. Zhang, E. Kraft, I. Henderson, J. Callis, and S. E. Jacobsen. 2007. 'The SRA

- methyl-cytosine-binding domain links DNA and histone methylation', *Current Biology*, 17: 379-84.
- Jones, R. S., and W. M. Gelbart. 1993. 'The Drosophila Polycomb-group gene Enhancer of zeste contains a region with sequence similarity to trithorax', *Mol Cell Biol*, 13: 6357-66.
- Kim, D., J. M. Paggi, C. Park, C. Bennett, and S. L. Salzberg. 2019. 'Graph-based genome alignment and genotyping with HISAT2 and HISAT-genotype', *Nat Biotechnol*, 37: 907-15.
- Kinoshita, T., R. Yadegari, J. J. Harada, R. B. Goldberg, and R. L. Fischer. 1999. 'Imprinting of the MEDEA polycomb gene in the Arabidopsis endosperm', *Plant Cell*, 11: 1945-52.
- Kohler, C., D. R. Page, V. Gagliardini, and U. Grossniklaus. 2005. 'The Arabidopsis thaliana MEDEA Polycomb group protein controls expression of PHERES1 by parental imprinting', *Nat Genet*, 37: 28-30.
- Kueng, S., B. Hegemann, B. H. Peters, J. J. Lipp, A. Schleiffer, K. Mechtler, and J. M. Peters. 2006. 'Wapl controls the dynamic association of cohesin with chromatin', *Cell*, 127: 955-67.
- Lambing, C., K. Choi, A. R. Blackwell, and I. R. Henderson. 2020. 'Chromatin Immunoprecipitation of Meiotically Expressed Proteins from Arabidopsis thaliana Flowers', *Methods Mol Biol*, 2061: 219-36.
- Lambing, C., F. C. Franklin, and C. R. Wang. 2017. 'Understanding and Manipulating Meiotic Recombination in Plants', *Plant Physiol*, 173: 1530-42.
- Lamke, J., K. Brzezinka, S. Altmann, and I. Baurle. 2016. 'A hit-and-run heat shock factor governs sustained histone methylation and transcriptional stress memory', *EMBO J*, 35: 162-75.
- Lengronne, A., Y. Katou, S. Mori, S. Yokobayashi, G. P. Kelly, T. Itoh, Y. Watanabe, K. Shirahige, and F. Uhlmann. 2004. 'Cohesin relocation from sites of chromosomal loading to places of convergent transcription', *Nature*, 430: 573-8.
- Lengronne, A., J. McIntyre, Y. Katou, Y. Kanoh, K. P. Hopfner, K. Shirahige, and F. Uhlmann. 2006. 'Establishment of sister chromatid cohesion at the S. cerevisiae replication fork', *Mol Cell*, 23: 787-99.
- Liao, Y., G. K. Smyth, and W. Shi. 2019. 'The R package Rsubread is easier, faster, cheaper and better for alignment and quantification of RNA sequencing reads', *Nucleic Acids Res*, 47: e47.
- Lichten, M. 2001. 'Meiotic recombination: breaking the genome to save it', *Curr Biol*, 11: R253-6.
- Lister, R., R. C. O'Malley, J. Tonti-Filippini, B. D. Gregory, C. C. Berry, A. H. Millar, and J. R. Ecker. 2008. 'Highly integrated single-base resolution maps of the epigenome in Arabidopsis', *Cell*, 133: 523-36.
- Litwin, I., E. Pilarczyk, and R. Wysocki. 2018. 'The Emerging Role of Cohesin in the DNA Damage Response', *Genes (Basel)*, 9.
- Liu, C., F. Lu, X. Cui, and X. Cao. 2010. 'Histone methylation in higher plants', *Annu Rev Plant Biol*, 61: 395-420.
- Liu, N. Q., M. Maresca, T. van den Brand, L. Braccioli, Mmga Schijns, H. Teunissen, B. G. Bruneau, E. P. Nora, and E. de Wit. 2021. 'WAPL maintains a cohesin loading cycle to preserve cell-type-specific distal gene regulation', *Nat Genet*, 53: 100-09.
- Lou, Y., X. F. Xu, J. Zhu, J. N. Gu, S. Blackmore, and Z. N. Yang. 2014. 'The tapetal AHL family protein TEK determines nexine formation in the pollen wall', *Nat Commun*, 5: 3855.
- Love, M. I., W. Huber, and S. Anders. 2014. 'Moderated estimation of fold change and dispersion for RNA-seq data with DESeq2', *Genome Biol*, 15: 550.
- Lu, F., X. Cui, S. Zhang, T. Jenuwein, and X. Cao. 2011. 'Arabidopsis REF6 is a histone H3 lysine 27

- demethylase', *Nat Genet*, 43: 715-9.
- Lu, F., X. Cui, S. Zhang, C. Liu, and X. Cao. 2010. 'JM14 is an H3K4 demethylase regulating flowering time in Arabidopsis', *Cell Res*, 20: 387-90.
- Lu, F., G. Li, X. Cui, C. Liu, X. J. Wang, and X. Cao. 2008. 'Comparative analysis of JmjC domain-containing proteins reveals the potential histone demethylases in Arabidopsis and rice', *J Integr Plant Biol*, 50: 886-96.
- Luger, K., A. W. Mader, R. K. Richmond, D. F. Sargent, and T. J. Richmond. 1997. 'Crystal structure of the nucleosome core particle at 2.8 Å resolution', *Nature*, 389: 251-60.
- Lynch, J. T., W. J. Harris, and T. C. Somerville. 2012. 'LSD1 inhibition: a therapeutic strategy in cancer?', *Expert Opin Ther Targets*, 16: 1239-49.
- Ma, H. 2006. 'A molecular portrait of Arabidopsis meiosis', *Arabidopsis Book*, 4: e0095.
- Ma, LiJuan, ZhongNan Yang, and Sen Zhang. 2013. 'DEX1, a plasma membrane-localized protein, functions in microspore development by affecting CalS5 expression in Arabidopsis thaliana', *Chinese Science Bulletin*.
- Macaisne, N., M. Novatchkova, L. Peirera, D. Vezon, S. Jolivet, N. Froger, L. Chelysheva, M. Grelon, and R. Mercier. 2008. 'SHOC1, an XPF endonuclease-related protein, is essential for the formation of class I meiotic crossovers', *Curr Biol*, 18: 1432-7.
- MacQueen, A. J., M. P. Colaiacovo, K. McDonald, and A. M. Villeneuve. 2002. 'Synapsis-dependent and -independent mechanisms stabilize homolog pairing during meiotic prophase in C-elegans', *Genes & Development*, 16: 2428-42.
- Maeda, I., D. Okamura, Y. Tokitake, M. Ikeda, H. Kawaguchi, N. Mise, K. Abe, T. Noce, A. Okuda, and Y. Matsui. 2013. 'Max is a repressor of germ cell-related gene expression in mouse embryonic stem cells', *Nat Commun*, 4: 1754.
- Makrantonis, V., and A. L. Marston. 2018. 'Cohesin and chromosome segregation', *Curr Biol*, 28: R688-R93.
- Martin, K., K. Kopperud, R. Chakrabarty, R. Banerjee, R. Brooks, and M. M. Goodin. 2009. 'Transient expression in Nicotiana benthamiana fluorescent marker lines provides enhanced definition of protein localization, movement and interactions in planta', *Plant J*, 59: 150-62.
- Martini, E., R. L. Diaz, N. Hunter, and S. Keeney. 2006. 'Crossover homeostasis in yeast meiosis', *Cell*, 126: 285-95.
- McKim, K. S., B. L. Green-Marroquin, J. J. Sekelsky, G. Chin, C. Steinberg, R. Khodosh, and R. S. Hawley. 1998. 'Meiotic synapsis in the absence of recombination', *Science*, 279: 876-8.
- Mercier, R., S. Jolivet, D. Vezon, E. Huppe, L. Chelysheva, M. Giovanni, F. Nogue, M. P. Doutriaux, C. Horlow, M. Grelon, and C. Mezard. 2005. 'Two meiotic crossover classes cohabit in Arabidopsis: one is dependent on MER3, whereas the other one is not', *Curr Biol*, 15: 692-701.
- Metzger, E., M. Wissmann, N. Yin, J. M. Muller, R. Schneider, A. H. Peters, T. Gunther, R. Buettner, and R. Schule. 2005. 'LSD1 demethylates repressive histone marks to promote androgen-receptor-dependent transcription', *Nature*, 437: 436-9.
- Miura, A., M. Nakamura, S. Inagaki, A. Kobayashi, H. Saze, and T. Kakutani. 2009. 'An Arabidopsis jmjC domain protein protects transcribed genes from DNA methylation at CHG sites', *EMBO J*, 28: 1078-86.
- Morant, M., K. Jorgensen, H. Schaller, F. Pinot, B. L. Moller, D. Werck-Reichhart, and S. Bak. 2007. 'CYP703 is an ancient cytochrome P450 in land plants catalyzing in-chain hydroxylation of

- lauric acid to provide building blocks for sporopollenin synthesis in pollen', *Plant Cell*, 19: 1473-87.
- Moreno-Romero, J., H. Jiang, J. Santos-Gonzalez, and C. Kohler. 2016. 'Parental epigenetic asymmetry of PRC2-mediated histone modifications in the Arabidopsis endosperm', *EMBO J*, 35: 1298-311.
- Nakayama, J., J. C. Rice, B. D. Strahl, C. D. Allis, and S. I. Grewal. 2001. 'Role of histone H3 lysine 9 methylation in epigenetic control of heterochromatin assembly', *Science*, 292: 110-3.
- Ng, D. W., T. Wang, M. B. Chandrasekharan, R. Aramayo, S. Kertbundit, and T. C. Hall. 2007. 'Plant SET domain-containing proteins: structure, function and regulation', *Biochim Biophys Acta*, 1769: 316-29.
- Ng, S. S., W. W. Yue, U. Oppermann, and R. J. Klose. 2009. 'Dynamic protein methylation in chromatin biology', *Cell Mol Life Sci*, 66: 407-22.
- Ning, Y. Q., Z. Y. Ma, H. W. Huang, H. Mo, T. T. Zhao, L. Li, T. Cai, S. Chen, L. Ma, and X. J. He. 2015. 'Two novel NAC transcription factors regulate gene expression and flowering time by associating with the histone demethylase JM14', *Nucleic Acids Res*, 43: 1469-84.
- Nishiyama, T., R. Ladurner, J. Schmitz, E. Kreidl, A. Schleiffer, V. Bhaskara, M. Bando, K. Shirahige, A. A. Hyman, K. Mechtler, and J. M. Peters. 2010. 'Sororin mediates sister chromatid cohesion by antagonizing Wapl', *Cell*, 143: 737-49.
- Noh, B., S. H. Lee, H. J. Kim, G. Yi, E. A. Shin, M. Lee, K. J. Jung, M. R. Doyle, R. M. Amasino, and Y. S. Noh. 2004. 'Divergent roles of a pair of homologous jumonji/zinc-finger-class transcription factor proteins in the regulation of Arabidopsis flowering time', *Plant Cell*, 16: 2601-13.
- Onn, I., J. M. Heidinger-Pauli, V. Guacci, E. Unal, and D. E. Koshland. 2008. 'Sister chromatid cohesion: a simple concept with a complex reality', *Annu Rev Cell Dev Biol*, 24: 105-29.
- Page, S. L., and R. S. Hawley. 2001. 'c(3)G encodes a Drosophila synaptonemal complex protein', *Genes & Development*, 15: 3130-43.
- Pan, J., M. Sasaki, R. Kniewel, H. Murakami, H. G. Blitzblau, S. E. Tischfield, X. Zhu, M. J. Neale, M. Jasin, N. D. Socci, A. Hochwagen, and S. Keeney. 2011. 'A hierarchical combination of factors shapes the genome-wide topography of yeast meiotic recombination initiation', *Cell*, 144: 719-31.
- Parelho, V., S. Hadjur, M. Spivakov, M. Leleu, S. Sauer, H. C. Gregson, A. Jarmuz, C. Canzonetta, Z. Webster, T. Nesterova, B. S. Cobb, K. Yokomori, N. Dillon, L. Aragon, A. G. Fisher, and M. Merckenschlager. 2008. 'Cohesins functionally associate with CTCF on mammalian chromosome arms', *Cell*, 132: 422-33.
- Pasini, D., P. A. Cloos, J. Walfridsson, L. Olsson, J. P. Bukowski, J. V. Johansen, M. Bak, N. Tommerup, J. Rappsilber, and K. Helin. 2010. 'JARID2 regulates binding of the Polycomb repressive complex 2 to target genes in ES cells', *Nature*, 464: 306-10.
- Pauli, A., F. Althoff, R. A. Oliveira, S. Heidmann, O. Schuldiner, C. F. Lehner, B. J. Dickson, and K. Nasmyth. 2008. 'Cell-type-specific TEV protease cleavage reveals cohesin functions in Drosophila neurons', *Dev Cell*, 14: 239-51.
- Peng, H., G. E. Begg, D. C. Schultz, J. R. Friedman, D. E. Jensen, D. W. Speicher, and F. J. Rauscher, 3rd. 2000. 'Reconstitution of the KRAB-KAP-1 repressor complex: a model system for defining the molecular anatomy of RING-B box-coiled-coil domain-mediated protein-protein interactions', *J Mol Biol*, 295: 1139-62.
- Petela, N. J., T. G. Gligoris, J. Metson, B. G. Lee, M. Voulgaris, B. Hu, S. Kikuchi, C. Chapard, W. Chen, E.

- Rajendra, M. Srinivisan, H. Yu, J. Lowe, and K. A. Nasmyth. 2018. 'Scc2 Is a Potent Activator of Cohesin's ATPase that Promotes Loading by Binding Scc1 without Pds5', *Mol Cell*, 70: 1134-48 e7.
- Peters, A. H., D. O'Carroll, H. Scherthan, K. Mechtler, S. Sauer, C. Schofer, K. Weipoltshammer, M. Pagani, M. Lachner, A. Kohlmaier, S. Opravil, M. Doyle, M. Sibilia, and T. Jenuwein. 2001. 'Loss of the Suv39h histone methyltransferases impairs mammalian heterochromatin and genome stability', *Cell*, 107: 323-37.
- Peterson, Ross, Janet P Slovin, and Changbin Chen. 2010. 'A Simplified Method for Differential Staining of Aborted and Non-Aborted Pollen Grains', *International Journal of Plant Biology*.
- Powers, N. R., E. D. Parvanov, C. L. Baker, M. Walker, P. M. Petkov, and K. Paigen. 2016. 'The Meiotic Recombination Activator PRDM9 Trimethylates Both H3K36 and H3K4 at Recombination Hotspots In Vivo', *PLoS Genet*, 12: e1006146.
- Pradillo, M., A. Knoll, C. Oliver, J. Varas, E. Corredor, H. Puchta, and J. L. Santos. 2015a. 'Involvement of the Cohesin Cofactor PDS5 (SPO76) During Meiosis and DNA Repair in Arabidopsis thaliana', *Frontiers in Plant Science*, 6.
- . 2015b. 'Involvement of the Cohesin Cofactor PDS5 (SPO76) During Meiosis and DNA Repair in Arabidopsis thaliana', *Front Plant Sci*, 6: 1034.
- Quilichini, T. D., M. C. Friedmann, A. L. Samuels, and C. J. Douglas. 2010. 'ATP-binding cassette transporter G26 is required for male fertility and pollen exine formation in Arabidopsis', *Plant Physiol*, 154: 678-90.
- Quilichini, T. D., E. Grienenberger, and C. J. Douglas. 2015. 'The biosynthesis, composition and assembly of the outer pollen wall: A tough case to crack', *Phytochemistry*, 113: 170-82.
- Rea, S., F. Eisenhaber, D. O'Carroll, B. D. Strahl, Z. W. Sun, M. Schmid, S. Opravil, K. Mechtler, C. P. Ponting, C. D. Allis, and T. Jenuwein. 2000. 'Regulation of chromatin structure by site-specific histone H3 methyltransferases', *Nature*, 406: 593-9.
- Rodriguez-Granados, N. Y., J. S. Ramirez-Prado, A. Veluchamy, D. Latrasse, C. Raynaud, M. Crespi, F. Ariel, and M. Benhamed. 2016. 'Put your 3D glasses on: plant chromatin is on show', *J Exp Bot*, 67: 3205-21.
- Roeder, GS 1990. 'Chromosome synapsis and genetic recombination: their roles in meiotic chromosome segregation', *Trends in Genetics*.
- Rolef Ben-Shahar, T., S. Heeger, C. Lehane, P. East, H. Flynn, M. Skehel, and F. Uhlmann. 2008. 'Eco1-dependent cohesin acetylation during establishment of sister chromatid cohesion', *Science*, 321: 563-6.
- Rollins, R. A., P. Morcillo, and D. Dorsett. 1999. 'Nipped-B, a Drosophila homologue of chromosomal adherins, participates in activation by remote enhancers in the cut and Ultrabithorax genes', *Genetics*, 152: 577-93.
- Rotili, D., and A. Mai. 2011. 'Targeting Histone Demethylases: A New Avenue for the Fight against Cancer', *Genes Cancer*, 2: 663-79.
- Salome, P. A., K. Bomblies, J. Fitz, R. A. Laitinen, N. Warthmann, L. Yant, and D. Weigel. 2012. 'The recombination landscape in Arabidopsis thaliana F2 populations', *Heredity (Edinb)*, 108: 447-55.
- Sanchez, R., and M. M. Zhou. 2011. 'The PHD finger: a versatile epigenome reader', *Trends Biochem Sci*, 36: 364-72.
- Sanders, Paul M., Anhthu Q. Bui, K. N Koen Weterings, Yung-Chao Hsu McIntire, Pei Yun Lee, Mai Thy

- Truong, T. P. Beals, and R. B. Goldberg. 1999. 'Anther developmental defects in *Arabidopsis thaliana* male-sterile mutants', *Sexual Plant Reproduction*.
- Saze, H., A. Shiraishi, A. Miura, and T. Kakutani. 2008. 'Control of genic DNA methylation by a jmjC domain-containing protein in *Arabidopsis thaliana*', *Science*, 319: 462-5.
- Schubert, D., L. Primavesi, A. Bishopp, G. Roberts, J. Doonan, T. Jenuwein, and J. Goodrich. 2006. 'Silencing by plant Polycomb-group genes requires dispersed trimethylation of histone H3 at lysine 27', *EMBO J*, 25: 4638-49.
- Schuldiner, O., D. Berdnik, J. M. Levy, J. S. Wu, D. Luginbuhl, A. C. Gontang, and L. Luo. 2008. 'piggyBac-based mosaic screen identifies a postmitotic function for cohesin in regulating developmental axon pruning', *Dev Cell*, 14: 227-38.
- Schultz, D. C., K. Ayyanathan, D. Negorev, G. G. Maul, and F. J. Rauscher, 3rd. 2002. 'SETDB1: a novel KAP-1-associated histone H3, lysine 9-specific methyltransferase that contributes to HP1-mediated silencing of euchromatic genes by KRAB zinc-finger proteins', *Genes Dev*, 16: 919-32.
- Scott, R. J., M. Spielman, and H. G. Dickinson. 2004. 'Stamen structure and function', *Plant Cell*, 16 Suppl: S46-60.
- Sexton, T., E. Yaffe, E. Kenigsberg, F. Bantignies, B. Leblanc, M. Hoichman, H. Parrinello, A. Tanay, and G. Cavalli. 2012. 'Three-dimensional folding and functional organization principles of the *Drosophila* genome', *Cell*, 148: 458-72.
- Shi, J., M. Cui, L. Yang, Y. J. Kim, and D. Zhang. 2015. 'Genetic and Biochemical Mechanisms of Pollen Wall Development', *Trends Plant Sci*, 20: 741-53.
- Shi, Y. J., C. Matson, F. Lan, S. Iwase, T. Baba, and Y. Shi. 2005. 'Regulation of LSD1 histone demethylase activity by its associated factors', *Mol Cell*, 19: 857-64.
- Shi, Y., F. Lan, C. Matson, P. Mulligan, J. R. Whetstone, P. A. Cole, R. A. Casero, and Y. Shi. 2004. 'Histone demethylation mediated by the nuclear amine oxidase homolog LSD1', *Cell*, 119: 941-53.
- Shu, J., C. Chen, R. K. Thapa, S. Bian, V. Nguyen, K. Yu, Z. C. Yuan, J. Liu, S. E. Kohalmi, C. Li, and Y. Cui. 2019. 'Genome-wide occupancy of histone H3K27 methyltransferases CURLY LEAF and SWINGER in *Arabidopsis* seedlings', *Plant Direct*, 3: e00100.
- Sidhu, G. K., C. Fang, M. A. Olson, M. Falque, O. C. Martin, and W. P. Pawlowski. 2015. 'Recombination patterns in maize reveal limits to crossover homeostasis', *Proc Natl Acad Sci U S A*, 112: 15982-7.
- Simon, L., and A. V. Probst. 2018. 'High-Affinity LNA-DNA Mixmer Probes for Detection of Chromosome-Specific Polymorphisms of 5S rDNA Repeats in *Arabidopsis thaliana*', *Methods Mol Biol*, 1675: 481-91.
- Smagulova, F., I. V. Gregoretto, K. Brick, P. Khil, R. D. Camerini-Otero, and G. V. Petukhova. 2011. 'Genome-wide analysis reveals novel molecular features of mouse recombination hotspots', *Nature*, 472: 375-8.
- Song, M., B. Zhai, X. Yang, T. Tan, Y. Wang, X. Yang, Y. Tan, T. Chu, Y. Cao, Y. Song, S. Wang, and L. Zhang. 2021. 'Interplay between Pds5 and Rec8 in regulating chromosome axis length and crossover frequency', *Sci Adv*, 7.
- Sorensen, A. M., S. Krober, U. S. Unte, P. Huijser, K. Dekker, and H. Saedler. 2003. 'The *Arabidopsis* ABORTED MICROSPORES (AMS) gene encodes a MYC class transcription factor', *Plant J*, 33: 413-23.

- Springer, N. M., C. A. Napoli, D. A. Selinger, R. Pandey, K. C. Cone, V. L. Chandler, H. F. Kaeppler, and S. M. Kaeppler. 2003. 'Comparative analysis of SET domain proteins in maize and Arabidopsis reveals multiple duplications preceding the divergence of monocots and dicots', *Plant Physiol*, 132: 907-25.
- Stacey, N. J., T. Kuromori, Y. Azumi, G. Roberts, C. Breuer, T. Wada, A. Maxwell, K. Roberts, and K. Sugimoto-Shirasu. 2006. 'Arabidopsis SPO11-2 functions with SPO11-1 in meiotic recombination', *Plant J*, 48: 206-16.
- Stassen, M. J., D. Bailey, S. Nelson, V. Chinwalla, and P. J. Harte. 1995. 'The Drosophila trithorax proteins contain a novel variant of the nuclear receptor type DNA binding domain and an ancient conserved motif found in other chromosomal proteins', *Mech Dev*, 52: 209-23.
- Stavropoulos, P., G. Blobel, and A. Hoelz. 2006. 'Crystal structure and mechanism of human lysine-specific demethylase-1', *Nat Struct Mol Biol*, 13: 626-32.
- Stedman, W., H. Kang, S. Lin, J. L. Kissil, M. S. Bartolomei, and P. M. Lieberman. 2008. 'Cohesins localize with CTCF at the KSHV latency control region and at cellular c-myc and H19/Igf2 insulators', *EMBO J*, 27: 654-66.
- Stroud, H., M. V. Greenberg, S. Feng, Y. V. Bernatavichute, and S. E. Jacobsen. 2013. 'Comprehensive analysis of silencing mutants reveals complex regulation of the Arabidopsis methylome', *Cell*, 152: 352-64.
- Suja, J. A., and J. L. Barbero. 2009. 'Cohesin complexes and sister chromatid cohesion in mammalian meiosis', *Genome Dyn*, 5: 94-116.
- Sumara, I., E. Vorlaufer, C. Gieffers, B. H. Peters, and J. M. Peters. 2000. 'Characterization of vertebrate cohesin complexes and their regulation in prophase', *J Cell Biol*, 151: 749-62.
- Sung, P., and D L Robberson. 1995. 'DNA strand exchange mediated by a RAD51-ssDNA nucleoprotein filament with polarity opposite to that of RecA', *Cell*.
- Suzuki, T., and N. Miyata. 2011. 'Lysine demethylases inhibitors', *J Med Chem*, 54: 8236-50.
- Tachibana, M., M. Nozaki, N. Takeda, and Y. Shinkai. 2007. 'Functional dynamics of H3K9 methylation during meiotic prophase progression', *Embo Journal*, 26: 3346-59.
- Takada, Y., C. Naruse, Y. Costa, T. Shirakawa, M. Tachibana, J. Sharif, F. Kezuka-Shiotani, D. Kakiuchi, H. Masumoto, Y. Shinkai, K. Ohbo, A. H. Peters, J. M. Turner, M. Asano, and H. Koseki. 2011. 'HP1gamma links histone methylation marks to meiotic synapsis in mice', *Development*, 138: 4207-17.
- Takeuchi, T., Y. Yamazaki, Y. Katoh-Fukui, R. Tsuchiya, S. Kondo, J. Motoyama, and T. Higashinakagawa. 1995. 'Gene trap capture of a novel mouse gene, jumonji, required for neural tube formation', *Genes Dev*, 9: 1211-22.
- Toledo-Ortiz, G., E. Huq, and P. H. Quail. 2003. 'The Arabidopsis basic/helix-loop-helix transcription factor family', *Plant Cell*, 15: 1749-70.
- Toyoda, Y., and M. Yanagida. 2006. 'Coordinated requirements of human topo II and cohesin for metaphase centromere alignment under Mad2-dependent spindle checkpoint surveillance', *Mol Biol Cell*, 17: 2287-302.
- Tschiersch, B., A. Hofmann, V. Krauss, R. Dorn, G. Korge, and G. Reuter. 1994. 'The protein encoded by the Drosophila position-effect variegation suppressor gene Su(var)3-9 combines domains of antagonistic regulators of homeotic gene complexes', *EMBO J*, 13: 3822-31.
- Tsukada, Y., J. Fang, H. Erdjument-Bromage, M. E. Warren, C. H. Borchers, P. Tempst, and Y. Zhang. 2006. 'Histone demethylation by a family of JmjC domain-containing proteins', *Nature*, 439:

811-6.

- Underwood, C. J., K. Choi, C. Lambing, X. Zhao, H. Serra, F. Borges, J. Simorowski, E. Ernst, Y. Jacob, I. R. Henderson, and R. A. Martienssen. 2018. 'Epigenetic activation of meiotic recombination near *Arabidopsis thaliana* centromeres via loss of H3K9me2 and non-CG DNA methylation', *Genome Res*, 28: 519-31.
- Van Leene, J., D. Eeckhout, B. Cannoot, N. De Winne, G. Persiau, E. Van De Slijke, L. Vercruyse, M. Dedecker, A. Verkest, K. Vandepoele, L. Martens, E. Witters, K. Gevaert, and G. De Jaeger. 2015. 'An improved toolbox to unravel the plant cellular machinery by tandem affinity purification of *Arabidopsis* protein complexes', *Nature Protocols*, 10: 169-87.
- Vass, S., S. Cotterill, A. M. Valdeolmillos, J. L. Barbero, E. Lin, W. D. Warren, and M. M. Heck. 2003. 'Depletion of Drad21/Sccl in *Drosophila* cells leads to instability of the cohesin complex and disruption of mitotic progression', *Curr Biol*, 13: 208-18.
- Vaur, S., A. Feytout, S. Vazquez, and J. P. Javerzat. 2012. 'Pds5 promotes cohesin acetylation and stable cohesin-chromosome interaction', *EMBO Rep*, 13: 645-52.
- Vrielynck, N., A. Chambon, D. Vezon, L. Pereira, L. Chelysheva, A. De Muylt, C. Mezard, C. Mayer, and M. Grelon. 2016. 'A DNA topoisomerase VI-like complex initiates meiotic recombination', *Science*, 351: 939-43.
- W.Parish, Roger, and Song F.Li. 2010. 'A programme of developmental altruism', *Plant Science*, 178.
- Wang, J., C. Y. Yu, S. B. Zhang, J. Y. Ye, H. Dai, H. K. Wang, J. Y. Huang, X. F. Cao, J. B. Ma, H. Ma, and Y. X. Wang. 2020a. 'Cell-type-dependent histone demethylase specificity promotes meiotic chromosome condensation in *Arabidopsis* (vol 46, pg 212, 2020)', *Nature Plants*, 6: 1194-94.
- Wang, J., C. Yu, S. Zhang, J. Ye, H. Dai, H. Wang, J. Huang, X. Cao, J. Ma, H. Ma, and Y. Wang. 2020b. 'Cell-type-dependent histone demethylase specificity promotes meiotic chromosome condensation in *Arabidopsis*', *Nat Plants*, 6: 823-37.
- Wang, Q., P. Liu, H. Jing, X. F. Zhou, B. Zhao, Y. Li, and J. B. Jin. 2021. 'JMJ27-mediated histone H3K9 demethylation positively regulates drought-stress responses in *Arabidopsis*', *New Phytol*, 232: 221-36.
- Wang, Y., Z. Cheng, P. Lu, L. Timofejeva, and H. Ma. 2014. 'Molecular cell biology of male meiotic chromosomes and isolation of male meiocytes in *Arabidopsis thaliana*', *Methods Mol Biol*, 1110: 217-30.
- Watrin, E., and J. M. Peters. 2006. 'Cohesin and DNA damage repair', *Exp Cell Res*, 312: 2687-93.
- Watrin, E., A. Schleiffer, K. Tanaka, F. Eisenhaber, K. Nasmyth, and J. M. Peters. 2006. 'Human Sccl is required for cohesin binding to chromatin, sister-chromatid cohesion, and mitotic progression', *Curr Biol*, 16: 863-74.
- Wendt, K. S., K. Yoshida, T. Itoh, M. Bando, B. Koch, E. Schirghuber, S. Tsutsumi, G. Nagae, K. Ishihara, T. Mishiro, K. Yahata, F. Imamoto, H. Aburatani, M. Nakao, N. Imamoto, K. Maeshima, K. Shirahige, and J. M. Peters. 2008. 'Cohesin mediates transcriptional insulation by CCCTC-binding factor', *Nature*, 451: 796-801.
- Wilson, Z. A., S. M. Morroll, J. Dawson, R. Swarup, and P. J. Tighe. 2001. 'The *Arabidopsis* MALE STERILITY1 (MS1) gene is a transcriptional regulator of male gametogenesis, with homology to the PHD-finger family of transcription factors', *Plant J*, 28: 27-39.
- Wilson, Z. A., and D. B. Zhang. 2009. 'From *Arabidopsis* to rice: pathways in pollen development', *J Exp Bot*, 60: 1479-92.
- Wysocka, J., T. Swigut, H. Xiao, T. A. Milne, S. Y. Kwon, J. Landry, M. Kauer, A. J. Tackett, B. T. Chait, P.

- Badenhorst, C. Wu, and C. D. Allis. 2006. 'A PHD finger of NURF couples histone H3 lysine 4 trimethylation with chromatin remodelling', *Nature*, 442: 86-90.
- Xiao, J., U. S. Lee, and D. Wagner. 2016. 'Tug of war: adding and removing histone lysine methylation in Arabidopsis', *Curr Opin Plant Biol*, 34: 41-53.
- Xu, J., Z. Ding, G. Vizcay-Barrena, J. Shi, W. Liang, Z. Yuan, D. Werck-Reichhart, L. Schreiber, Z. A. Wilson, and D. Zhang. 2014. 'ABORTED MICROSPORES Acts as a Master Regulator of Pollen Wall Formation in Arabidopsis', *Plant Cell*, 26: 1544-56.
- Xu, J., C. Yang, Z. Yuan, D. Zhang, M. Y. Gondwe, Z. Ding, W. Liang, D. Zhang, and Z. A. Wilson. 2010. 'The ABORTED MICROSPORES regulatory network is required for postmeiotic male reproductive development in Arabidopsis thaliana', *Plant Cell*, 22: 91-107.
- Yan, W., D. Chen, C. Smaczniak, J. Engelhorn, H. Liu, W. Yang, A. Graf, C. C. Carles, D. X. Zhou, and K. Kaufmann. 2018. 'Dynamic and spatial restriction of Polycomb activity by plant histone demethylases', *Nat Plants*, 4: 681-89.
- Yang, C., Y. Hamamura, K. Sofroni, F. Bower, S. C. Stolze, H. Nakagami, and A. Schnittger. 2019. 'SWITCH 1/DYAD is a WINGS APART-LIKE antagonist that maintains sister chromatid cohesion in meiosis', *Nat Commun*, 10: 1755.
- Yang, C., G. Vizcay-Barrena, K. Conner, and Z. A. Wilson. 2007. 'MALE STERILITY1 is required for tapetal development and pollen wall biosynthesis', *Plant Cell*, 19: 3530-48.
- Yang, H., P. Lu, Y. Wang, and H. Ma. 2011. 'The transcriptome landscape of Arabidopsis male meiocytes from high-throughput sequencing: the complexity and evolution of the meiotic process', *Plant J*, 65: 503-16.
- Yang, Z., Q. Qiu, W. Chen, B. Jia, X. Chen, H. Hu, K. He, X. Deng, S. Li, W. A. Tao, X. Cao, and J. Du. 2018. 'Structure of the Arabidopsis JM14-H3K4me3 Complex Provides Insight into the Substrate Specificity of KDM5 Subfamily Histone Demethylases', *Plant Cell*, 30: 167-77.
- Yao, X., H. Feng, Y. Yu, A. Dong, and W. H. Shen. 2013. 'SDG2-mediated H3K4 methylation is required for proper Arabidopsis root growth and development', *PLoS One*, 8: e56537.
- Zhang, L., S. Wang, S. Yin, S. Hong, K. P. Kim, and N. Kleckner. 2014. 'Topoisomerase II mediates meiotic crossover interference', *Nature*, 511: 551-6.
- Zhang, S., B. Zhou, Y. Kang, X. Cui, A. Liu, A. Deleris, M. V. Greenberg, X. Cui, Q. Qiu, F. Lu, J. A. Wohlschlegel, S. E. Jacobsen, and X. Cao. 2015. 'C-terminal domains of a histone demethylase interact with a pair of transcription factors and mediate specific chromatin association', *Cell Discov*, 1.
- Zhang, W., Y. Sun, L. Timofejeva, C. Chen, U. Grossniklaus, and H. Ma. 2006. 'Regulation of Arabidopsis tapetum development and function by DYSFUNCTIONAL TAPETUM1 (DYT1) encoding a putative bHLH transcription factor', *Development*, 133: 3085-95.
- Zhang, X., Y. V. Bernatavichute, S. Cokus, M. Pellegrini, and S. E. Jacobsen. 2009. 'Genome-wide analysis of mono-, di- and trimethylation of histone H3 lysine 4 in Arabidopsis thaliana', *Genome Biol*, 10: R62.
- Zhang, X., J. Yazaki, A. Sundaresan, S. Cokus, S. W. Chan, H. Chen, I. R. Henderson, P. Shinn, M. Pellegrini, S. E. Jacobsen, and J. R. Ecker. 2006. 'Genome-wide high-resolution mapping and functional analysis of DNA methylation in Arabidopsis', *Cell*, 126: 1189-201.
- Zhang, Z. B., J. Zhu, J. F. Gao, C. Wang, H. Li, H. Li, H. Q. Zhang, S. Zhang, D. M. Wang, Q. X. Wang, H. Huang, H. J. Xia, and Z. N. Yang. 2007. 'Transcription factor AtMYB103 is required for anther development by regulating tapetum development, callose dissolution and exine formation in

- Arabidopsis', *Plant J*, 52: 528-38.
- Zheng, J., F. Chen, Z. Wang, H. Cao, X. Li, X. Deng, W. J. J. Soppe, Y. Li, and Y. Liu. 2012. 'A novel role for histone methyltransferase KYP/SUVH4 in the control of Arabidopsis primary seed dormancy', *New Phytol*, 193: 605-16.
- Zheng, S., H. Hu, H. Ren, Z. Yang, Q. Qiu, W. Qi, X. Liu, X. Chen, X. Cui, S. Li, B. Zhou, D. Sun, X. Cao, and J. Du. 2019. 'The Arabidopsis H3K27me3 demethylase JUMONJI 13 is a temperature and photoperiod dependent flowering repressor', *Nat Commun*, 10: 1303.
- Zhu, J., Y. Lou, X. Xu, and Z. N. Yang. 2011. 'A genetic pathway for tapetum development and function in Arabidopsis', *J Integr Plant Biol*, 53: 892-900.
- Zickler, D., and N. Kleckner. 1999a. 'Meiotic chromosomes: Integrating structure and function', *Annual Review of Genetics*, 33: 603-754.
- . 1999b. 'Meiotic chromosomes: integrating structure and function', *Annu Rev Genet*, 33: 603-754.
- Zilberman, D., X. Cao, and S. E. Jacobsen. 2003. 'ARGONAUTE4 control of locus-specific siRNA accumulation and DNA and histone methylation', *Science*, 299: 716-9.

7 Appendix

Abbreviation:

IBM1: increase in BONSAI methylation

H3K9me2: histone 3 lysine 9 dimethylation

H3K4me1: histone 3 lysine 4 monomethylation

H3K27me3: histone 3 lysine 27 trimethylation

FYRN: FY-rich N-terminus

FYRC: FY-rich C-terminus

JmjC: Jumonji C

PHD: plant homeodomain)

CMT3: CHROMOMETHYLASE 3

PCD: programmed cell death

NAC: NAM, ATAF1 and CUC1/CUC2

SC: synapotomal complex

dex1: DEFECTIVE IN EXINE FORMATION 1

TEM:transmission electron microscopic

RSC: Remodels the Structure of Chromatin

S. pombe: Schizosaccharomyces pombe

TADs: topologically associated domains

A. tumefaciens: Agrobacterium tumefaciens

N. benthamiana:Nicotiana benthamiana

TEs: Transposable Elements

AGDP1: Agenet domain (AGD)-containing p1

Dot1: Disruption of telomeric silencing 1

SET: Su(var), E(z), and Trithorax

KMTs: Histone Lysine Methyltransferases

KDMs: Histone Lysine Demethylases

E(Z): Enhancer of zeste

trxG: trithorax group

PRC2: Polycomb Repressive Complex 2

PcG: Polycomb group

DEGs: Differentially Expressed Genes

DSBs: Double Strand Breaks

ATAC-seq: Assay for Transposase-Accessible Chromatin using sequencing

Hi-C: High-throughput chromosome conformation capture

Supplementary Table 1: List of primers used in this study

Gene ID	primers	used for
AT5G52290	CCTTTGGTGTTAACTTGTGGC	Chip_qPCR
	CCATCCGTACACAACAACAAC	
	TGAGACGATTGAACCCCAAG	
	CCTTTGAGCCTATAAGCTCC	
	TCGAAGCTGCTAAGACTACC	
	GCATACCACCAGATCTACATG	
AT1G22260	GCCGTTAGTCGAATTAATCGAC	Chip_qPCR
	TTGCGCTCTCGAATTGTGTG	
	CGAATTTGAACTCACTGCAG	
	GTCGAAATCATCATAACAGTCG	
	AAAAGACGAGTGTTCACTG	
	CTTCTAACCTCCTGCTCTG	
AT1G22275	TCTGAGTCTCTGACATCAGC	Chip_qPCR
	GCTCTCGAAATTGTGTGAGC	
	CTCTCAACGAAGACTCTGTG	
	CATCCTGAACTTGAGAAGCC	
	AAGTACGAGAAACTGCAGGC	
	GGCTCTCACTCTTTCTGC	
AT5G48390	ACATTTAAAACGGCATAACGTAC	Chip_qPCR
	TCGATTTCAAGAGGGAGATGG	
	TGCAGAAGGGAGAGTTGAG	
	TCCATCACTACCATTTCCTCC	
	GCCATTGGTCAGATCGATGC	
	TCATGCGCTGAAAGGGAAAG	
AT1G67370	CGCGTCGTTACACAATTAGTC	Chip_qPCR
	GTGAGGGAGTCTGGGAGATC	
	GACGACATGCAAGATGATGG	
	CTGAATCAGAAGGCTGGTCA	
AT5G61960	AGGTAAGAGTTGGTTCGCTG	Chip_qPCR
	ACGATTAGGTACATCCAGAAGC	
	TGAAAACAGACATGATGCCTG	
	CAGCTGGTAACTTTCAGATGTC	
AT2G42890	GGAAGAGAGGAGGAGGAAGAG	Chip_qPCR
	CGGAGAAGCAAAGGAGAAGAG	
	ATATGCCATCTTTGCTGAGTAG	
	GAGCTTGAGAACATGCTGAG	
AT5G07290	GAGTTGGTTCTTCTCTGCTTC	Chip_qPCR

	CAAAATTCGGAATTA AAAACGCC	
	AACAATCCAATGCCTGAAGG	
	GAGAGAGCTGGTAACTGTCAG	
	TCTCCATAAATCAAGGATCCC	
	CACATCATGCCACTTGACTG	
AT5G52290	GTCTCAAATGATAAAGGGAGACG	RT_qPCR
	TCAGATTCTTGAGGCATGGAG	
AT5G48390	AGAAGAAGCTGAAAAGCTTGAG	RT_qPCR
	TCATGCGCTGAAAGGGAAAG	
AT1G22275	ACCAACAAATCATTAAGGACAAGG	RT_qPCR
	TAATTGCCTGGTCATTCTCTG	
AT1G67370	ATGGAGAGGTTGATGAAGATGAC	RT_qPCR
	CGAGCTGATCCATGATTTCTTC	
AT3G13220	CTCGGCCTCGAAAGATGCCG	RT_qPCR
	GGTGGCAGAAGTGGAGTCAAG	
AT4G35420	CAAGCGCTTCCAGGTCTGG	RT_qPCR
	CGAGGACATCGGAAGCTGTAG	
AT1G66170	TGTCGTTGCACAGGTTGGAG	RT_qPCR
	CCATTGACACATACCAAATGACC	
AT2G28560	CCACCATGTCAATCTGCTCG	RT_qPCR
	ACCAATACCAGGAGGACCAAC	
AT3G07610	GCTGCTACCACTAGTTGCCAG	<i>ibm1-4</i> (SALK_035608) genotyping
	ACTGCCACGATAATGAGGTTG	
AT4G00990	ACGCAATGTATGTCTTGGGTC	<i>jmj27-2</i> (SALK_092672) genotyping
	ATCCATTGCCAATTTTCACAG	
AT2G16910	CTCTCAGCCATCAGGTTCTTG	<i>ams</i> (SALK_152147) genotyping
	ACAGGTTTGTGAAGTGGATGG	
AT5G47690	CTTGCAGCATCTCTAACGTCC	<i>pds5a</i> (SALK_114556) genotyping
	GAAGTGCCTATCTTACCAG	
AT1G77600	CGCCAGTTCTCTCATTGAAAG	<i>pds5b</i> (SALK_092843) genotyping
	GGAAAAAGATCATCGGAGAGC	
AT1G80810	TTCGAATCAATTCAGGTCAGG	<i>pds5c</i> (SALK_013481) genotyping
	ATGTGAAGGGACATTCAGTGC	
AT1G15940	GTCTGCAGTTTGCTCTTTTGC	<i>pds5e</i> (SAIL_287_D07) genotyping
	TCTGCCTTGTAAGTAAAATTCC	
AT5G05490	CTCATATTCACGGTGCTCCC	<i>rec8</i> (SAIL_807_B08) genotyping
	GGGGGAAAAGAGAAAGGTTT	
AT3G07610	GCGGGTACCCTTCGATCACAAATTAGAGGAAAT	construction for IBM1 promoter
	GCGGTCGACTTTTCGAAAATCAAATTTCTCAATCGTC	
AT3G07610	GCGGTCGACATGGATTCTGTGGAGGAAGAAGG	construction for IBM1 CDS
	GCGGGATCCATCTTCTCAATTTCTAATCTGTCAATG	
AT3G22880	GCGCTCGAGCACGAATATAATTGCGAAGAATAG	construction for AtDMC1 promoter
	GCGGTCGACTTTCTCGCTCTAAGAGTCTCTAAG	

AT5G05490	GCGGGTACCCCAGCCAAGACATTGTGATC	construction for REC8 promoter
	GCGGTCGACTTCCTTTCTACTATCTGCCAATTTAG	
AT5G51330	GCGGGTACCTTGACATTGTGAGAGTAACGGAG	construction for SWI1 promoter
	GCGGAATTCGATTTTTGCTCTCGATAATCTTCG	
AT5G05490	GATAGAATAGAATGGCGTGGCATTCTCTCTTTTGTATTCC	construction for <i>REC8</i> knock down
	GAATGCCACGCCATTCTATTCTATCAAAGAGAATCAATGA	
	GAATACCACGCCATTGTATTCTTTACAGGTCGTGATATG	
	GAAAGAATACAATGGCGTGGTATTCTACATATATATTCT	
AT3G07610	GATAATTTAGTATCTAGACGCACTCTCTCTTTTGTATTCC	construction for <i>IBM1</i> knock down
	GAGTGCGTCTAGATACTAAATTATCAAAGAGAATCAATGA	
	GAGTACGTCTAGATAGTAAATTTTACAGGTCGTGATATG	
	GAAAATTTACTATCTAGACGTA CTCTACATATATATTCT	

8 Acknowledgement

Firstly, I want to express my deepest grateful to my supervisor Hua Jiang for providing the opportunity to being as the PhD candidate in his group, for giving the guidance, for being always available for discussion, and for being able to express my ideas freely and practice them, and also for many training I have got during my PhD study. Thank you very much.

I want to thank all members of the Applied Chromosome Biology (ACB) group. Many thanks to Leane Gottschalk for much help in study and life. Thanks to Ewa Piskorz, Linhao Xu, Jothipriya Ramakrishnan, Kim Mungyeong, Yingrui Ma, Shiwei Zheng for their help in scientific support and also comfort for difficult life. It's a great time to meet all of you during my PhD study. Thank you very much.

I also want to thanks ME group member Dr. Stefan Heckmann to provide ZYP1 antibody, and Dr. Maria Cuacos, Dr. Chao Feng, Jana Lorenz, Mohammad Abdelmordy Ayoub, Stefan Steckenborn Diaz Coria for their technical help during my PhD study.

I would like to thank Dr. Twan Rutten for training in microscopy and our cooperater Dr. Michael Melzer for light microscope and transmission electron microscopy observation in my mutants, Prof. Dr Klaus D Grasser and Valentin Bergér for AP-MS, Prof. Dr Arp Schnitger and Chao Yang to kindly provide us plant materials and plasmid for Y2H.

I am very grateful for the help from CSF group members to share machines and stuff during my study.

Many thanks to my roommates Fang Liu and Daiyan Li for their help in my life.

Many thanks to Dr. Britt Leps for her help that made my life easier in Gatersleben, and also the gardners to provide much help in my study.

I also want to thanks my parents, my brother, and my sister. Thank them for supporting all the decisions I have made, and their selfless love and encouragement that keep me moving forward.

9 Curriculum Vitae

Name: Jinping Cheng

Gender: female

Date of birth: 1991/10/07

Education:

2018.03.22-present: **PhD** in Biology, Leibniz-institute of Plant Genetics and Crop Plant Research (IPK), Gatersleben, and enrolled at Martin Luther University, Halle, Germany,

Supervisor: Prof. Dr. Hua Jiang, Applied Chromosome Biology group

PhD thesis: **H3K9 demethylation is required for reproduction in *Arabidopsis***

2014.09.03-2017.06.25 **M.Sc.** Biochemistry and Molecular Biology, College of Life Sciences, Fudan University, Shanghai, China

Supervisor: Prof. Dr. Binglian Zheng

Thesis: **The identification and function of lariat RNAs in *Arabidopsis***

2010.09.07-2014.06.21 **B.Sc.** Biotechnology, College of Life Sciences, Sichuan University, Chengdu, China

Poster Presentation

Jinping Cheng. Epigenetic alterations in *Arabidopsis* polyploids. Poster. Plant Science Student Conference, Halle, Germany, 2018.

Jinping Cheng. The function of H3K9 demethylase during meiosis. Plant Science Student Conference, Halle, Germany, 2019.

Attended Conferences

2021. June 3: MAYosis series seminar, online

2021.July.13-15: 23rd International Chromosome Conference (ICC), online

Publication:

Cheng J, Zhang G, Xu L, Liu C, Jiang H. Altered H3K27 trimethylation contributes to flowering time variations in polyploid *Arabidopsis thaliana* ecotypes. *J Exp Bot.* 2021 Oct 26:erab470. doi: 10.1093/jxb/erab470. Epub ahead of print. PMID: 34698830

Jinping Cheng, Linhao Xu, Valentin Berg er, Astrid Bruckmann, Chao Yang, Klaus D Grasser, Arp Schnittger, Hua Jiang. H3K9 demethylation-mediated transcriptional activation is required for male meiosis in *Arabidopsis thaliana*. (Under Review)

Cheng, J., Zhang, Y., Li, Z. et al. A lariat-derived circular RNA is required for plant development in Arabidopsis. *Sci. China Life Sci.* (2018).
Doi:10.1007/s11427-017-9182-3

Li Z, Wang S, **Cheng J**, et al. Intron Lariat RNA Inhibits MicroRNA Biogenesis by Sequestering the Dicing Complex in Arabidopsis. *PLoS Genet.* 2016;12(11):e1006422. Published 2016 Nov 21. doi:10.1371/journal.pgen.1006422

Su, C., Li, Z., **Cheng, J.**, Li, L., Zhong, S., Liu, L., Zheng, Y. and Zheng, B. (2017). The Protein Phosphatase 4 and SMEK1 Complex Dephosphorylates HYL1 to Promote miRNA Biogenesis by Antagonizing the MAPK Cascade in Arabidopsis. *Dev Cell* 41, 527-539 e5.

Zhang X, Zhang Y, Wang T, Li Z, **Cheng J**, Ge H, Tang Q, Chen K, Liu L, Lu C, Guo J, Zheng B, Zheng Y. A Comprehensive Map of Intron Branchpoints and Lariat RNAs in Plants. *Plant Cell.* 2019 May;31(5):956-973. doi: 10.1105/tpc.18.00711. Epub 2019 Mar 20. PMID: 30894459; PMCID: PMC6533014

10 Eidesstattliche Erklärung/Declaration under Oath

Ich erkläre an Eides statt, dass ich die Arbeit selbstständig und ohne fremde Hilfe verfasst, keine anderen als die von mir angegebenen Quellen und Hilfsmittel benutzt und die den benutzten Werken wörtlich oder inhaltlich entnommenen Stellen als solche kenntlich gemacht habe.

I declare under penalty of perjury that this thesis is my own work entirely and has been written without any help from other people. I used only the sources mentioned and included all the citations correctly both in word or content.

Datum / Date

*Unterschrift des Antragstellers /
Signature of the applicant*

11 Erklärung über bestehende Vorstrafen und anhängige Ermittlungsverfahren/Declaration concerning Criminal Record and Pending Investigations

Hiermit erkläre ich, dass ich weder vorbestraft bin noch dass gegen mich Ermittlungsverfahren anhängig sind. / I hereby declare that I have no criminal record and that no preliminary investigations are pending against me.

Datum / Date

Unterschrift des Antragstellers /
Signature of the applicant